ABSTRACT

Title of dissertation: ON SYMMETRY: A FRAMEWORK FOR AUTOMATED SYMMETRY DETECTION

Hyoungjune Yi, Doctor of Philosophy, 2013

Dissertation directed by: Professor Yiannis Aloimonos
Department of Computer Science

Symmetry has weaved itself into almost all fabrics of science, as well as in arts, and has left an indelible imprint on our everyday lives. And, in the same manner, it has pervaded a wide range of areas of computer science, especially computer vision area, and a copious amount of literature has been produced to seek an algorithmic way to identify symmetry in digital data.

Notwithstanding decades of endeavor and attempt to have an efficient system that can locate and recover symmetry embedded in real-world images, it is still challenging to fully automate such tasks while maintaining a high level of efficiency.

The subject of this thesis is symmetry of imaged objects. Symmetry is one of the non-accidental features of shapes and has long been (maybe mistakenly) speculated as a pre-attentive feature, which improves recognition of quickly presented objects and reconstruction of shapes from incomplete set of measurements. While symmetry is known to provide rich and useful geometric cues to computer vision, it has been barely used as a principal feature for applications because figuring out how to represent and recognize symmetries embedded in objects is a singularly difficult

task, both for computer vision and for perceptual psychology.

The three main problems addressed in the dissertation are: (i) finding approximate symmetry by identifying the most prominent axis of symmetry out of an entire region, (ii) locating bilaterally symmetrical areas from a scene, and (iii) automating the process of symmetry recovery by solving the problems mentioned above.

Perfect symmetries are rare in the extreme in natural images and symmetry perception in humans allows for qualification so that symmetry can be graduated based on the degree of structural deformation or replacement error. There have been many approaches to detect approximate symmetry by searching an optimal solution in a form of an exhaustive exploration of the parameter space or surmising the center of mass. The algorithm set out in this thesis circumvents the computationally intensive operations by using geometric constraints of symmetric images, and assumes no prerequisite knowledge of the barycenter. The results from an extensive set of evaluation experiments on metrics for symmetry distance and a comparison of the performance between the method presented in this thesis and the state of the art approach are demonstrated as well.

Many biological vision systems employ a special computational strategy to locate regions of interest based on local image cues while viewing a compound visual scene. The method taken in this thesis is a bottom-up approach that causes the observer favors stimuli based on their saliency, and creates a feature map contingent on symmetry. With the help of summed area tables, the time complexity of the proposed algorithm is linear in the size of the image. The distinguished regions are then delivered to the algorithm described above to uncover approximate symmetry.

ON SYMMETRY: A FRAMEWORK FOR AUTOMATED SYMMETRY DETECTION

by

Hyoungjune Yi

Dissertation submitted to the Faculty of the Graduate School of the
University of Maryland, College Park in partial fulfillment
of the requirements for the degree of
Doctor of Philosophy
2013

Advisory Committee:
Professor Yiannis Aloimonos, Chair/Advisor
Dr. Cornelia Fermuller, Co-Advisor
Professor Amitabh Varshney
Professor Dan Butts
Professor Shihab Shamma

Dedication

Dedicated to *Yu Yangyeon*, my first and greatest teacher ...

Acknowledgments

First all, I owe my advisor, Dr. Yiannis Aloimonos, and co-advisor, Dr. Cornelia Fermüller, a debt of gratitude for all their support, patience, and guidance throughout graduate school.

I would also like to express my deepest gratitude to my committee members: Dr. Amitabh Varshney, Dr. Dan Butts; and Dr. Shihab Shamma, for their advice, insightful comments, and suggestions during the oral examination.

I also would like to place my sincere thanks to all the faculty members of the Department of Computer Science for their motivation, enthusiasm, and help.

My sincere appreciation is extended to my brother, Yongseok, and my sister-in-law. Without their encouragement, I would not have a chance to be here.

Last but not least, I want to thank all the people who have set theoretical and empirical foundations of symmetry research. Without them I would never have made it this far.

Table of Contents

List of Figures

List of Abbreviations

AoI	Area of Interest
AoS	Area of Symmetry
CBIR	Content-Based video/Image Retrieval
DoS	Degree of Symmetry
FIT	Feature Integration Theory
GST	Generalized Symmetry Transform
HA	Holographic Approach
LBS	Line Based Symmetry detection
LHC	Large Hadron Collider
PoI	Point of interest
RoI	Regions of Interest
SAT	Summed Area Table
SD	Symmetry Distance
SfM	Structure from Motion
SIFT	Scale-Invariant Feature Transform
SLS	Smoothed Local Symmetries
SUSY	Supersymmetry
TA	Transformational Approach

Chapter 1

Introduction

Science is based on symmetry. The three main ingredients of science, *i.e.*, reproducibility, predictability, and reduction, are all symmetries [186][1]. To build the scientific veracity of a claim, the results can be replicated at different times and locations (reproducibility), the possible outcome can be expressed in advance to formulate laws on the phenomena examined (predictability), and last but not least, the produced results should be unaffected by and independent of the possible changes in the rest of the universe(reduction).

The goal of this chapter is providing a brief précis on the general understanding of symmetry from various perspectives ranging from art and physics to biology and human psychology. While this chapter certainly will not cover all the empirical or theoretical issues on symmetry, it will provide enough insight into the perceptual underpinnings of the proposed model.

1.1 Definition of Symmetry

Numerous entities in the world, both natural and man-made, are strongly constrained by symmetry. Symmetry is all-pervasive [58, 62, 86, 119, 139, 237], and comprehended in a loose sense, *i.e.*, besides geometric symmetries, everyone has

[1]There are four other forms it manifests itself in science, Rosen claims. Symmetry of evolution, symmetry of states, gauge symmetry and symmetry at quantum theory.

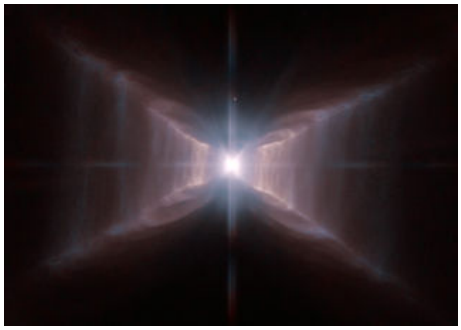

(a) The star HD 44179

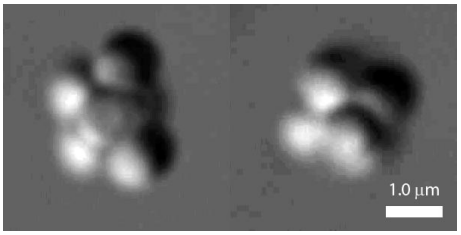

(b) Colloidal clusters

Figure 1.1: Symmetry as big as nebula to as small as colloidal clusters. 1.1(a) The star HD 44179 surrounded by a structure known as the Red Rectangle. The images of it in visible and near infrared light show a highly symmetric nebula. The nebula is approximately 2,300 light years distant from Earth. 1.1(b) Highly symmetric colloidal clusters. Scale bar, 1 μm.[141]

their own idea of what symmetry means. It can be an instance in mathematical programming that should be removed from a problem to reduce the computation times of enumerative algorithms for the given optimization problem [115], or a relation between a boson and a corresponding fermion with the same mass and internal quantum numbers but differ by half a unit of spin. Musicians may consider it as one of the fundamental principles that has a huge importance in music in tandem with contrast [100], someone finds it from the positions and movements involved in T'ai Chi Chuan, the Chinese martial art [74], or a child prodigy just says "Symmetry is what we see at a glance"[2]. It is also construed as an equivalence between decidability and verifiability in the complexity class P, and the lack thereof in the class NP. It delivers an important parameter in physical and chemical processes[5] and is an important criterion in medical diagnosis[142].

[2]In the Pensées. Blaise Pascal. 1660.

Irrespective of various opinions as to what it means to be symmetric, there is one common characteristic shared by most people: invariance. Like in physics symmetry means invariance. It is immune to possible changes or transformation that could perturb observational activity, measurement. For this reason there should be an operation (transformation) you can do on something and after you do the operation on it, still some aspects of it remain the same [186]. As an illustrative instance, here is a phrase: "rats live on no evil star", and you read it backward. You do the operation (reading in the reverse direction) on a phrase and yet it reads the same, then we call the phrase symmetric under reading in the reverse direction. Phrases with this type of bilateral symmetry are dubbed palindromes.

Formally, if $S \in R^n$, a symmetry of S is an isometry f (a transformation that preserves all pairwise distances between metric spaces, *e.g.*, the rotation of a plane) with the property that $f(S) = S$. There are only four mathematically well-defined primitive symmetry types in 2D Euclidean space (Figure 1.2): Reflection ($f(x,y) = f(-x,y)$)[3], Rotation ($f\,(x,y) = f\left(r\,cos\left(\frac{2\pi}{n}\right), r\,sin\left(\frac{2\pi}{n}\right)\right), r = \sqrt{x^2+y^2}$), Translation ($f(x,y) = f(x+\triangle x, y+\triangle y)$), and Glide reflection ($f(x,y) = f(-x, y+\triangle y)$)[118].

[3] A more rigorous geometrical definition is given at http://mathworld.wolfram.com/Reflection.html. Given a vector v in Euclidean space R^n, the reflection in the hyperplane orthogonal to a is given by

$$\mathrm{Ref}_a(v) = v - 2\frac{v \cdot a}{a \cdot a}a$$

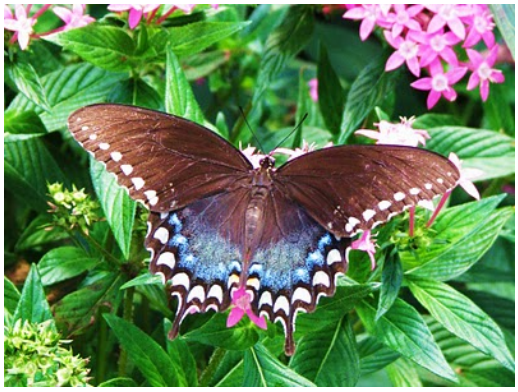

(a) Refletive Symmetry

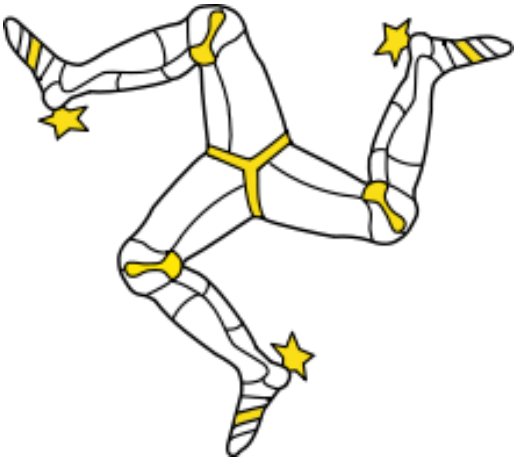

(b) Rotational Symmetry

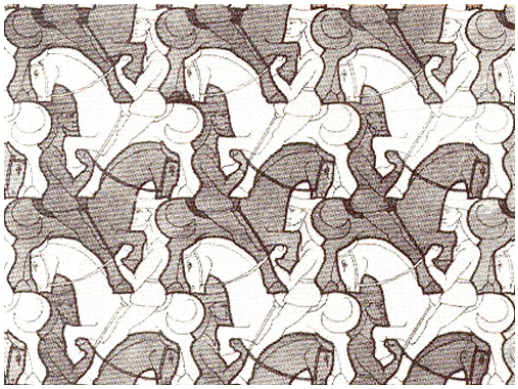

(c) Translational Symmetry

(d) Glide reflective Symmetry

Figure 1.2: Primitive geometrical symmetries in 2D Euclidean space. 1.2(a): also called bilateral symmetry and has one or more axes of symmetry, 1.2(b): the center of rotation is the only invariant point, 1.2(c): in fact, the figure also contains glide reflection in shape space, 1.2(d): the composition of two glide reflections commensurates with a translational symmetry.

(a) Taj Mahal (b) Mumtaz Mahal

Figure 1.3: Taj Mahal facing the long reflecting pool and Mumtaz Mahal. Taj Mahal was constructed by her husband as her final resting place.

1.2 Symmetry in Art

Symmetry, and especially bilateral symmetry, is said to be aesthetically linked to our emotional sensibility and credited with beauty[238]. The Taj Mahal (Figure 1.3(a)), one of the world's most amazing jewel of traditional architecture renowned for its natural beauty, is a mausoleum and the incarnation of symmetry[4]. Even the pool of water in front of the building reflects the symmetrical features of structure on its stationary surface. When his beloved wife (Figure 1.3(b).) died during the birth of their 14^{th} child, the grief-stricken husband, Emperor Shah Jahan, decided to build her a tomb, so that she can rest in its perfection and beauty: symmetry.

It is, in point of fact, hard to think of any architectural tradition without symmetry. Aesthetic value of an object is the satisfaction we can get from its beauty

[4]Yet there are flaws, albeit not critical, in the symmetry in the placement of the two coffins and slightly tilted minarets.

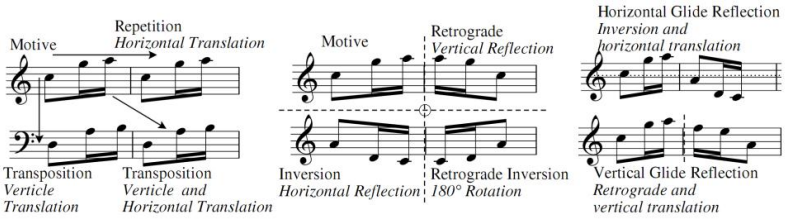

Figure 1.4: Isometric transformations in musical space. Adapted from [75]

and symmetry is regarded to form a canon of beauty in art as in nature [155].

The symmetry does not have to be visual or spatial: a fugue begins with the exposition and the subject that is introduced at the beginning will recur throughout the fugue, repeating the theme at the same time interval (Figure 1.4).

Although symmetry seems to provide stable and attractive sensation towards the whole structure, it also conveys inflexible platitude that makes it less appealing than more dynamic and unforeseeable charm of asymmetry. Even Immanuel Kant agreed that mathematical regularity is "inherently repugnant to taste" [5]. When the underlying symmetry is evident, asymmetry can evoke feelings of excitement and curiosity, so many painters in the Italian Renaissance chose to use it [139].

1.3 Alan Turing and Symmetry

In the last paper before his committing suicide in 1952 [216], Alan Turing ushered in the first applications of computer modeling in developmental biology and tried to find out how the symmetric morphology of a spatially homogeneous mass

[5] "All stiff regularity (such as borders on mathematical regularity) is inherently repugnant to taste, in that the contemplation of it affords us no lasting entertainment." in "Kant's Critiques: The Critique of Pure Reason, The Critique of Practical Reason, The Critique of Judgment"

of identical cells could be broken (Symmetry breaking) by reactants, called morphogens, with different diffusion rates. He considered asymmetrical patterns that are later manifested in the anatomical structure of an organism as the result of an array of biochemical reactions among morphogens. He claimed a small aberration from homogeneity caused by stochastic fluctuations can be amplified and the inherent symmetry of a form would be dissipated. While it had fallen short of explaining any particular question up until recently (a natural Turing pattern was found on the skin of an angelfish [103]), and there are no evidences to support the exact theory as set out by him, the importance of his claim is that the loss of homogeneity could be explained in a quantitatively rigorous way.

1.4 Symmetry and Natural Selection

Symmetry is more than obtaining aesthetic gratification from artwork; it might be emerging from natural selection [54, 221] that decides which species survive and which perish. The surviving predators must be very sensitive to bilateral gait asymmetries since that trait can reveal a pathological vulnerability that can help an attack [194].

The advent of animals with bilateral symmetry goes back more than five hundred million years [198, p. 215]. It has been established that in the world of animal mating, perfect bilateral symmetry is regarded as a sign of good health and superior genetic quality, and asymmetry is deemed as an evidence of vulnerability to parasitic infection [153, 145]. Therefore, bilateral symmetry serves as a determinant of

mate choice as well as a fitness indicator [145, 146, 117].

Symmetry also gives the conceivable fitness benefits to plants with symmetrical flowers, and influences their reproductive prospects. Pollinating insects have keen sensory biases for symmetry to discern subtle differences in the petals of a flower and prefer the most symmetric ones for good reason; the more symmetric the blossom gets, the more nectar it yields and the better a food source it comes to for pollinators [146]. As a result of more frequent visits from pollinators, symmetrical plants have more favorable opportunity to be pollinated or to pollinate other flowers than asymmetrical ones, which more often results in the fruition of a desire.

1.5 Symmetry in Physics

More often than not, symmetry, in physics, means that the laws of physics are independent of a frame of reference in space, time, and motions of an observer. Inherently, symmetry means conservation laws in physics. As first brought to notice by Emmy Noether, there is a connection between continuous symmetries and conservation laws [151], such as the principles of conservation of energy, and angular momentum. Momentum is conserved due to the invariance under spatial transformation (the isometry of space) and energy is conserved on account of time translational invariance (the isometry of time). Any feature (physical property) of the system that is invariant against certain continuous transformations is defined as a symmetry of the system.

There is another concept of symmetry conjectured by theoretical physicists

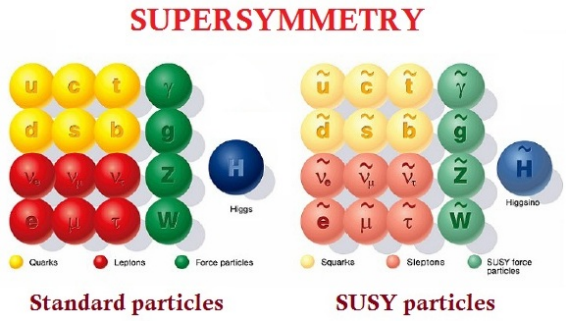

Figure 1.5: Every particle in the Standard Model has its "superpartner" particle awaiting to be found. (Illustration: CERN & I.E.S de SAR)

in the 1960s that can be consistently added to the symmetries of Einsteins theory: Supersymmetry (SUSY). The idea is that every type of elementary particle in nature has one or more twins (superpartners). Fermions (matter carrier particles. *e.g.*, electron) have bosons (force carrier particles. *e.g.*, photon) as superpartners, and vice versa (Figure 1.5). SUSY makes the unification of strong, weak, and electromagnetic forces in the Minimal Supersymmetric Standard Model (MSSM), and helps solve many problems in particle physics including the Hierarchy problem.

1.6 Approximate Symmetry and Global Information; Symmetry in Real Life.

In the face of scientific endeavors to find symmetries, the universe obstinately shows asymmetry at all levels, against the best efforts to make it otherwise. An archetypal example is human faces which are generally considered as "symmetric"; however, supplanting the left half of the image with a reflection of the right half we obtain an image which is not the same as that obtained by replacing the left half of

the image with the reflection of the right half.

After the lack of success of the Large Hadron Collider (LHC) to uncover superpartners and extra spatial dimensions, even the SUSY is considered to be "broken" or "approximate", and people established that the superpartners should all be heavier than their counterparts [240]. In the visual world, loss of exact symmetry is further enhanced; even perfectly symmetric objects loose their exact symmetry when projected onto the image plane or the retina.

The lack of perfect symmetry defined by mathematics of group theory, and the ability of human brain that readily perceives departures from perfect symmetry but still gives a feeling of the exactness make the field of computational symmetry extremely challenging.

In bridging the gap between a dichotomous definition of symmetry, to wit, everything that is not symmetric is asymmetric, and the great flexibility of human perception, the global information of an entire object becomes critically important because the deviation from the idealized perfect symmetry can only reliably be determined in conjunction with a symmetry that holds at all elements of the object under consideration.

Scientists who aim to solve the global symmetry are facing two grave adversities due to the nature of the problem. Firstly, we need to establish a threshold value while validating the global symmetry and the value can be an arbitrary constant which is hard to verify its veracity; how can we tell the approximate symmetry from asymmetry? The second is the time complexity of ascertaining the relative fitness for each candidate; all the elements should engage in the decision process.

1.7 Human Symmetry Perception

More than one hundred years ago, Mach attracted people by the fact that symmetry is a salient feature and a vertical symmetry is more easily noticeable than a horizontal symmetry [130, 56]. He also suggests that human do mental rotation/normalization to perceive symmetry and nature seems to be predisposed to prefer vertical symmetry by virtue of the force of gravity operating straight up and down (Gardner [68] also claims that the perfect spherical symmetry is broken by the vertical force of gravity). Since then there have been substantial number of nice reviews on human symmetry perception [212, 218, 217, 219, 229]. In this section, we focus on the bilateral symmetry that is the most salient type of symmetry [69] out of its family of isometries (others are rotational and translational symmetries[6]) and address the characteristics of human perception of symmetry ascertained by empirical observation.

1.7.1 Symmetry and Gestalt Principles

Gestalt psychology, like behaviorism, arose as a competition to the molecular approach of structuralism. It is founded on the idea that psychological behavior should be considered as unified wholes rather than a mere sum of individual parts and processes, so it clearly dissociates itself from reductionistic approaches that break psychological phenomena down into their smallest constituent part.

The Gestaltists are inclined to think symmetry as one of the "whole properties"

[6]sometimes they are called repetition and centric symmetry [219]

Figure 1.6: An example of the law of symmetry

(the other two are closure and equilibrium) that has a high level of goodness[7], and assume it as an important unit-forming factor in the perceptual grouping in human vision. For the Gestalt psychologists, symmetry signifies not just similarity of parts, but "the logical correctness of a part considered relative to the whole in which that part occurs" [53].

The main claim of Gestalt psychology is the human is inclined to shape visual stimuli into perceptual groups by a set of principles. According to the law of prägnanz, we have a tendency to reduce our experience into the simplest form with minimum cognitive effort. If more than one of the Gestalt laws are at work, they are either cooperating or competing. By the law of proximity, two pairs of square and curled brackets in Figure 1.6 should be grouped together considering they are in immediate proximity to each other. We, however, tend to detect three pairs of symmetrical brackets, as opposed to two asymmetrical pairs and two singles as the effect of symmetry prevails over proximity in this case. Although there actually exists a preponderance among the Gestalt laws for grouping, it still remains unclear if we could predict *a priori* which laws determine the configuration we see[8].

[7]The goodness is a general term for detectability, discriminability and insensitivity to noise [219]. Symmetry is deemed to have a high level of goodness for the reason that it can be detected fast, easily discriminated, and can be found in the middle of noise.

[8]This is the one of the reasons the Gestalt principles are criticized as rules of little more than

1.7.2 The Role of Symmetry

Symmetry serves an important role in providing balance and form to an object structure and its appearance. If grouped parts give rise to emergent features, *e.g.*, closure and symmetry, those features can give configural superiority effects to the whole shapes so that they become more distinguishable from the previously isolated contours [162, 171]. Symmetry is often called a local Gestalt glue[9] or perceptual glue that connects individual parts into unified whole forms. In summary, symmetry is a piece of information that informs which part of a pattern in a shape is related to another part of itself. If a pattern features symmetry, symmetry imposes structure on the pattern and groups the individual stimulus into a coherent whole, *e.g.*, the effect of symmetry on figure-ground segregation (Figure 1.7).

There is little doubt that symmetry is an all-pervasive property of a shape, acts as an one-object cue that signifies the presence of a single object, holds the attention for perceptual analysis, and the benefit of symmetry in artificial objects is apparent as it gives balance, stability and affordance to them [212], but does it provide any benefits for its detectors other than aesthetic enjoyment?

Other patterns are mainly used for identifying a given shape from the past memory and the main point in question is how to represent the relevant matching-pattern of objects in memory for the future retrieval. Symmetry perception, however, is a bit peculiar in that a memory of patterns is not necessary at all, and the

ceteris paribus [92]

[9] A recent study suggests symmetry detection is based on other grouping properties. Accordingly, a deficit in the integration of local orientation information can lead to severely impaired mirror symmetry detection. The Gestalt psychologists, still, suggest symmetry is a fundamental grouping property of perceptual organization.

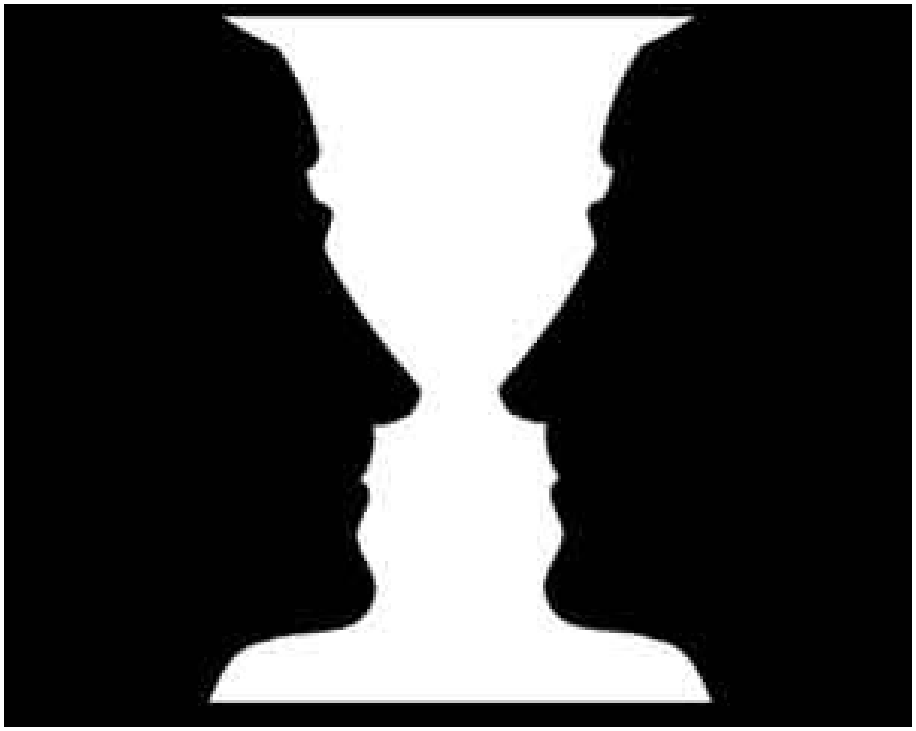

Figure 1.7: Rubin's vase: The force of symmetry on figure-Ground segregation. The perceptual distinction between figure and ground depends on how we relate borders to adjoining image regions in a scene. In this classic example, if we associate the contrast border between the black and white regions with the white region in the center, we perceive a goblet-shaped figure in front of a uniform black background. If we instead associate the border with the black region of the image, we perceive juxtaposed face-shaped figures in front of a uniform white background. Thus, we must decide which region corresponds to the closer, occluding surface that gave rise to the border *i.e.*, which region "owns" the border. Reproduced from Pettijohn

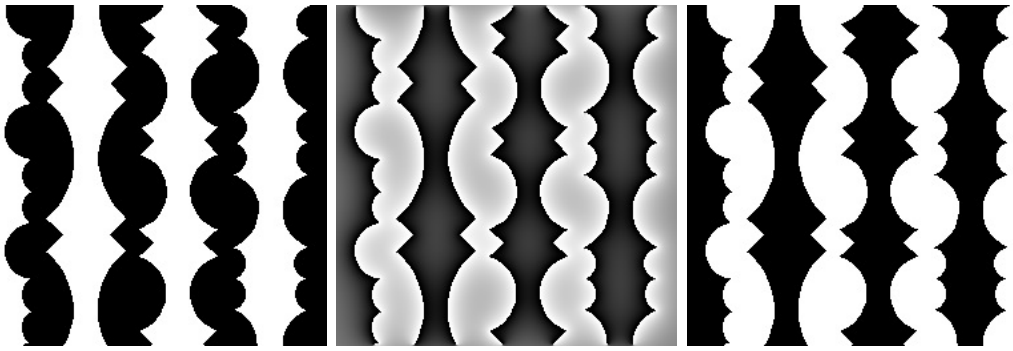

(a) (b) (c)

Figure 1.8: Figure-ground segregation does not depend on object recognition. Even in scenes such as this, which contain no recognizable objects, our visual system still demands a distinction between figure and ground. In psychophysics experiments using stimuli such as these, Gestalt psychologists observed that basic geometric properties of image regions-*e.g.*convexity or symmetry in the shapes of the regions' borders-guide our impressions of figure and ground. Over 92% of people notice the convex shapes as the figures and the concave ones as ground. Whether the convex shapes are black or white does not affect the decision. Reproduced from [97].

patterns to be compared are all presented contiguously in the same image.

1.7.3 Symmetry and Human Visual Attention

When spatial symmetry is brought into a scene, structural irregularity or complexity of the view is reduced, and the field of view becomes less informative than its asymmetric counterpart. That being so, the symmetrical view should receive less visual exploration and achieves less attention than asymmetrical scene. Yet we select the visual information we need in a more involved and sophisticated way than merely looking at information entropy of an image. It is well known that psychophysical thresholds for the shape detection would be decidedly lower when the given shape is symmetric than asymmetric [212]. During visual exploration this less arousal but more accessible, let alone its aesthetically pleasurable [156], feature catches the eye. Again, the detection of symmetry and subsequent physiological arousal seem to be mediated by global information [124].

We did not dismiss the idea that asymmetric entities could receive more visual exploration than symmetric bodies. Actually they do [123]. Figure 1.9 exhibits eye-movement records for symmetrical and asymmetrical shapes. Firstly, visual fixations and fixation time increase with stimulus complexity measured by the number of sides of the shape. It does not matter whether the shape is symmetric or not. Second, the number of fixations and their duration are symmetry-blind, too. But the fixation patterns for symmetrical and asymmetrical shapes are in stark contrast to each other. Symmetrical shapes display one-sided scanning patterns, while asymmetric

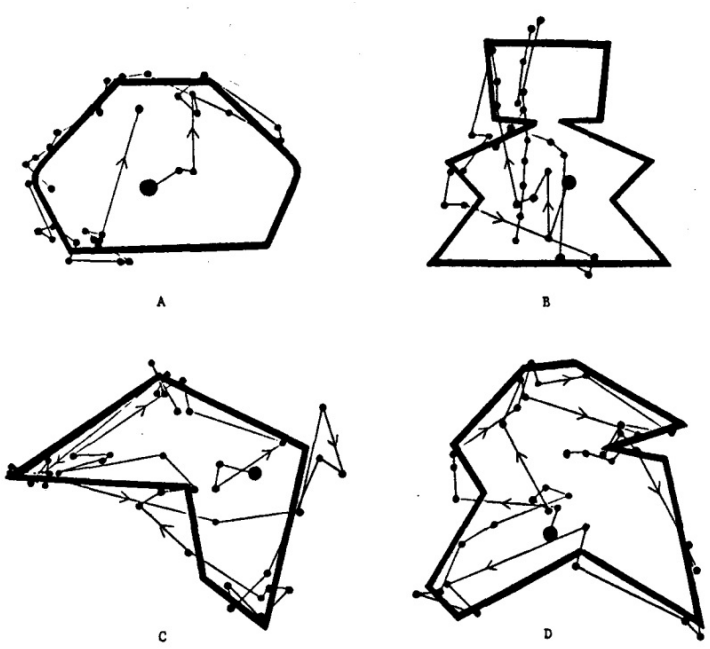

Figure 1.9: Eye-movement records for symmetrical and asymmetrical shapes with different complexity. Adapted from [123]

ones show two-sided patterns. If our visual system finds redundant shapes while moving eyes, there is no point in fixating those shapes.

For the purpose of this thesis, we mainly pay attention to the computational models of attention. For an extensive survey on models of visual attention, please refer to [60].

Since the computational power of the human brain is limited by the order of 10^{17} operations per second [168, 49, 71], only a small amount of visual information can be processed and utilized. Directing more attention to a selected stimulus leaves other visual input unattended (Winner-takes-it-all). There are two factors that drive visual attention by influencing the selectivity: bottom-up bias and top-down control [50]. Salient visual cues (stimulus salience) in the environment, such

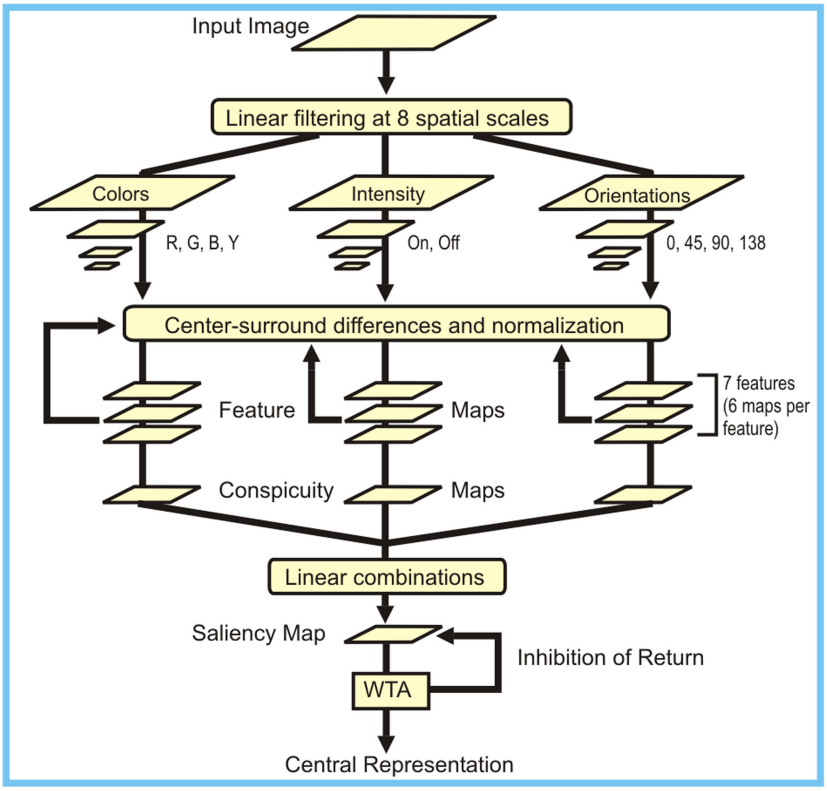

Figure 1.10: The control of bottom-up attention based on Koch and Ullman's hypothesis [102]. A centralized saliency map can provide an efficient control strategy for the deployment of attention. Adapted from [90, 91]

as bright colors, high contrast or fast motion contrasts, can introduce a bottom-up (target-independent) bias toward the stimulus (stimulus-driven) (Figure 1.10), while, in contrast, contextual target information derived from the requirement of a task guides top-down control (goal-driven) [150]. (This type of attention control is sometimes disapproved as being a failed theoretical dichotomy [7]).

In feature integration theory (FIT) [214], there are two stages of visual attention: a preattentive stage and an attentive stage. Preattentive vision functions in

a spatially parallel manner without attentional constraints (or attentional bottlenecks), while on the contrary attentive vision allocates attentional resources to the limited scope of the visual field where the visual target is likely to show itself. The finding of the existence or nonexistence of a primitive feature during visual search tasks is known to be irrespective of the number of stimuli (usually the number of elements in a given scene) [214]. Since the detection of primitive features takes place preattentively, the location of attention in the visual field is of little consequence.

This dichotomy was a departure from the Gestalt theory and restricted the preattentive stage to a single stimulus (primitive feature) dimension, *e.g.*, size, brightness, orientation, color, and direction of movement (later FIT had to include a master map of locations to reconcile results that reported highly efficient conjunction searches [149]). Detected primitive features are interacting with each other on their own dimension prior to conscious perception. When attention is focused at a particular location, the features in that position are attended to. During the first stage of FIT, the features of unattended entities do not bind (this can produce lots of false positives in the end). Therefore it is possible to detect the existence of interesting features without exact information of the location. In other words, the normal order of operation (attention to a location precedes identification of an interesting object) can be broken by separation of locating a feature from detecting it. FIT considers symmetry as a basic feature that can be used as a bounding condition that limits the candidate locations for the spotlight. As a response to the FIT, the Guided Search Model has been proposed [242]. In this model, parallel processes use information about primitive features to guide attention in the search

for conjunctions.

In 1985, Christof Koch and Shimon Ullman proposed a hypothesis based on bottom-up attention of FIT [102]. They claimed the set of early representations of individual visual features that contributes to selective attention is encoded into a topographically oriented map called the "Saliency map". It combines the normalized information from the feature maps into a comprehensive measure of conspicuity. In their hypothesis, similar to the center-surround representations, the bottom-up saliency of a given location is computed by a difference between the primitive feature and its surround at many different scales. The salient locations (usually the positions of the local maxima in the map) in the "Saliency map", accordingly, would be good candidates for attentional selection. This selection is done by a Winner-Take-All mechanism. Once the selection is drawn, inhibition of return mechanism[10] takes effect and the selection is shifted to the location of the next highest value in the saliency map. This process would keep going until no interesting point is left in the saliency map, and the trace of this selections frames the scan of the scene given. The diagram in Figure 1.10 is based on this hypothesis that a centralized saliency map provides an efficient control over the deployment of attention based on bottom-up biases. The saliency map is then examined by attention. Top-down control and training can fine-tune most stages of the bottom-up model.

[10] A mechanism that suppresses the last attended position in the saliency map, so that attention can shift to the next most salient location.

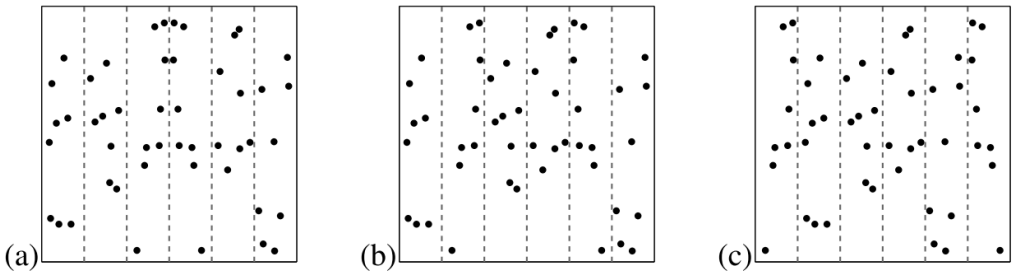

Figure 1.11: The effects of location on sensitivity of symmetry detection in a dot pattern. (a) Near the axis of symmetry. (b) Intermediate stripes. (c) Outermost stripes. Adapted from [212]

1.7.4 Outline versus Interior Area on Symmetry Detection

Most psychological research papers on symmetry [11, 94, 152] have dealt mainly with dot patterns or blobs which are not typical patterns to human observers. In the test of random-dot arrays, the outline is not required and has no effect on the decision of a symmetry axis whereas the area close to the axis of symmetry plays a major role in symmetry detection [11, 234]. The symmetric patterns located between the axis of the symmetry stripe and the outermost stripes (the intermediate stripes) are the hardest to detect (Figure 1.11).

1.7.5 Symmetry as a Preattentive Feature and Its Automatic Detection

We assume symmetry detection, just like grouping processes, is automatic, that is, it is not involving cognitive control, for the sake of its fast detection [11, 19] and its contribution to figure-ground segregation [10, 15, 243]. Yet is it preattentive

(automatic processes usually depend on attention[11])? Though there are supporting results [11, 14, 122, 230] that static symmetry can be detected preattentively with a duration[12] threshold of 40 msec[13] to help efficiently guide attention to relevant objects, and consistent with specific predictions from a simple feedforward processing model [61], the most recent study [37] shows its detection is not always rapid (varied from 28–568 msec) and suggests a strong dependence on the context. Again, symmetry detection is rapid and highly accurate on a simple stimulus, however, attention seems to play an important part in symmetry perception [154, 233].

On initial consideration, it is surprising that symmetry is a preattentive feature considering its perceptual complexity of relating different kinds of spatial information (locations and angles; both cues do not belong to a single stimulus component) around an axis. The human visual system is not able to catch much simpler conjunctions (relating single stimulus to others) without applying proper attention [214, 213]. If symmetry detection happens in the fast and parallel preattentive stage, it should not require a time-costly computation, *i.e.*, through a computationally intensive point-by-point comparison of visual cues across the axis.

All in all, it is plausible that symmetry is a preattentive feature that distinguishes one region from the other but that explicit symmetry information would not be delivered to the higher systems without attention [154]. Accordingly, static symmetry should be located quickly during preattentive perception in a coarsely

[11]there is another hypothesis objects this assertion citing inattention blindness is just inattention amnesia or a lack of awareness; still not detectable

[12]time of stimulus exposure

[13]the maximum limit of preattentive perception is less than 160 msec.; a time period that does not allow attentional scan by eye movements.

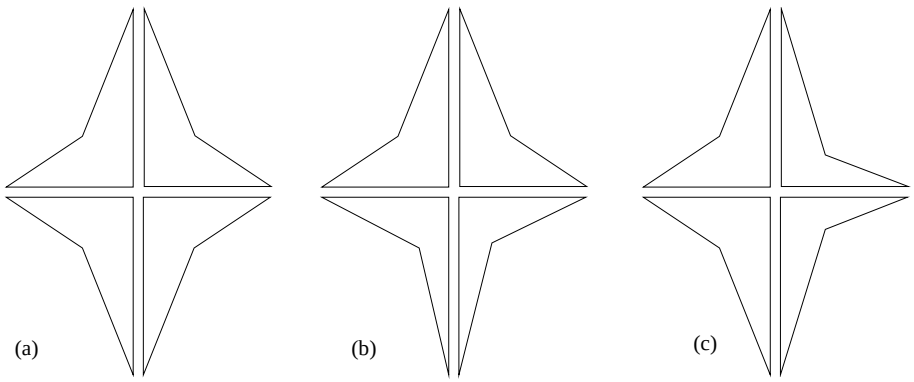

Figure 1.12: An experiment on the orientation of symmetry. Adapted from [247]

manner, and immediately afterward more scrutinous and detailed exploration on that attended region would be carried out. The two-phase symmetry detection scheme described above is the main proposition of this thesis.

1.7.6 Anisotropicity of Symmetry

Figure 1.12 shows that patterns deformed so that vertical symmetry is preserved (though horizontal symmetry is destroyed) are more similar to the original than the same pattern deformed so that horizontal symmetry is maintained (vertical symmetry is broken).

In measures of preference, symmetries along the vertical seem to have a perceptual advantage over other symmetries, because they are congruent with the bilateral shape of the visual system [159, 235]. Studies on the anisotropy of symmetry failed to show identical or consistent results, however, vertical and horizontal show strong saliences over obliques (Figure 1.13), and this advantage might stem from retinal

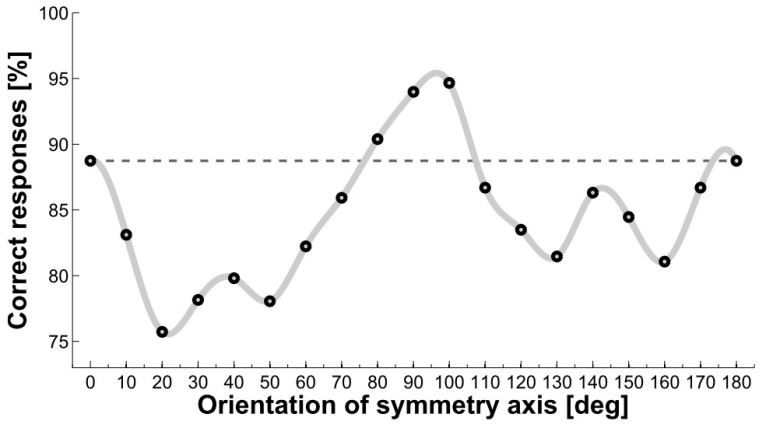

Figure 1.13: Sensitivity to symmetry as a function of the orientation. Adapted from [212]

coordinates.

On structural grounds, nonvertical symmetries would be found only after they are mentally aligned to the anatomical vertical [41] (A mental rotation model. See Section 1.7.11), and response time to determine symmetry would be increased linearly with increasing angular displacement from gravitational vertical.

Foveation of the symmetry axis is not an essential condition for its detection, yet detectability drops considerably with deviation from the center [191].

1.7.7 Symmetry in 3D

First, it can be argued that symmetry detection solely depends on the retinal image, or it is affected by the perception of objects. When viewers are given randomly created asymmetric 2D images, they get a bias that takes asymmetric retinal projections as oblique views of symmetrical objects (Figure 1.14). As a result, they

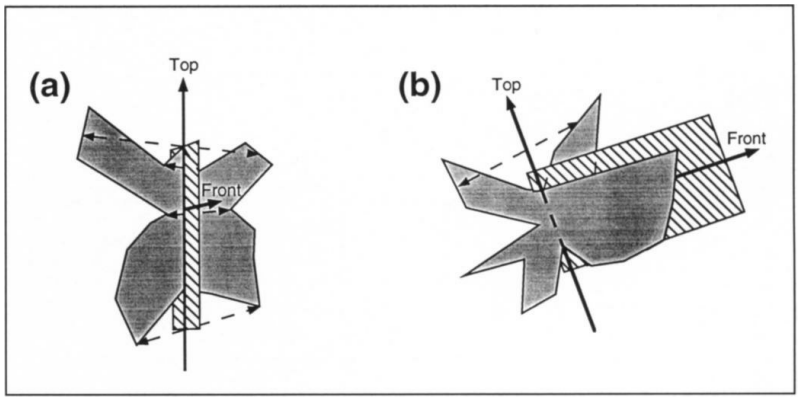

Figure 1.14: Interpreted axes of symmetry from silhouettes. Viewers consider the polygons as silhouettes that have a near-vertical axis of symmetry. The dotted arrows show conceptually interpreted matching parts. (a) Near symmetric figures result in planes of symmetry perpendicular to the picture plane, (b) Near asymmetric figures result in planes of symmetry parallel to the picture plane. Adapted from [138]

universally construe the shapes as silhouettes of bilaterally symmetric 3D objects because 3D symmetry can be a strong heuristic for limiting orientation [138].

It could be possible that human visual system selects 3D cues, determines the 3D orientation of the shape, mentally rotates the images to the fronto-parallel plane, and detects symmetry in it (use the mentally rotated image rather than the retinal image) [207]. However the drops in performance observed in [223] can not be explained by this hypothesis.

If the symmetry in the retinal image is deteriorated, its perceptual salience is also weakened (symmetry detection is not obstructed when an image is rotated about the x-axis but it is severely hampered by rotations about the y-axis). The data from [223] implies the visual system analyzes the retinal projections of 3D rotated symmetries as an integral part of 3D object perception; not as a post-normalization

process.

1.7.8 Symmetry Effect and Asymmetry Effect

It is well known that if the deviation from exact symmetry is not too huge, approximate symmetry can still convey the visual impression of symmetry [11]. The mechanism of symmetry detection is not highly accurate and symmetry perception becomes less sensitive when the location of the axis is not central [81].

The assumption of symmetry effect is that forms with high degree of symmetry would be so exaggerated by perceivers that the forms are considered more symmetric than they actually are [65]. This is a bias in detecting global symmetry and a small local departure from global symmetry is not noticeable for cost-effective representations of stimuli. A nearly symmetric form is found more similar to (or more confusable with) a more symmetric pick than to a less symmetric choice: Symmetry effect. (Figure 1.15)

The disposition to the more symmetric form prevails only in highly symmetric conditions. In low symmetric conditions, an asymmetric alternative is chosen: Asymmetry effect.

By the holographic model (Section 1.7.9.2), these effects are not induced by an erroneous assessment of the degree of symmetry, rather by a correct estimate of the symmetry-to-noise ratio [48].

Figure 1.15: Tripartite comparison of a pedestal's imperfect symmetry (upper) with a more symmetrical object (down-left) and a less symmetrical object (down-right). The task is deciding which of the two targets at bottom is more similar to the pedestal at top. Adapted from [65]

1.7.9 Representational Models of Symmetry Detection

Representational models try to detect visual regularities from stimulus elements by specifying the structures and geometric relationships between them.

1.7.9.1 Transformational Approach(TA)

TA takes symmetries as one of visual regularities that leaves its configuration invariant under reflection. It claims the human visual system is sensitive to these kinds of invariant group transformations, *e.g.*, translation, rotation and reflection [158]. But TA could not explain why symmetry (reflection) is more salient than repetition (translation).

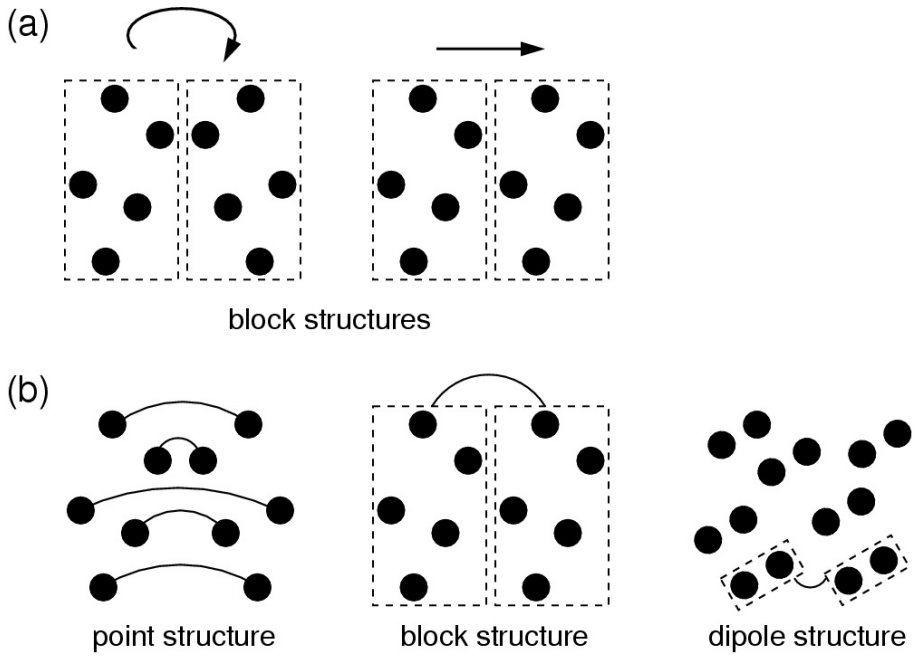

Figure 1.16: (a) The transformational approach (invariance under motion); it puts a block structure to symmetry (left) and repetition (middle), because the whole symmetry halves and the all duplicates are the units associated with each other. (b) The holographic approach (invariance under growth); it gives a point structure to symmetry, a block structure to repetition, and a dipole structure to Glass patterns (right), because corresponding pairs, blocks, and dipoles are the units that can be stretched out while preserving the regularity of the structure in them. Adapted from [222]

1.7.9.2 Holographic Approach(HA)

HA is about goodness [219], *i.e.*, the detectability of regularities and nested regularities regardless of noise, and unlike TA's invariance under motion, HA is about invariance under growth.

According to HA, bilateral symmetries have a point structure, and repetitions a block structure that can be used to quantify the goodness of a regularity by the weight of evidence. (Figure 1.16)

1.7.10 Scale Invariance

When we are trying to gauge the strength of symmetry stimuli, there are numerous candidates: peak spatial frequency that covers the symmetry integration region, numerosity (number of elements), element density (number of elements per unit area), or display size. Interestingly, the results of the experiment manifest that the spatial integration region, a place integrates information, for symmetry is unaffected by changes in stimulus spatial frequency, numerosity, or size [178]. That is, the amount of information garnered from a stimulus is constant against size, number of elements and spatial frequency.

1.7.11 Template Model and Mental Rotation Model

There are 2 descriptive models of the perceptual reference frames (similar to [40] in object perception) in the context of symmetry perception:

- Template model - There is a template for each angle of symmetry axis that detects the symmetry in a pattern (Orientation-dependent).
- Mental rotation model - There is a single mechanism to detect symmetry and all other reflective symmetries are detected by mentally rotating the shape to align it's vertical symmetry axis (Object-centered).

Several experiments were done to test these two models, however, the results are still open to interpretation. Zabrodsky [247] claims that there is more than one strategy for symmetry detection on the basis of conflicting results.

1.7.12 Symmetry Detection Can Be Learned?

The controversy over whether the symmetry detection is innate or learned often gets answered with "It is somewhere in between"; Infants discriminate vertically symmetric forms from asymmetrical ones (or horizontally symmetrical ones), which validates sensitivity to the symmetrical pattern rather than components in the pattern [63, 172]. This finding corroborates the claim that symmetry has a prevailing position in early perceptual development over other perceptual components and that newborns tend to perceive a pattern as a whole. Zabrodsky [247] argues symmetry detection has some initial bases in anatomical and physiological mechanisms, however, is fine-tuned by our experience and learning.

1.7.13 Structure-From-Motion (SfM) and Symmetry in 3D Representation

One of the important task of the visual system is to institute a 3D representation from the visual stimuli affecting the retina. To achieve this goal, it utilizes many depth cues including but not limited to shading, texture gradients, and motion. Out of those cues, the kinetic depth effect known as structure-from-motion (SfM) can elicit strong volumetric perception [26].

Symmetry, a strong one-object cue, can give a structural cue to this 3D representation because conceptual thresholds for shape detection become much lower when the shape considered is symmetric than asymmetric [212].

A study on the relation between symmetry and SfM found that at the level of

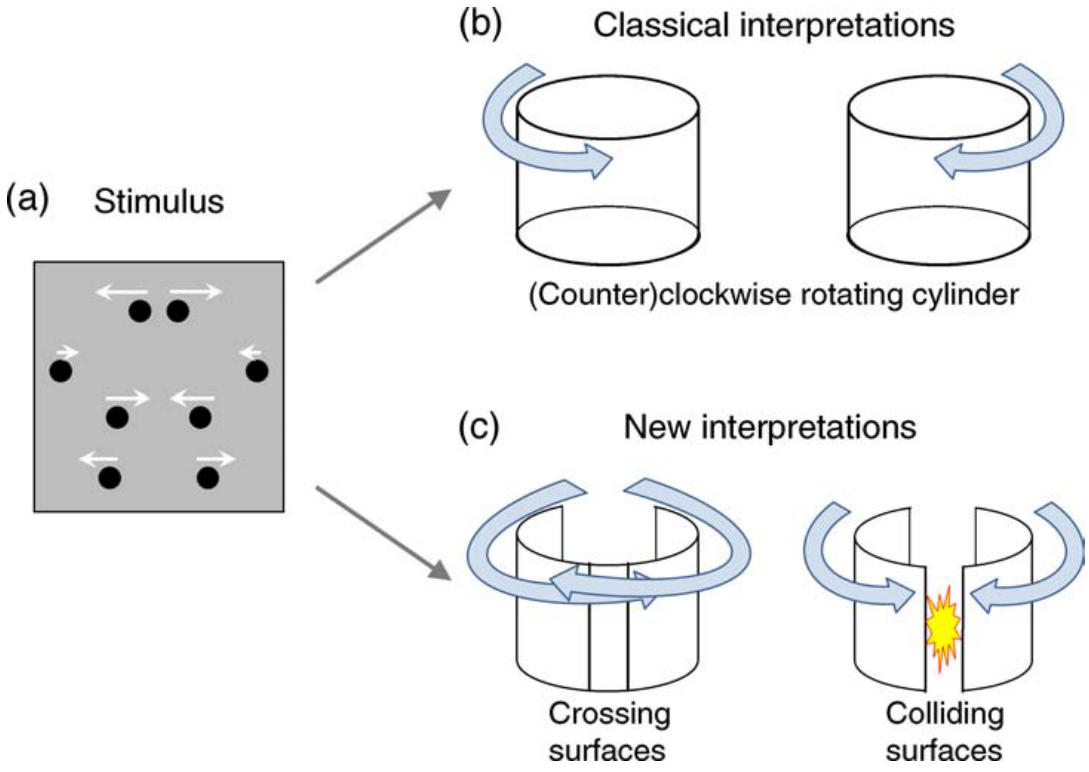

Figure 1.17: Conflicting perceptual interpretations of a symmetric motion. (a) Scheme of the vertically symmetrical stimulus, (b) Interpretations of a rotating cylinder, and (c) Symmetric surfaces either crossing or colliding each other. Adapted from [211]

surface perception the perceptual competition between the symmetric surfaces and the rotating cylinder surface is resolved [211]. According to these results, SfM is regarded as an interactive process, which subsumes not only motion cues but also form cues, *i.e.*, symmetry (Figure 1.17, 1.18, 1.19).

1.7.14 Symmetry Related Brain Parts

A functional MRI (fMRI) experiment shows robust activity of higher-order regions of human visual cortex (areas V3A, V4, V7, and LO) associated with the

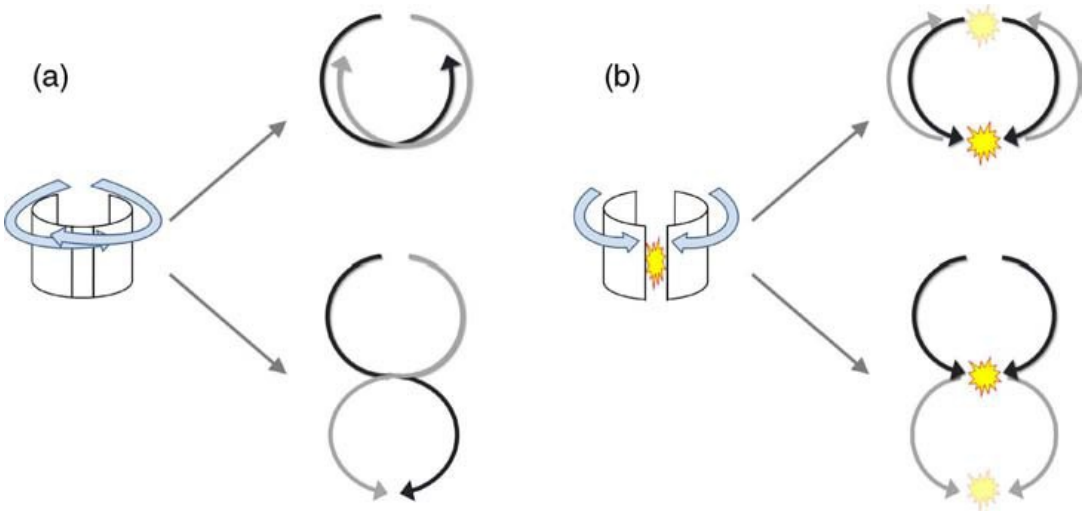

Figure 1.18: Four possible interpretations of the motion direction of symmetry surfaces. (a) and (b): For both crossing surfaces or colliding surfaces, either the two surfaces rotate at fixed position (upper) or wind toward the observer without touching physically. Adapted from [211]

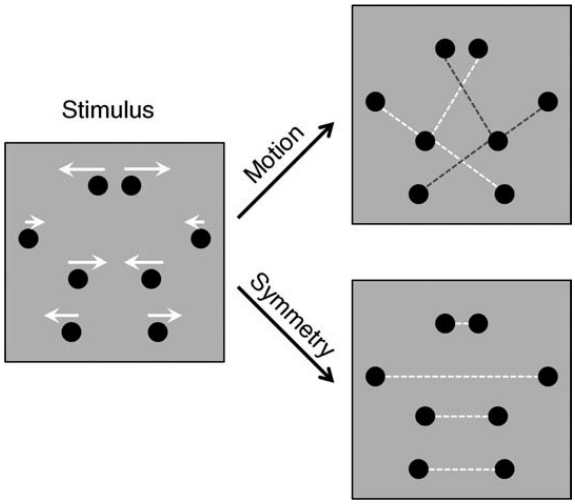

Figure 1.19: Competition between grouping by motion (common fate) and grouping by symmetry. The perceptual choice decides the depth difference between the groups. Adapted from [211]

visual exposure (both with and without attention control) to symmetric stimuli (Especially, V3A and LOC are known for the designated region for feature integration) but no meaningful symmetry-specific reaction in MT/V5 (regions for surface interpolation) [194]. The dot (not line) stimuli might induce the lack of robust activity in V1 and V2.

Against symmetric dot stimuli, symmetry axes manifest the same tilt-aftereffects as luminance-defined contours [224]. Judging from these results, similar mechanisms might support the encoding of symmetry as well as the orientation. This result is in agreement with studies [179, 178] that indicate the concurrent processing of symmetry perception at various spatial scales and for different orientations, implying that simple filters in V1 [14] could be involved in symmetry perception.

1.7.15 Some Interesting Factoids

There are some interesting factoids based on evolutionary theory about the relationships between symmetry and human behavior on attractiveness [227].

- Departures from symmetry mirror an individual's inability to keep developmental homeostasis [163].
- Predilection for a symmetrical mate is an evolutionary adaptation for the positive genetic effects on offspring survival not due to perceptual preference [70].
- Facial symmetry is more susceptible to environmental perturbations [70].

[14] Clusters of neurons in V1 and V2 respond to bars of specific orientations, or combinations of bars in a selective manner. These orientation selective neurons in area V1 respond to a line segment of a particular orientation in a specific visual area.

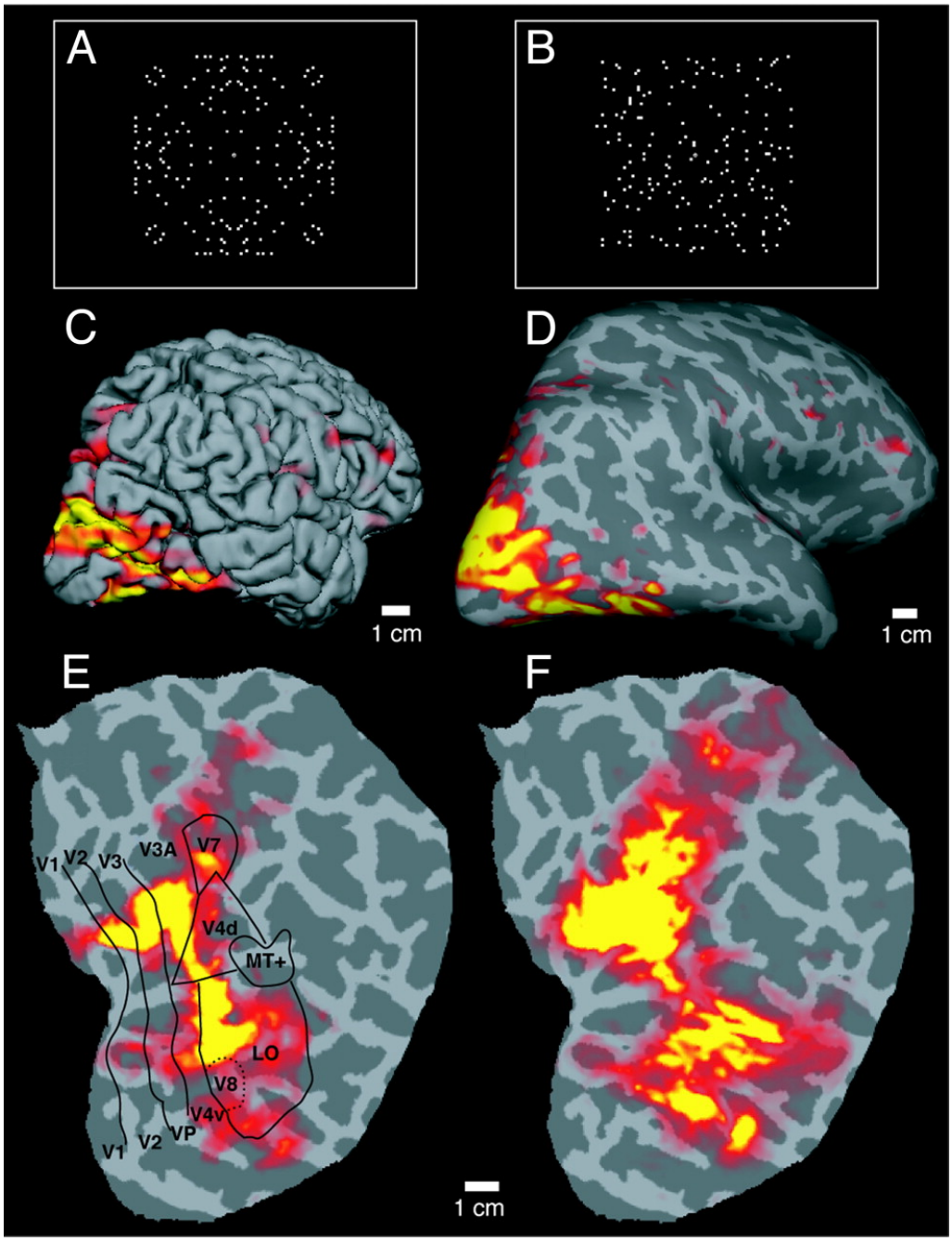

Figure 1.20: Brain activation caused by symmetric patterns. (A), (B) Example of the dot stimuli. (C) Brain activation in the right hemisphere (posterior-lateral view), (D) The "inflated" cortex format. (E) Symmetry-biased activation in the "flattened" cortex format, (F) Average symmetry-biased activation. Adapted from [194].

- Men and women look more attractive when their faces and bodies are close to symmetrical [13, 165]; the attractiveness of symmetry is cross-cultural/cross-racial agreement [183]. However, several recent studies have shown that symmetry is not a principal factor in an attractiveness assessment [251] and functionally asymmetrical faces can be perceived as attractive [250].

- Facial symmetry serves as a certificate of health in regard to mate potential [13].

- Higher symmetry induce greater procreative potentiality [29].

- Female breast symmetry takes part in mate choice related adaptations since it is linked to best care for children [228]. Women with symmetrical breasts have more children.

- Men who use breast symmetry as a cue for mate selection would gain a selective advantage concerning reproductive success because breast symmetry is hereditary and their daughters should be subjected to greater mating success and fertility [147].

- Men with pleasing voices have broader shoulders and women with beautiful voices have hourglass figures [88]. As symmetry grows, ratings of vocal attractiveness increase [87].

- Symmetrical men are deemed as better protectors of their mates [66].

- Symmetry is associated with cognitive ability [12].

- Low facial asymmetry men are more likely to commit adultery [66].
- The overall symmetry can predict the lifetime number of sexual partners and extra-pair copulations (EPCs) [208].
- Faster middle distance runners have more symmetrical ears and openings of the nose than slower runners [131].
- Symmetrical men were considered as better dancers than asymmetrical men and dance is a sexually selected courtship signal [27].
- Men and women with more symmetrical faces are more extroverted [174].
- Psychopathic individuals have greater symmetry than non-psychopathic individuals [180].
- Alcohol intoxication reduces detection of asymmetry, increases perceptions of facial attractiveness [202].
- Although the outline of bilateral symmetrical dot patterns participate in symmetry detection, the elimination of the outline by a surrounding random-dot figure merely diminishes the performance by a fixed measure [234].
- Monocular symmetry is neither necessary nor sufficient for bilateral symmetry perception [236].
- The mechanisms of symmetry perception are inherently color-blind [148].

1.8 Applications of Symmetry

1.8.1 Symmetry and Multimedia Searching

With an explosive growth in the number of digital images and videos in the world, content-based video/image retrieval (CBIR) has been an active topic of vision research [76, 77, 210]. Regrettably, to the best of our knowledge, up until now there is no commercial CBIR search engines that explicitly label or search symmetric contents. We speculate that computationally expensive algorithms of current state-of-the-art detection methods might conjure a strong barrier that thwarts employing symmetry constraints.

1.8.2 Robotics, Image Compression

RoboCup is an international robotics competition founded in 1997 with an aim to promote robotics and AI research. To enable a soccer robot to navigate a RoboCup soccer field efficiently, symmetry detection methods were employed to gather the location information (especially the lines) of the field [82].

Theoretically, one symmetry axis can reduce the amount of information needed to be coded by half. For example, a perfect circle can be compressed to one single line. Symmetry can be used to increase the efficiency of medical image compression [192] (improvement of 15%), or natural image compression [160].

1.8.3 Symmetry and Its Underutilization

Symmetry is a rich source of structural information in images. Despite its intuitive appeal as an essential and ubiquitous concept in nature, symmetry, more specifically global symmetry, has been underutilized in computer vision. Some researches [77, 205, 210] adopted a local-symmetry-structure based approach [181, 126] on applications where limited symmetry information on the overall shape would not be much helpful, while a great portion of researches that can benefit from symmetry just have disregarded it.

One of the possible causes for the underutilization is that symmetry is not the only cue that encodes shape information through the relations between features, besides it is obtained at relatively high expense of computational cost; the high computational cost of symmetry detection makes it extremely unattractive to applications that involve fast merging of very large volumes of images. An incidence relation among points and lines, for example, may also provide enough information to describe the underlying shapes of objects. The high computational complexity of symmetry detection arise from a global exploration of the search space, whereas the other cues can be obtained from local information.

A mathematical representation of symmetry also casts doubts on the usefulness of symmetry. By the mathematical definition of symmetry, it is a binary feature of an object; an object is either symmetric or not. Yet the symmetry around us rarely follows the strict definition of mathematics, and all sorts of errors and inaccuracies in measurements lead to the conclusion that "everything is anything but symmetric".

Chapter 2

Symmetry Detection in Computational Models: Previous Approaches

2.1 Introduction

Automatic detection of symmetry embedded in digital images has long been pursued by many scientists, yet we are still, after decades of effort, baffled by the lack of efficient and robust algorithms applicable to a wide range of problems from computer generated images to natural scene images. For instance, we are having a multitude of edge or corner (both are considered as preattentive features) detectors [252] or operators for edge/corner detection, *e.g.*, Prewitt, Sobel, Kirsch, Harris and Stephens, Laplacian of Gaussian (LoG) and difference of Gaussians (DoG), however, the only bilateral symmetry detector whose standing is roughly commensurate with the reputation of those edge/corner detectors is a Generalized Symmetry Transform (GST) [181].

In this chapter, we selectively review some of the prominent algorithms for (mostly bilateral) symmetry detection and briefly put forward several enhanced algorithms we developed based on the existing algorithms. A more detailed and in-depth comparison between a qualitative approach and a quantitative method is given in Section 3.1.

2.2 Previous Work by Other Researchers

2.2.1 Generalized Symmetry Transform (GST)

This point of interest operator [181] is a typical isotropic symmetry detector that extracts local symmetry based on spatial positions and gradient information. This operator compares the gradients of two adjacent points and assigns a value to the midpoint between them in a symmetry map. This process can be implemented as range voting (cardinal ratings or ratings summation) or plurality voting (first-past-the-post voting) [181, 126]. If you keep track of the voting record and double back on the points after voting, the result would be very similar to segmentation by symmetry (see Figure 2.22). Because the symmetry found is dependent only on the points voted to it, this approach is less adversely affected by background noise or other independent symmetry structures around it. The value assigned to the midpoint location in the symmetry map is controlled by a phase function that favors symmetrically oriented gradients. The resulting symmetry map can be interpreted as a map of interesting points (Figure 2.1). Various modified versions of the GST also have been suggested in 2D [113, 114, 112] and 3D applications [144].

Each list of elements in the set of point-pairs $\Gamma(p)$ has a distance weight func-

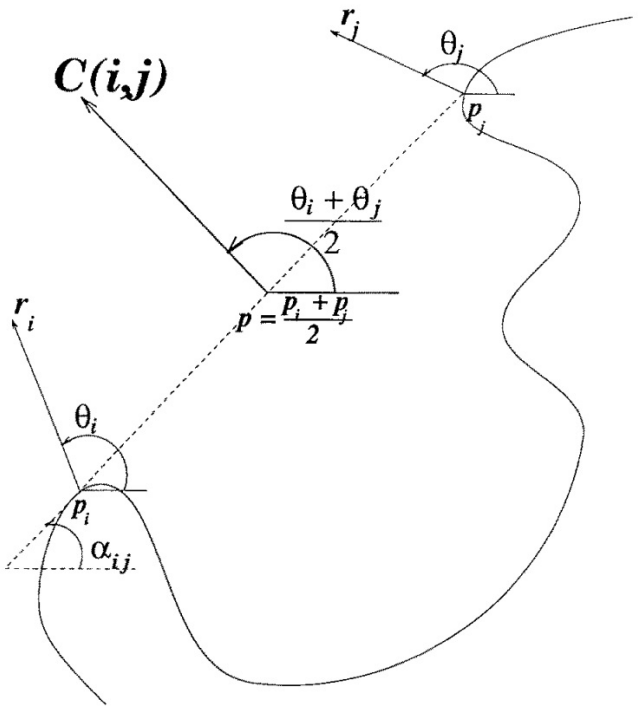

Figure 2.1: The contribution to symmetry of the gradients at p_i and p_j in [181].

tion $D_\sigma(i,j)$ and a phase weight function $P(i,j)$ such that

$$\Gamma(p) = \left\{ (i,j) | \frac{p_i + p_j}{2} = p \right\},$$

$$D_\sigma(i,j) = \frac{1}{\sqrt{2\pi}\sigma} e^{-\frac{||p_i - p_j||}{2\sigma}},$$

$$P(i,j) = (1 - cos(\theta_i + \theta_j - 2\alpha_{ij}))(1 - cos(\theta_i - \theta_j)),$$

where θ_i is the gradient of the intensity at point p_i. The term $(1 - cos(\theta_i + \theta_j - 2\alpha_{ij}))$ in the phase weight function $P(i,j)$ implies the constraint that a line connecting a pair of bilaterally symmetric points should be perpendicular to the axis of symmetry. The other term $(1 - cos(\theta_i - \theta_j))$ favors a pair of gradients with opposite directions and handicaps vectors with the same direction.

With these functions, the contribution function $C(i,j)$ of the points p_i and p_j is defined as

$$C(i,j) = D_\sigma(i,j)\ P(i,j)\ r_i\, r_j,$$

where r_k is a logarithmic function of the pixel p_k's gradient intensity,

$$r_k = log(1 + \|\nabla p_k\|).$$

The contributions of all points features the symmetry magnitude M_σ of each point

p such that

$$M_\sigma(p) = \sum_{(i,j)\in\Gamma(p)} C(i,j)$$

that adds up the symmetry value over all orientations. The direction of the contribution of the points p_i and p_j is specified (Figure:2.1) as

$$\varphi(i,j) = \frac{\theta_i + \theta_j}{2}$$

The symmetry direction of the point p, $\phi(p)$, is defined as

$$p_{maxDir} = \{(a,b) | \arg\max_{(i,j)\in\Gamma(p)} C(i,j)\},$$

$$\phi(p) = \varphi(x,y),$$

where $(x,y) = p_{maxDir.}$

Finally, the symmetry of the point p, $S_\sigma(p)$, is stated as

$$S_\sigma(p) = (M_\sigma(p), \phi(p)).$$

This operator is based on a simple and straightforward algorithm and often criticized for its high computational cost, $O(n^2)$, where n is the number of feature points in the input scene image. The framework of this algorithm is very close to *smoothed local symmetries* (SLS) [25] that provides a way of describing a 2D shape through image gradient based local symmetries (Figure 2.2). The definition

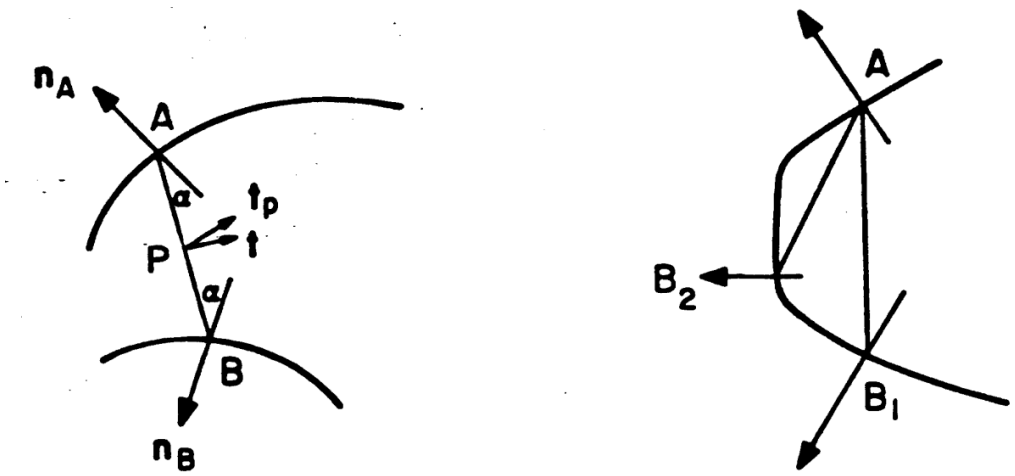

Figure 2.2: The geometry of local symmetries in SLS. Adapted from [25]

of local symmetry in SLS is virtually identical, a bit stricter, to the GST, they both depend heavily on the accuracy of the tangent angle computed by Canny [30] like edge detector, and even the time complexity of SLS, $O(n^2)$, is the same as that of the GST because SLS also tests every contour point against every other (n is the number of contour points).

This approach mainly deals with perfect or nearly perfect symmetry and even a small perturbation of the image edge or image deformation by perspective distortion can result in incorrect outcomes. Besides, each pair of points in the image votes to a center of them, not to the best candidate for the symmetry axis; strong local disruptions might disproportionately affect the result.

In an effort to improve the performance of the GST, several attempts have been made to reduce the n in $O(n^2)$. Instead of random sampling of points, as in [144], an improved version of the GST [126] takes a scale-invariant feature detector such as SIFT [125] ($p_i = (x_i, y_i, \phi, s_i)$ is a point feature contains its location, orientation

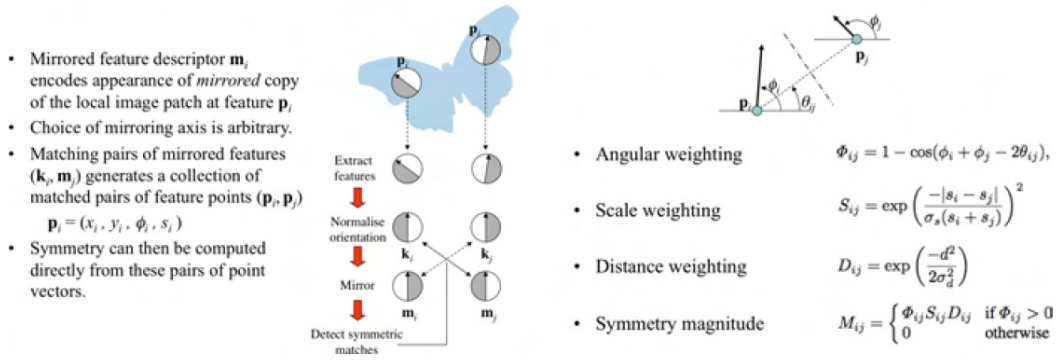

Figure 2.3: An improved version of the GST [126]. Adapted from [121]

and scale information) and uses its descriptor (k_i is the 128-dimensional vector that describes the appearance of the image patch) (see Figure 2.3).

The predominant orientation is retrieved from the maximum of the histogram of gradient orientations (8 bins are used to quantize the orientations, and their histogram values are quadratically interpolated) and the mirrored version (m_i) of its descriptor (k_i) is also made. The symmetry magnitude for each matched pair of SIFT features (M_{ij}) is mainly decided by the phase weighting function, and the polar coordinates of the potential axis of symmetry are pre-computed from Cartesian coordinates. It also relaxes the constraint on the symmetry diameter to measure a symmetry magnitude and can get much reliable information on symmetry direction (the GST does not vote for a symmetry direction but for a midpoint) by voting in Hough space (Figure 2.4). By virtue of the voting in (r, θ) space, the distance between the feature points are obscured and the fixation tendencies based on symmetry magnitude also become indistinct. Despite the fact that the computational complexity of this method is $T(n) = O(n^2)$ as in the GST, the

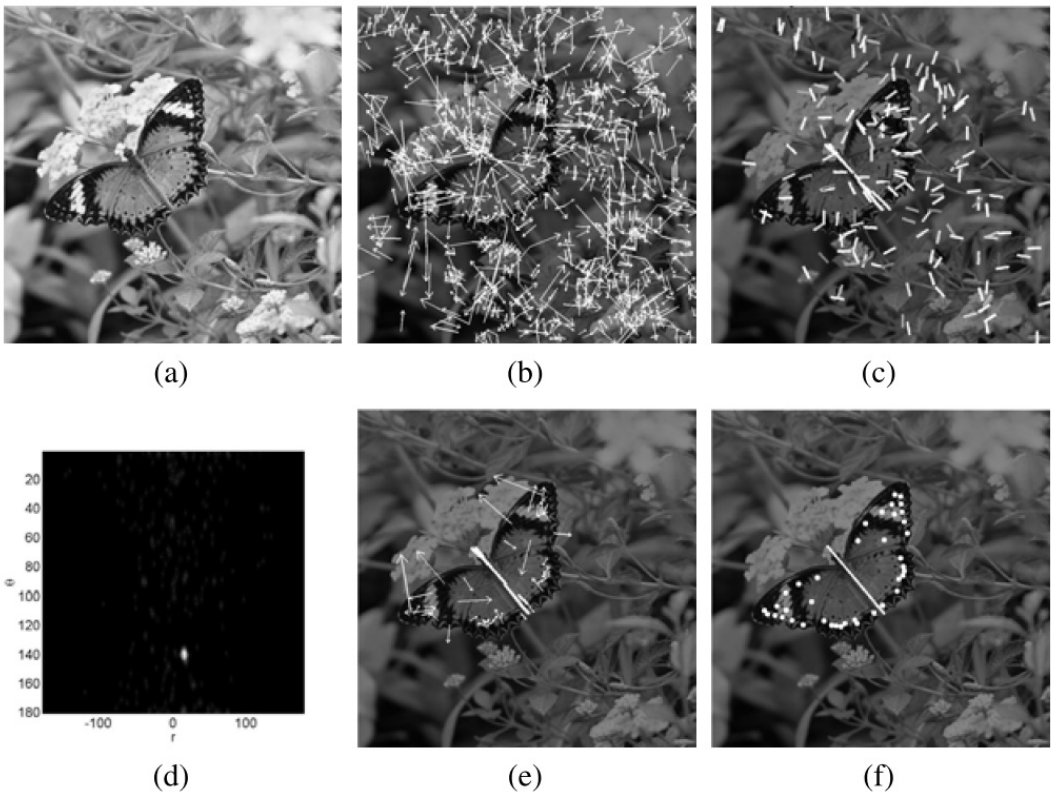

Figure 2.4: An example of detection result by the improved version of the GST [126]. (a) Input image; (b) SIFT feature points detected; (c) Axes of symmetries related to the reflective matches among SIFT feature points. M_{ij} decides the intensity in (d) Voting results on the potential symmetry axes in Hough space; (e) Matched symmetric features linked to the dominant symmetry axis; (f) Principal axis of symmetry and its symmetric features that voted for the axis. Adapted from [126]

absolute number of comparisons is claimed to be significantly reduced, because n, the number of feature points, becomes smaller.

According to a recent research study on the performance evaluation of symmetry detectors [161] and a result of the first symmetry detection competition [89], the improved version of the GST [126] was found the best algorithm. We choose this algorithm for performance-comparison of symmetry detection since it has proven to

be the best among all the other detection methods. We also raise two important questions about this approach:

- Are the scale-invariant features salient features for symmetry detection?
- Does this algorithm decrease the computational burden across the board?

The first question is about whether it provides necessary and sufficient information to find an axis of symmetry. The second is about the subquadratic-time algorithm of this approach as the dimension of the descriptor (SIFT descriptor is a 128-dimensional vector) can be an issue even with the Best-Bin-First (BBF) search method[1].

2.2.2 Radial Symmetry Detection

This approach uses either the gradient of an image [127] or curvature of circular shapes and responses of oriented filters [170] to locate points of high radial (co-circular) symmetry. The radial symmetry is most common in flowering plants and more constrained than bilateral symmetry. Although radial symmetry is not considered in this thesis, we are still able to combine this algorithm with the point of interest detector discussed later (Chapter 4).

The algorithm is quite simple and fast since it operates at a pair of equidistant locations along the image gradient $\mathbf{g(p)}$ where $\mathbf{p}$ is a point in an image (Figure 2.5). The radial symmetry contribution is calculated by multiplying a normalized *orientation projection image* O_n that counts the number of points that positively/negatively

[1]SIFT descriptors with lower dimensionality do not perform well

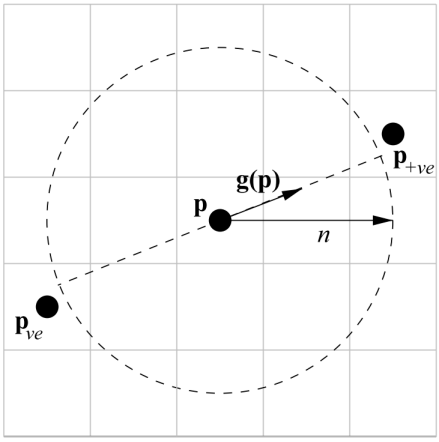

Figure 2.5: A pair of locations $p_{+ve}(p)$ and $p_{-ve}(p)$ is affected by the gradient information $\mathbf{g(p)}$ for a range of 2. Adapted from [127]

affects $\mathbf{p}$ with their gradients by a normalized *magnitude projection image* M_n that accumulates the gradients that influence $\mathbf{p}$. The full transformation is the sum of the contributions made during the previous step.

The time complexity this algorithm is $O(KN)$ for an image of N pixels with $K \times K$ neighborhood structure.

2.2.3 Symmetry Detection by Phase Relation

The symmetry detection of this model [157] is based on the phase relationships of frequency components. Since the filter kernels are either symmetric or antisymmetric, they encode spatial frequencies, such that if the harmonics are in phase at zero crossing, an edge is detected and if phase congruence happens at peaks or troughs, a line is detected. In a perfectly symmetrical patch, the model put the pixels where frequency components are at their extrema on the axes of

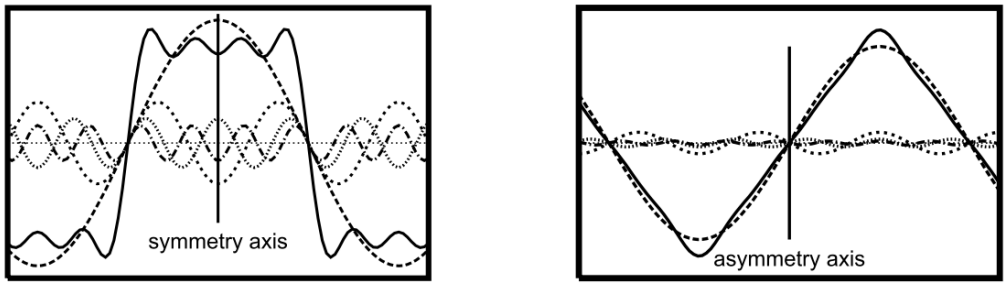

Figure 2.6: Phase patterns at symmetric point and antisymmetric point. Adapted from [105]

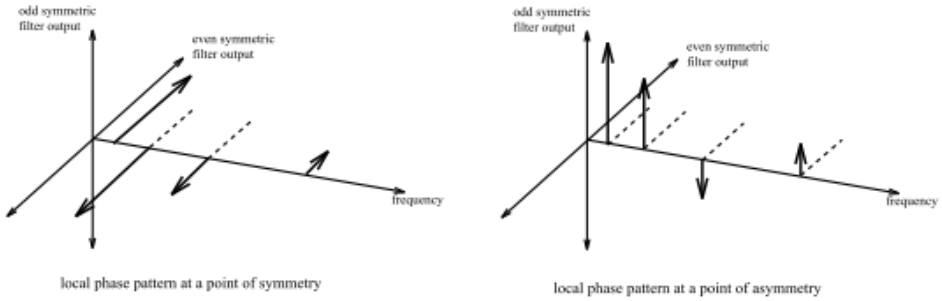

Figure 2.7: The local phase pattern would be that even-symmetric filters will respond to a symmetric point, and odd-symmetric filters to a asymmetric point. Adapted from [105]

symmetry (Figure 2.6). More intuitively, at a symmetric point the absolute output value of the even-symmetric filter would be large and the absolute output value of the odd-symmetric filter would be small (Figure 2.7). Because asymmetries reduce the phase congruency, the model has an inherent bias to perfect symmetry and asymmetry makes axes less detectable.

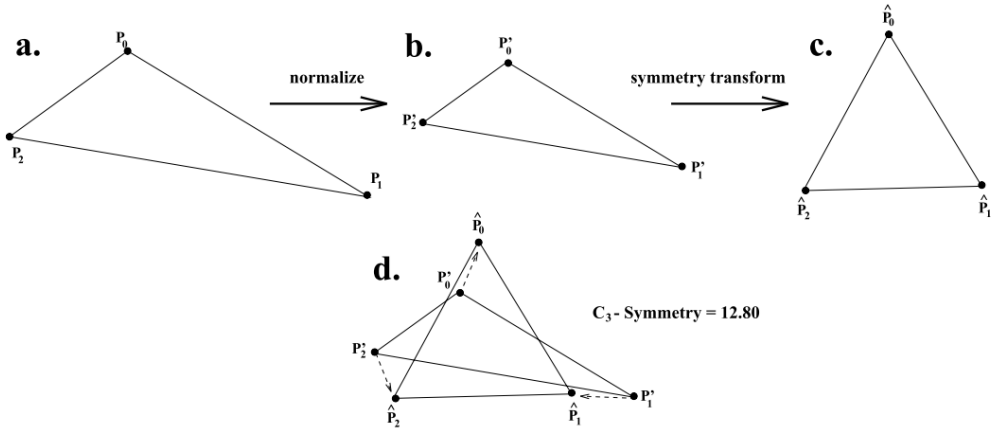

Figure 2.8: From an original shape (a), Zabrodsky *et al.* [249] normalize the distances so that the maximum distance to the barycenter is 1 (b), then applies the symmetry transform to get a symmetric shape $\hat{\mathrm{P}}$ (c). The value of SD is the average distance from feature points in P to those in $\hat{\mathrm{P}}$ (d). Adapted from [249]

2.2.4 Symmetry Distance

Zabrodsky *et al.* [248, 249] define the Symmetry Distance (SD) of a shape as a minimum effort required to turn a given shape into a symmetric shape. SD is the mean of the square distances each point should be moved from its location in the original shape to its corresponding location in the symmetric shape (Figure 2.8).

During the symmetry transform of a shape P to its closest symmetric shape $\hat{\mathrm{P}}$, the SD of a shape P (the distance between P ($\{P\}_{i=0}^{n-1}$) and $\hat{\mathrm{P}}$) is:

$$SD = \frac{1}{n}\sum_{i=0}^{n-1}\|P_i - \hat{P}_i\|.$$

In this approach, as symmetry is decided by a set of points that represents a shape of an object, the selection of representative points could be a non-trivial

problem. And moreover, an exhaustive search (rotating, folding and unfolding of points) for the nearest symmetric model is not computationally efficient.

2.2.5 Symmetropy

E. Yodogawa *et al.* [246] proposed a new quantity "symmetropy" based on Shannon entropy that gauges the combined symmetry and entropy of a given constellation or shape in the spatial domain. The measured quantity is the convolved projection value between the shape and the spatial distribution of units that captures symmetry of distributions as well as the spatial distribution. The definition of symmetropy utilizes a two-dimensional Walsh transformation.

The Walsh function (Figure 2.9) calculates projections into four principal classes of symmetries (vertical, horizontal, centro-symmetric, and double symmetry). Then Shannon's formula is applied and if the value of a symmetry component in the fracturing pattern is significantly higher than the others (*i.e.*, the symmetropy value is *low* when the symmetric pattern is present), the pattern is rich in the corresponding symmetry.

The main use of entropy was restricted to checking the uniformity of the filter output in their approach, and symmetry of a pattern was quantified not by entropy-related measures but by a two-dimensional discrete Walsh transform.

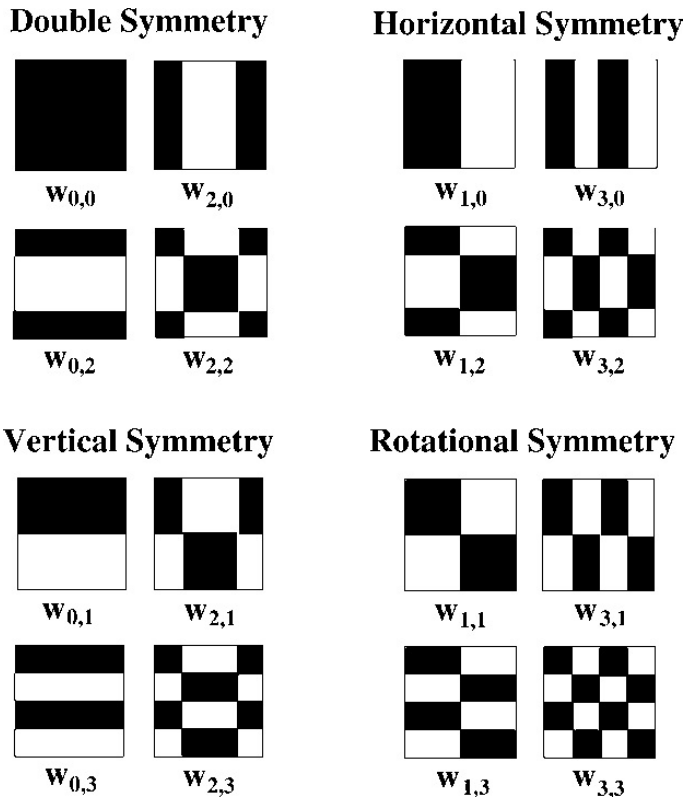

Figure 2.9: 2D discrete Walsh basis functions to detect four different kinds of symmetries. Black represents +1 and white -1. Adapted from [246]. [244] also contains a similar figure with a bigger window size.

2.2.6 Using Entropy for Similarity Measure

Measuring image similarity using entropy related divergence measures is popular for the image quality inspection [51], informative feature selection [209], texture retrieval [107] and image registration [128]. Most applications have accepted the idea of measuring image similarity between the marginal distributions of measurable feature sets; it is a fact that embracing entropy related divergence measures will be sufficiently applicable to the problems of symmetry finding.

2.2.7 The Symmetric Axis Transform (AKA Medial Axis Transform)

In terms of shape classification and description, the symmetric (or medial) axis is a set of points (centers of all *maximal disks*[2]) that are medial between the boundaries (Figure 2.10). The contours acquired from those points locally approximate an axis of reflection. In Figure 2.10, the symmetric axis forks at branch points and falls short of completely delineating the global symmetry of the given shape.

The symmetric axis transform [22] is a process that encodes a visual shape by giving it a pair of particular descriptions, namely the symmetric axis and the radii of disks (more precisely, radius function of position on the axis).

The serious flaw of the symmetric axis transform is its sensitivity to the details of boundary that small changes in boundary cause severe shifts in the symmetric axis (Figure 2.11). As a result of this sensitivity, two very similar shapes deliver two significantly different symmetric axes, and consequently the matching distance

[2]A maximal disk is a circular primitive entirely contained within the object boundaries but not enclosed by any other disk

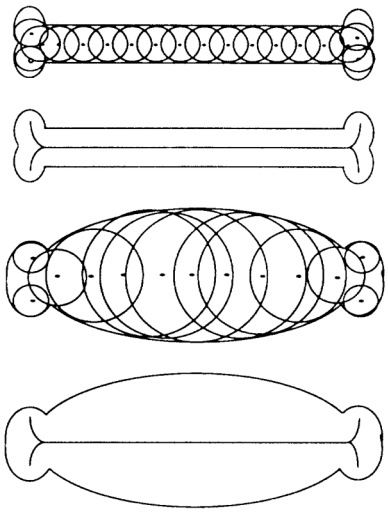

Figure 2.10: A set of maximal disks in shapes and the corresponding symmetric axis. Adapted from [167].

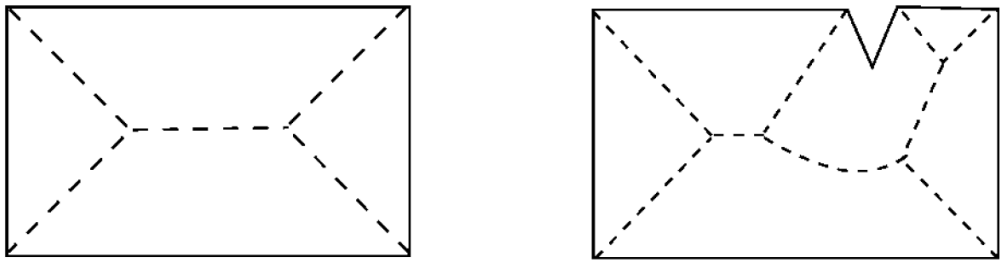

Figure 2.11: Sensitivity to noise in the boundary.

between the two axes becomes disproportionately large relative to the actual discrepancies between these otherwise similar shapes.

2.2.8 Medial Points by Superpixel Segmentation

The term superpixel [182] means a perceptually meaningful set of pixels that belongs to an atomic region which can replace the traditional pixel-grid. Levinshtein *et al.* [110] merge adjacent medial points of superpixels into a skeletal branch by

their symmetry affinity. The symmetry affinity between two adjacent superpixels is learned from shape (a fitted ellipse) components and appearance (color) components. Strictly speaking, this method is more about grouping by symmetry than detecting symmetry.

2.2.9 Spectral Symmetry Detection

To assess the relative similarity among all data points in an image, spectral clustering methods take advantage of the spectrum (a set of eigenvalues) of the similarity matrix to partition a dataset of points into clusters. The Normalized Cuts algorithm [200] is the most notable technique for this operation.

Seeing that a symmetrical shape bears pairs of similar local structures embedded in an image (a representation of self-similarity), the discovery of the self-alignment of points in the image can provide critical information regarding potential symmetry axes. Because the local features are not usually reflectionally-invariant, a reflected copy of the features [36] or a histogram of some feature value occurring in a window around a location [215] is employed for generating the affinity matrix; and afterward we can solve for the generalized eigenvectors [3] and find correspondences between the features [195, 18, 109].

2.2.10 Digital Papercutting

Symmetry can be used in an art of decorative paper cutting as it can provide folding lines that spawn various patterns. The digital papercutting algorithm [120]

is a typical example of an exhaustive search algorithm that probes every possible candidate of symmetry axis, characterized by (r, θ), to locate bilateral symmetry. This algorithm reflects the image across the given candidate axis, and then tallies the symmetry score by adding up the angle similarity (the cosine of the angle) between corresponding edges. The axis with the highest score would be the folding line or the axis of symmetry.

2.3 Our Different Approaches: Mainly Based on the Previous Work

2.3.1 Barycenter Assumption in a System

It is not clear whether a configural cue of symmetry is a necessary component of the segregation process, or the process can proceed without contributions from the cue thereof. With the parallel interactive model [129] that proposed mutually facilitatory connections between symmetry and area processes, we can reduce the problem space to segmented images.

If the domain of the problem is a set of single symmetric objects, there has to be a very simple and fast algorithm to find axes of symmetry. The main idea is that symmetric balance is created through an equilibrium between individual weights of components.

If a segmented image represents a single symmetric object, we can easily identify a point in the Euclidean space that an axis of symmetry passes through.

$$R = \frac{\sum m_i \cdot r_i}{\sum m_i},$$

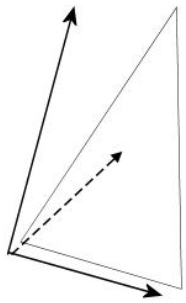

Figure 2.12: Orthogonal angles can shift the average angle.

where R is a barycenter, r_i is a position of a particle i and m_i is its mass.

A caveat of this approach is the orthogonality of the competing symmetry axes (Figure 2.12.) which shifts the barycenter to the sum of two symmetric-axes vectors. An expedient solution for this symptom is averaging the angles without the orthogonal angles and compute the differences between the orthogonal angles and average angles. Then the affected average angle pushes the difference to a lower value and generates local minima (Algorithm 1).

Algorithm 1 Find Axes of Symmetry from a segmented image

```
Read Image.
Compute edges and their gradients/Orientations from the image.
Find barycenter from the edges.
for all Angle i such that 0 ≤ i ≤ π do
   Value(i) = abs(average_{j≠i}(angle(j)) - i);
end for
Find local minima from Value
```

Figure 2.13 shows the detection results of the barycenter based algorithm with various single object images. The result clearly shows most of prevailing local sym-

metries of the image tested. Though some tested images are not perfectly symmetric, this algorithm still can produce results very close to the actual symmetry axes.

The search of symmetry becomes more difficult whenever the image contains noise or is perspectively distorted. The striking drawback of this approach is absence of robustness to noise and local perturbation as in Figure 2.14. For this reason, this algorithm can be used when well-segmented single object images are presented or you need approximate locations of the symmetry axes for the more elaborate and sophisticate algorithms that require far more computational time.

As described in Algorithm 1, this approach has a computational complexity of $max(O(n), O(g_a^2))$, where n is the total number of pixels in the input image and g_a is the angular granularity in Algorithm 1.

2.3.2 The Line-Based Symmetry Detection (LBS) Algorithm

If a scene contains more than one object or significant amount of noise, the naïve barycenter based method is doomed to fail. To choose the elements that shares the same axis of symmetry, an algorithm called a "voting scheme" has long been used. Eq. 3.2 serves as the symmetry measure in [126, 181] by voting to the line L_c. By tallying up the voting results, the local symmetries of the image emerge and each local maximum can be used as a candidate symmetry for an object in the image.

In this section, a method based on lines, a more sophisticated version of line-based voting algorithm that links edges into lines in a preprocessing step, is explained in detail. Considering that a surprisingly large number of man-made objects around

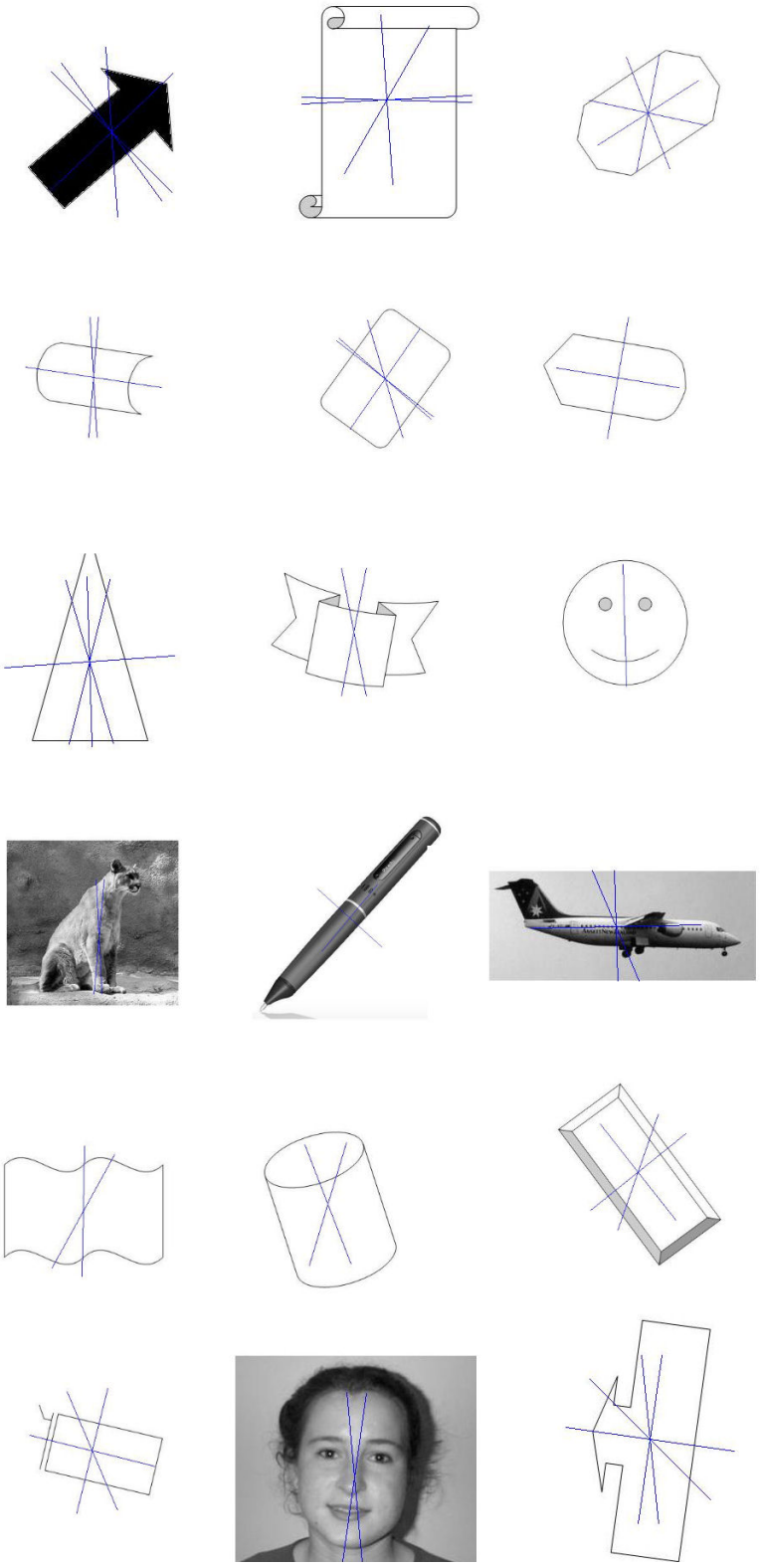

Figure 2.13: Detection results of barycenter approach (Success). The blue lines signify all the local minima found by the algorithm

Figure 2.14: Detection results of Barycenter approach. (Erroneous detections)

our environments have line pairs which are symmetric to each other with respect to axes of symmetries, we can easily identify the symmetries embedded in objects via a plain line matching scheme. Another advantage of using lines instead of all the pixels in an image is that one can remove the assumption of consistent color and achieve drastic speedups in detection time, empirically subquadratic time complexity.

The line-based symmetry detection (LBS) algorithm evaluates the symmetry between two lines by coupling a phase angle and the lengths of line segments. In this algorithm, all lines (or all points in Hough space) in an image are voting to determine the symmetry of the given image. Granted this algorithm has the appearance of a global approach - videlicet, all lines (or all points in Hough space) in an image contribute to determine the symmetry of the entire image -, it can be easily converted to the look of a local approach by a line-distance weight function.

Indeed, the LBS algorithm is a local approach in that the image features that decide the symmetry are a subset of the entire image. In that event we can not

entirely be sure the symmetry we found embodies a global symmetry. This method is very similar to [126] in that the voting for axes of symmetries happens in Hough space, but in place of SIFT descriptor environment, a contiguous set of points (line) is partaking the voting process. Besides, the LBS does not exclude non-extreme feature points in the scale space so that the algorithm is robust against missing feature points.

The LBS is a feature based approach, in which the locations of the visually salient features in an image are identified and common patterns of them conduce to more effective representation of the image. The main disadvantage of this approach is its sensitivity to measurement errors. In order to counter this unfavorable characteristic, a region based approach is proposed so that symmetry detection is more dependent on processing the overall shape of the object given, rather than the constituent parts of it.

2.3.2.1 Motivation

Image processing and psychophysical joint research has shown that line drawings are indeed much more informative than the edges extracted from photographs [193]. This result motivated us to think that a few lines on an image could supply enough information to recover symmetry. Unlike the silhouette boundaries which might compromise the capability of symmetry identification by missing crucial internal features, the LBS does not let these features get ignored.

Over the past decades, researchers in computer vision have explored a number

of aspects of symmetry to generate symbolic representations of shape and many algorithms have been developed for computing symmetries, particularly reflectional, of shapes. Understanding how to represent and recognize symmetries embedded in objects has, however, proven to be a remarkably difficult task, both for computer vision and for perceptual psychology. To our best knowledge, the algorithms developed either have high-complexity or provide limited information of shapes.

A symmetry detection algorithm introduced here is based on the line components in an image. This algorithm does not assume uniform object color, texture or lighting conditions, and does not rely on any specific a priori object model or assumption.

2.3.2.2 The Closest Study

The GST mentioned in Section 2.2.1 extracts local symmetry by an attention operator based on locations and gradient directions of edge points to produce a symmetry map. The GST decides the symmetry between two points by coupling a distance weight function, phase weight function, and logarithmic function of the gradient magnitudes for these two points. A symmetry map of this transform is interpreted as a map of interesting points in the image.

The algorithm presented here is somewhat similar to the GST, except an input image is reorganize into a set of lines in preference to edge orientations.

2.3.2.3 The LBS Using Hough Transform

The most peculiar aspect of the approach is, unlike previous voting schemes, we test pairs of lines in the given image for the decision of the symmetry axis. Since each line corresponds to a point in Hough space, a point with maximal votes is selected as the primary symmetry axis. It is known that normal voting schemes give rise to high computational complexity, and this approach can alleviate the computational burden associated with this shortcoming, because the number of possible pairs involved in the voting is limited. According to the Hough Transform, each line in image space corresponds to a point in Hough space and vise versa: therefore, the voting result is not the point of interest but the line of interest.

By Hough transform, we can carry out some feature-extraction procedures in a different parameter space other than the usual image space. Mostly we parameterize the lines in the Hough transform with two parameters, commonly referred to as r and θ that represent the distance between the line and the origin, and the angle of the vector from the origin to the closest point on the line respectively. The (r, θ) plane is called as Hough space for the set of straight lines in two dimensions.

2.3.2.4 Algorithm Description

The original images are first preprocessed by an appropriate edge filter. We tried the Canny and the Sobel edge-detection operators for this part and the Canny detector showed better performance.

From the binary edge image at the previous step, we make lists of connected

edge points by linking the edges. In this step, we also removed edges shorter than certain length as a process of noise rejection. The minimum edge length of interest depends on the size of the image and the distribution of edge lengths.

Using the lists of connected edge points, we derive straight line segments through a subsampling of its corresponding edge list such that straight line segments between these subsampled points do not deviate from the original points by more than the predefined maximum deviation.

Given 2 lines, $l = (a, b, c)^T$ and $l' = (a', b', c')^T$, the vector $x = l \times l'$, where '$\times$' means the cross product, is the intersection of two lines l and l'. It is trivial to find a line that bisects the angle between the two lines if we already have l, l' and its intersection point. The average of the two unit-vectors yields the midpoint of the base of the isosceles triangle the two unit-vectors make and it is a bisector. If we use the $r - \theta$ parameterization for lines found (*i.e.*, $r = x \cdot cos\theta + y \cdot sin\theta$), we can easily find polar coordinates (r, θ) in the Hough space (Figure 2.15).

Let H be a function that takes two lines with homogeneous representation and returns polar coordinates (r, θ) of the line that bisects the angle between them. The set of points $CL(r, \theta)$ can have a line-length contribution function $LL(r, \theta)$ as

$$CL(r, \theta) = \{(i, j) | H(l_i, l_j) = (r, \theta)\},$$

$$LL(r, \theta) = \sum_{(i,j) \in CL(r,\theta)} (\|l_i\| + \|l_j\|). \tag{2.1}$$

Alternatively the term $(\|l_i\| + \|l_j\|)$ can be modified to $(\|l_i\| \cdot \|l_j\|) \cdot cos(\alpha_{ij}/2)$,

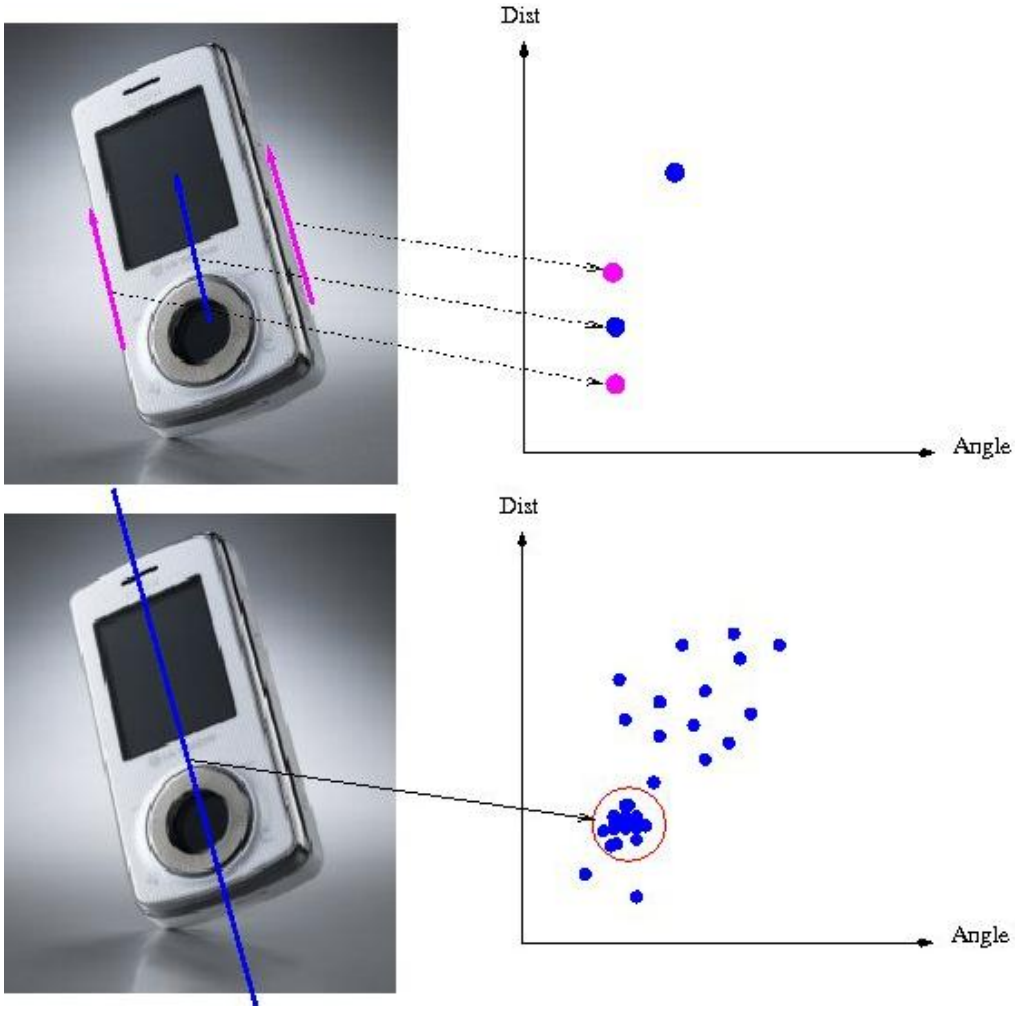

Figure 2.15: Hough Transform of lines to points (From Euclidean space(Left) to Hough space(Right))

where α_{ij} is the angle between two lines, l_i and l_j, if you want to exclude some edges perpendicular to the axis of symmetry concerned.

The $LL(r, \theta)$ definition above shows that the algorithm can deal with the case of occlusion by the repetition of adding.

To find axes of symmetry, we just choose the maximum values from 2D space of $LL(r, \theta)$.

$$l_{symm} = H^{-1}(\arg\max_{(r,\theta)} LL(r, \theta)) \tag{2.2}$$

2.3.2.5 Psychological Validation:

Up until now, a number of computational models for symmetry detection have been proposed to model the human visual system. The idea of the line based approach fits well into two stage model. Palmer *et al.* [159] suggest that symmetry is detected in two stages and the first stage is a fast and global analysis to choose a potential axis of symmetry by considering all the possible orientations of axis at the same time. Consequently, the first stage should be a global symmetry detection. In the wake of this stage, an explicit comparison of the two halves of the stimuli for more elaborate symmetry detection is performed.

2.3.2.6 Interpretation of the LBS: Centroid in Hough Space?

One of the prominent global approaches is based on moments. The moment of a 2D shape is described as

$$M_{pq} = \int_{-\infty}^{\infty} \int_{-\infty}^{\infty} x^p y^q I(x,y) dx dy \,, \tag{2.3}$$

where $I(x,y)$ is 1 at the inside of a shape and 0 otherwise. The central moment μ_{pq} is defined as

$$\mu_{pq} = \int_{-\infty}^{\infty} (x-\bar{x})^p (y-\bar{y})^q I(x,y) dx dy \,, \tag{2.4}$$

where $\bar{x} = \frac{M_{10}}{M_{00}}$ and $\bar{y} = \frac{M_{01}}{M_{00}}$ are the coordinates that represent the center of mass of the shape.

In the LBS, the axis of symmetry is *not* the centroid C: a weighted system of points such that $\sum_{i=1}^{m} w_i \overrightarrow{C} p_i \neq 0$ in Hough space, where p_i is a point that corresponds to a line in Euclidean space. The Figure 2.15 is somewhat misleading because the "midpoint-angle bisector" relationship holds only between the lines with the same slope as in the figure. Eq. 3.3 reveals the genuine symmetry constraints between two lines defined by the angle bisector.

2.3.2.7 Results of Experiment

A symmetry line map produced by the LBS algorithm is presented in Figure 2.16. Figure 2.16 shows the detection result of our line based algorithm with an image from [161]. The result shows a clear peak that represents an axis of sym-

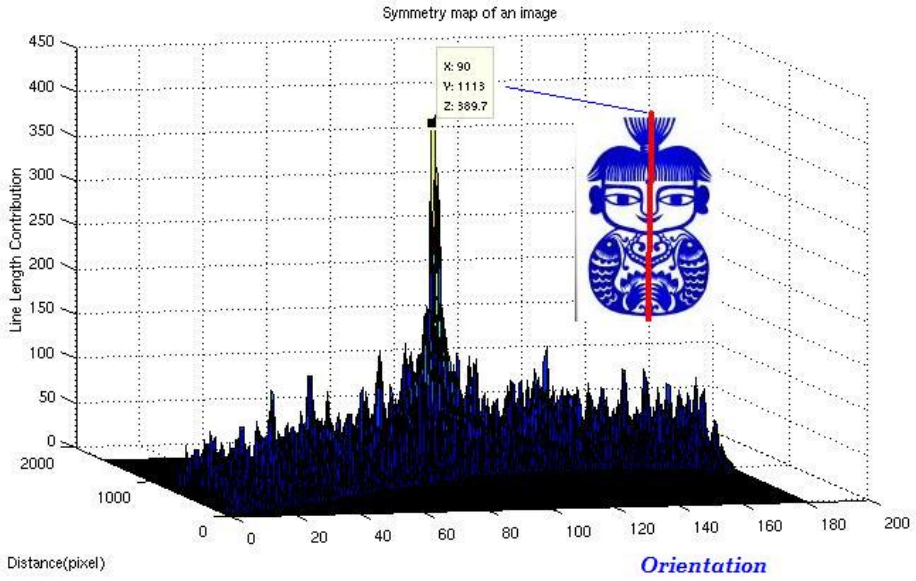

Figure 2.16: A symmetry map of an image.

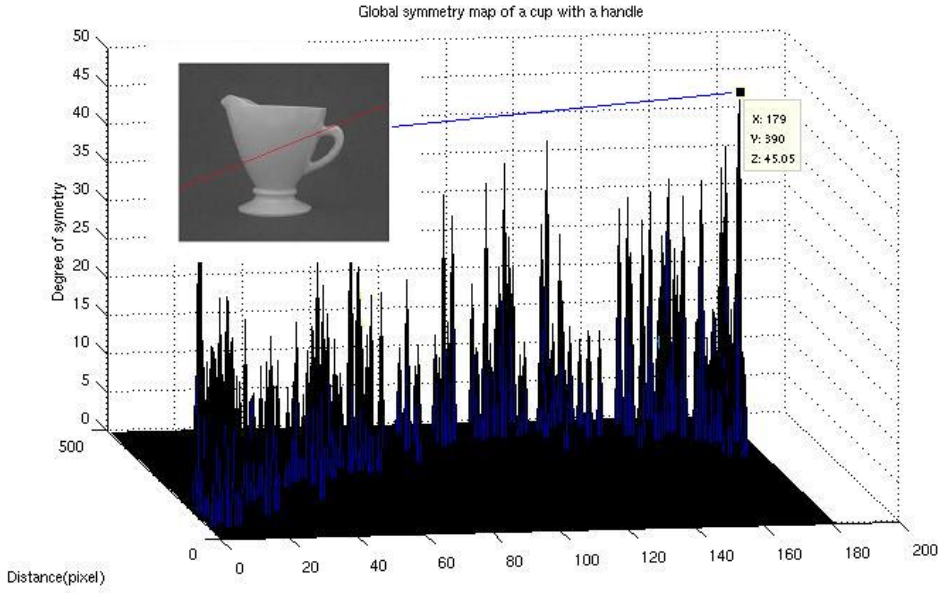

Figure 2.17: A symmetry map of a cup.

metry of the image tested. Figure 2.17, however, shows a case that fails to detect a desirable symmetry axis because the line components of the handle disrupt a global symmetry structure. Clearly, when the local symmetric assumption is forced on an locally asymmetric objects, the inference would be incorrect. The error that stems from local line features can be corrected by global symmetry detection algorithms.

2.3.2.8 Performance Comparison

The GST [181] has a computational complexity of $O(n^2)$, where n is the total number of pixels in the input image. Hough transform algorithm using mid-point pairs [245] has a complexity of $O(n_{edge}^4)$, where n_{edge} means the number of edge pixels. A real time symmetry detection algorithm [114] claims a complexity of $O(BINS_\theta \times n_{edge}^2)$, where $BINS_\theta$ is the number of Hough angle division.

The LBS approach performs symmetry detection by line-pairs of an image. All the line component pairs participate voting operations to decide axes of symmetry, and the algorithm requires $O(n_{line}^2)$ time complexity, where n_{line} represents the number of line components in the image. Though there is no rigorous basis to establish the relationship between the number of edges and that of lines in an image, in our experiment a line contains roughly 60 edge-pixels.

2.3.2.9 Applications of the LBS

Finding Areas of Interest: When we look at a scene, we concentrate on certain points more than others because people process visual information selectively. Those

areas that contains more interesting information than others are called areas of interest.

Consider a black and white image consists of N pixels in it. The total number of distinct pictures with N pixels are 2^N. The total number of distinct symmetry axes we can draw in the image is less than ${}_NC_2$ and for each symmetry axis we can have at most $2^{N/2}$ symmetric pictures.

Then the probability of observing symmetric image from the random permutation of the pixel is less than $\frac{N(N-1)}{2^{N/2}}$ and if $N = 10^4$, the probability becomes 10^{-1500}.

Therefore, if you detect a symmetry in an image, it is either a result of infinitesimal chance or a proof of existence of a symmetric object.

In Figure 2.18, two tree like structures in the front and a building structure in the back are detected when we choose the second and the third best axes of symmetries. This is due to the voting scheme that nicely subsumes local symmetries.

In Chapter 4, the issue of finding AoIs is investigated more thoroughly.

Object Alignment for Shape Matching: If we describe features of an object relative to the object itself, changes in viewpoint reshape the appearance of the object, yet they do not severely alter the position of a given feature relative to others in the object (objects can normally be assumed to be rigid). The most renowned example of an object-centered theory was proposed by Marr and Nishihara [134]. They proposed that an object's features are described relative to its axis of elongation or the axis of symmetry. Provided that an observer can capture those axes

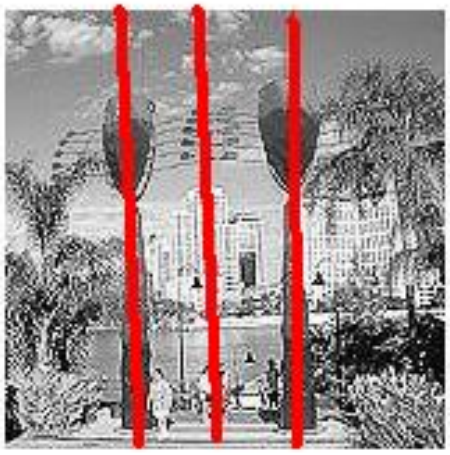

Figure 2.18: Symmetry detection results of trees and buildings (lines of interest).

for a given object, a canonical description of that object is framed and a single viewpoint-independent representation is built in visual memory for the recognition from all viewpoints.

It is trivial to rotate the image to align once we know the value of θ. This capability is especially useful for object classification or shape matching. For example, in shape matching and object recognition using shape contexts [16], rotation invariance is pretty hard to achieve because many points do not have reliable tangents for the relative frame. Therefore the primary symmetry axis of the object can be a good absolute frame for computing the shape context at each point (Figure 2.19).

Shape Recovery: Sometimes, if necessary, a continuous symmetric contour can be recovered by line segments on the two sides of symmetric objects. The evidence of a single line pair is reliable only if the local features around the lines are thoroughly

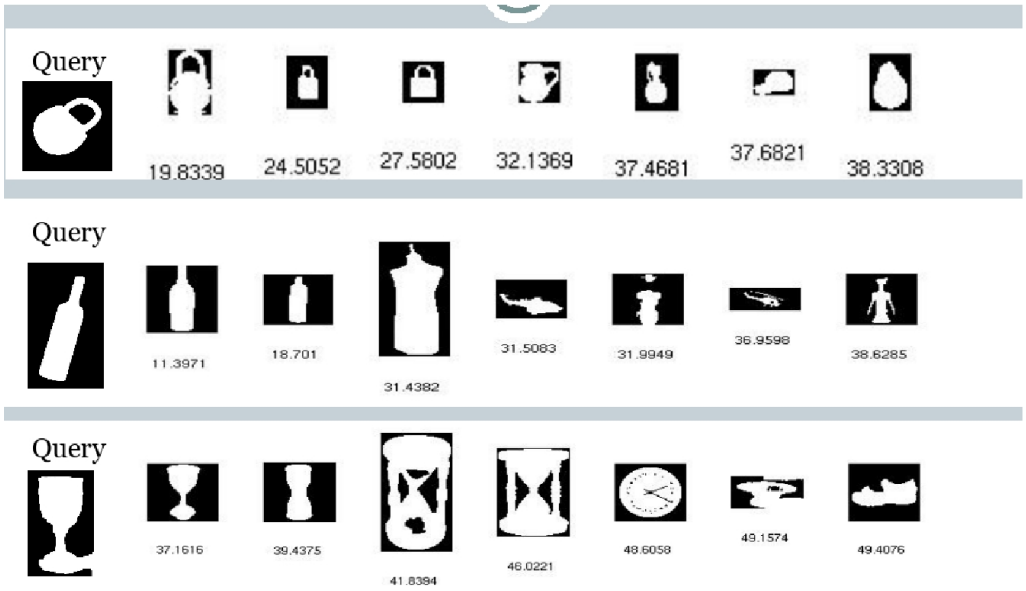

Figure 2.19: Shape Context with image alignment by symmetry detection. The numbers represent the matching scores.

reflected by the mirror transformation. If a line couldn't find its counterpart, yet its local geometric features surrounding it are mirrored by the symmetry axis, we can assume the matched pair is occluded or reduced to a useless line segment due to line-detection error. Shape recovery from occlusion and occlusion detection can be done by reconstructing the matched line pairs.

Contrary to this approach, there is a research that suggests symmetry does not play an important role in image segmentation and symmetry is important to the visual system only after the region is fixated [72].

Segmentation Using Areas of Interest (AoI) of an Image: In order to analyze an enormous amount of information involved in vision tasks under plausible time and space constraints, a vision system has to curtail redundant information by

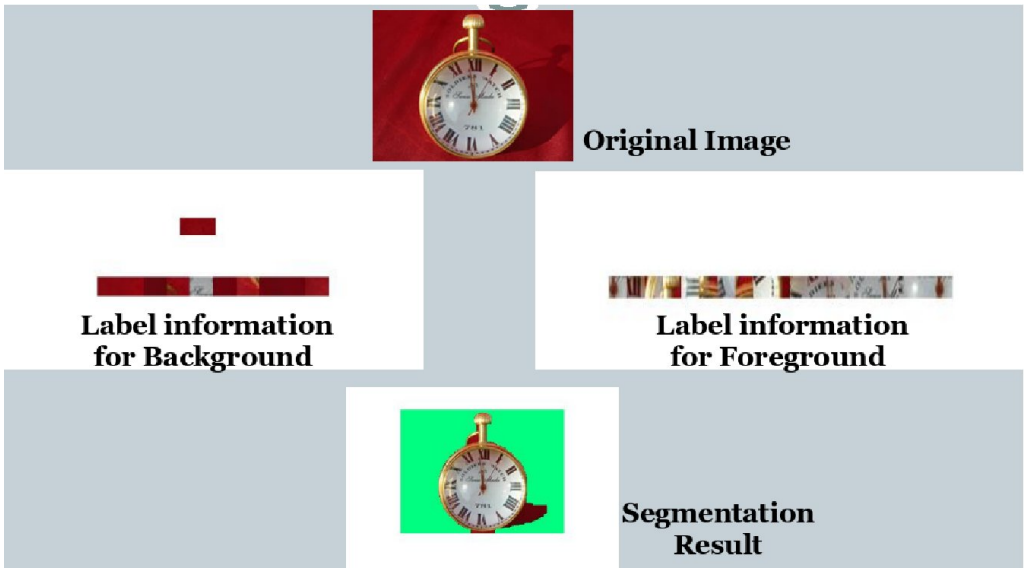

Figure 2.20: Object segmentation using symmetric areas.

directing its computational resources toward interesting areas [6] (also refer Section 1.7.3). Attention is shifted by fixating the eyes on these areas. A set of those areas serves as a guide for shifting the attention (or eyes) to fixation points in it.

Figure 2.20 shows the areas of interest distinguished by the LBS algorithm. Interestingly, the areas spotted by the detector were overlapped with the foreground object in the image. This finding justifies the use of symmetry as a salient cue that directs visual attention [127].

The pixel information from areas of interest is able to provide a more natural way to encode color features as segmentation cues. Then the foreground segmentation is obtained from local pixel similarities using iterated graph-cuts [24] (Figure 2.21). The results show a clear refinement against a naïve approach that assumes objects are around the center of the image.

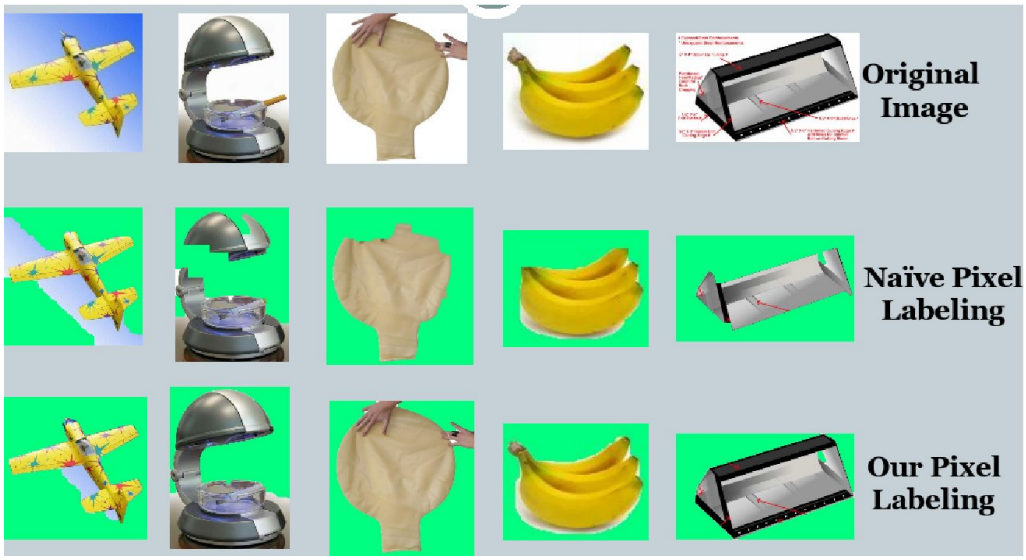

Figure 2.21: Comparison of results on foreground segmentation.

Segmentation by Retracing the Voting: When we keep track of the voting history, the group of edges or lines voted for the same candidate could provide a nice segmentation information. Figure 2.22 shows the results of backtracking from each local maximum of voting space.

2.3.3 Recovering Axes of Symmetry from Perspectively Distorted Images

The symmetry of an image is hard to detect. One reason is that real objects often are not perfectly symmetric and a small amount of perturbation may significantly affect the detection of symmetry. Even if an object is perfectly symmetric in $3D$, its $2D$ image under perspective projection might not be. Lighting variations only serve to aggravate the situation.

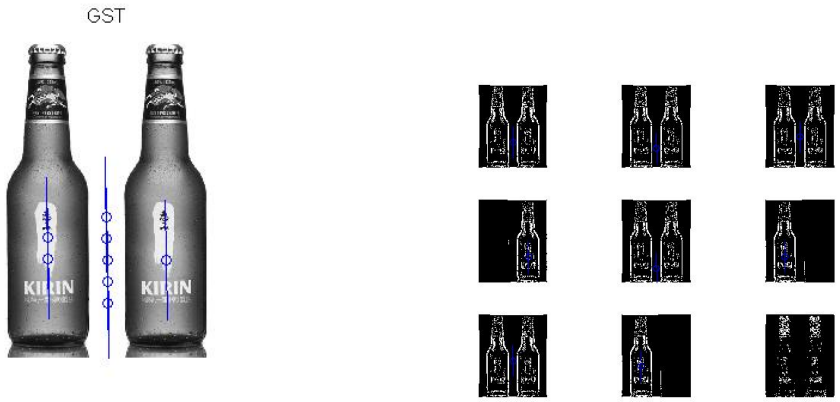

(a) Axes of symmetry found

(b) Results of backtracking from the axes of symmetry recovered.

Figure 2.22: Segmentation by retracing the voting result.

We proposed a method on computing bilateral symmetries of planar objects under perspective distortion. By exploiting the invariance of the cross ratio under perspectivities, we analytically compute a set of midpoints of the object as a function of the vanishing point. Then, we fit a straight line passing through the midpoints. The goodness-of-fit defines the likelihood of this line to be a symmetry axis. Using the proposed method, searching for the symmetry axis becomes searching for a vanishing point. This approach is global in the sense that we consider the whole image of the object rather than small parts of it. The results will show that the method presented here is capable of finding axes of symmetry from considerably distorted perspective images. See A.1 for the details of this method.

2.3.4 The Trace Transform Based Symmetry Detection (TTS) Algorithm

The trace transform [95, 96], a generalized Radon transform, traces an image with straight lines along with certain functionals of the image function. More specifically, for an arbitrary function $\rho(x, y)$, its trace transform, denoted as $T\{\rho(x, y)\}$, or simply $P(p, \phi)$, calculates the trace functional T of the image function $\rho(x, y)$ along a line (ray) L, criss-crossing its domain.

$$P(p, \phi) = T(\rho(x, y)), \tag{2.5}$$

where the path L is defined by

$$x \cdot cos\phi + y \cdot sin\phi = p, \tag{2.6}$$

where the parameters are ϕ, the orientation of the line, and p, the length of the normal from the axes origin, that characterize each line. It can be noted that the function $\rho(x, y)$ is not restricted to binary values such as 0 for the outside of a shape and 1 for the inside. It can be the intensity value of image pixel signals or the result of Laplacian operator.

Since we want to have a symmetry measure, We defined a new trace transform

$T(\rho(x,y))$ as

$$T(\rho(x,y)) = \\ \| \int_{-\infty}^{\infty} sin(\frac{r\pi}{2R})\rho(r)dr - \int_{0}^{\infty} cos(\frac{r\pi}{2R})\rho(r)dr + \int_{-\infty}^{0} cos(\frac{r\pi}{2R})\rho(r)dr \| , \quad (2.7)$$

where $r = x-c$, $R = max(||r||)$ where $\rho(r) \neq 0$, and and $c = median_x\{x, \rho(x,y)\}$.

Then along the column of the trace transform, the diametric function P, the integration of trace transform, is done.

The time complexity of this algorithm is defined by $O(kn)$, where n is the total number of pixels in the image and k is the number of angles tested (usually, $k \leq 180$).

2.3.4.1 View Point Selection and the Next-Action Decision for Active 3D Object Recognition.

The rationale for this approach is that when a 3D symmetric object is projected onto a 2D plane, it can take 2 forms of symmetry: parallel symmetry or/and skew symmetry. We claim that under the assumption of a flat object, for pairs of segment points which are possibly skew symmetric at a given skew angle, the trace transform T for the strip area made by these points through midpoints by the skew angle will give similar values on the symmetry trace transform (Eq. 2.7) unless the object is heavily concave or (a) hidden surface(s) of the object begin(s) to be captured by the camera of a robot. Accordingly, it is safe to say that in a small range of angles,

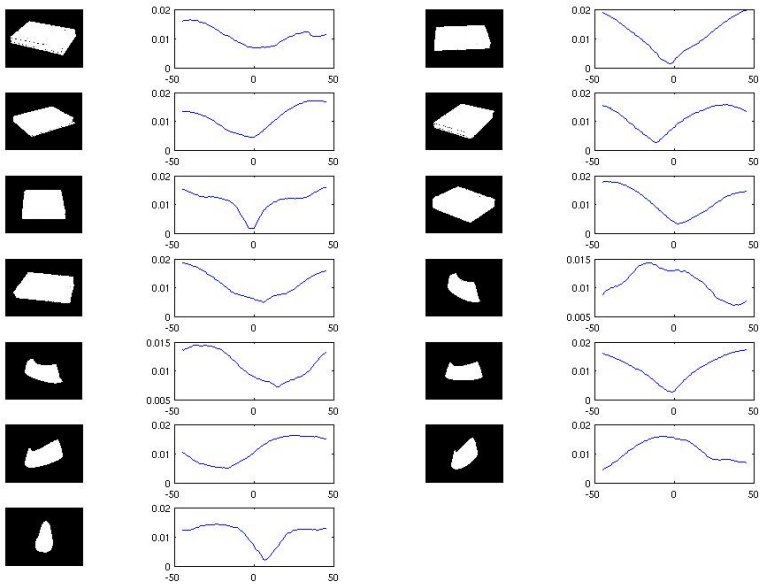

Figure 2.23: Measurement and estimation of symmetry degree.

the degree of symmetry predicted/measured by the trace transform (Eq. 2.7) of the flat symmetric object is reliable. Figure 2.23 supports this claim.

For all the claims we made in the prior paragraph assumed a bird's-eye view of a flat object. If an image captured is a side-view of an object, we can choose a better viewpoint by moving to the direction of the vanishing point that is obtained from A.1. The speed of movement can be constrained by

$$v = \frac{\nabla l}{\nabla t} = k \cdot \frac{1}{d_v}\,, \tag{2.8}$$

where k is a constant value and d_v is the distance between the center of the image captured and the vanishing point recovered.

Obviously the schemes above may not work well with non-flat 3D objects. Likewise, the poses of non-flat 3D images in a database are difficult to decide.

2.3.5 Robust Global Symmetry Detection By Entropy Measures

2.3.5.1 Psychological Motivation

All previous approaches are based on the assumption that symmetric balance is generated through an equilibrium between individual elements. However, McManus *et al.* [140] found that eliminating $10 \sim 30$ % from one end of the balanced picture makes "chopped" pictures that are also considered to be balanced. McManus *et al.* concluded that balance depends on an integration of the image as a unified whole, rather than on a simplistic adjustment of individual elements.

2.3.5.2 Computational Motivation

Measuring image similarity in the presence of noise is very fundamental and essential for a number of computer vision applications: object recognition, image search from database and video surveillance. The most prevalent types of measurement used to detect image similarity are mean squared error (MSE), cross correlation (CC) and peak signal-to-noise ratio (PSNR) and it has been shown that these measures lack the ability to attain reliable image similarity across distortion types [232].

In this section we introduce the concept of entropy as a measure of symmetry. Since entropy is tightly coupled with probability, it also can serve as a measure of symmetry that quantifies symmetries of objects in the world. This measure will

enable us to compare the degree of symmetry of different shapes as well as the degree of different symmetries in a single shape. As long as the domain has a probabilistic model, it can be applied universally.

2.3.5.3 Entropy and Symmetry

Entropy has been considered as an indispensable quantity that measures the amount of disorder or randomness in a system holding energy or information. The definition of the information entropy $H(X)$ devised by von Neumann [226] and Claude Shannon [197] is normally given as

$$H(X) = -\sum_{i=1}^{n}(p(x_i)\log_b p(x_i)), \tag{2.9}$$

where $p(x_i)$ is the discrete probability of the i^{th} microstate, n is the number of microstates and b represents the base-b logarithm.

Now we turn to a measure that quantitatively compares the similarity between two distributions. The entropy of a random variable is a measure of the amount of information required on the average to describe it.

The joint entropy $H(X,Y)$ of a pair of discrete random variables (X,Y) with a joint distribution $p(x,y)$ is defined as

$$H(X,Y) = -\sum_{x\in X}\sum_{y\in Y} p(x,y)\log_b p(x,y). \tag{2.10}$$

Finally, the mutual information $I(X;Y)$ that measures the amount of information that one random variable X contains about another random variable Y is

stated as follows:

$$I(X;Y) = \sum_{x \in X} \sum_{y \in Y} p(x,y) \log \frac{p(x,y)}{p(x)p(y)}. \tag{2.11}$$

If the two distributions p and q of the random variables X and Y are sufficiently similar to each other, the joint entropy $H(X,Y)$ and the mutual information $I(X;Y)$ approximate to $H(X)$ (or $H(Y)$). To eliminate the terms of joint/conditional probability, the relative entropy $D(p\|q)$ is devised.

The relative entropy $D(p\|q)$ is a measure of the inefficiency of inferring that the distribution is q when the true distribution is p. If we create a code with average description length $H(p)$, and use it for a distribution q, we should have $H(p) + D(p\|q)$ bits on the average to describe the random variable q. The relative entropy or Kullback-Leibler distance between two probability mass function provides such a measure.

In brief, if $p(x,y)$ and $q(x,y)$ of the random variables X and Y correspond to the half images of the same symmetric object in the scene, it is surmised that the minimum of the relative entropy $D(p\|q)$ is achieved when we dissociate one from the other. Finding symmetry is then interpreted as the process of uncovering the partition that increase the mutual information between the separated parts.

2.3.5.4 Divergence Measures Based on Entropy

In this section, we principally employ 2D reflective symmetry as an example of applying the concept of entropy to some important vision problems. The axis of

symmetry cleaves the 2D Euclidean plane into two parts and the degree of symmetry is usually involved in comparisons between two adjacent feature sets across the axis. If the probability distributions of features in each half-plane are similar to each other, by our definition, the degree of symmetry between the sets is set to high.

The simplest non-symmetric measure of the difference between two probability distributions P and Q of a discrete random variable is the Kullback-Leibler measure [106] of Q from P, also known as the measure of cross-entropy, defined as

$$D_{KL_I}(P,Q) = \sum_{j=1}^{n} P(j) \log \frac{P(j)}{Q(j)} \tag{2.12}$$

with the convention that, whenever $Q(j)$ is 0, $P(j)$ is set to 0 and $0 \log \frac{0}{0} = 0$. It is well known that $D_{KL_I}(P,Q)$ is non-negative, additive and not symmetric [106]. It is zero, if and only if $P = Q$.

Since the Kullback-Leibler measure is not symmetric, we need to symmetrize the divergence [93] as

$$D_{KL_J}(P,Q) = D_{KL_I}(P,Q) + D_{KL_I}(Q,R). \tag{2.13}$$

Eq. 2.13 means during the symmetry measurement, either P or Q serves as the *a priori* (true) distribution and the other one acts as a unknown distribution, and vice versa.

We also adopt the Jensen-Shannon divergence [116] described as

$$D_{JS}(P,Q) = \frac{1}{2}D_{KL_I}(P,M) + \frac{1}{2}D_{KL_I}(Q,M), \tag{2.14}$$

where M is the average of the two distributions,

$$M = \frac{1}{2}(P+Q). \tag{2.15}$$

We assumed whenever $Q(j)$ is 0, $P(j)$ is set to 0, and $0 \log \frac{0}{0} = 0$ when $D_{KL_I}(P,Q)$ is calculated. This rule removes the case that $D_{KL_I}(P,Q)$ is undefined if $Q(j) = 0$ and $P(j) \neq 0$ for any j, however, ignores the difference between $P(j)$ and $Q(j)$ too. $D_{JS}(P,Q)$ does not occasion this problem and has several other desirable properties - *i.e.*, non-negativity and boundedness [116].

We select $D_{KL_I}(P,Q)$ in Eq. 2.13 and $D_{JS}(P,Q)$ in Eq. 2.14 as divergence measures to estimate the "closeness" between two probability distributions of feature sets bisected by the axis of symmetry.

2.3.5.5 Results of Experiment

In this section, we illustrate our entropy scheme on several examples. We want to emphasize that the features used were the same for all examples. It is pointless to compare pixel-values to angles of line segments. The choices were determined by the performance of the algorithm used.

The approach specified below is contingent on the statistical information of

the lines in an image. A line represents a set of points that share the same gradient vector defined by an ordered pair of $(\frac{\partial f(x,y)}{\partial x}, \frac{\partial f(x,y)}{\partial y})$. The orientation of the gradient vector for every image pixel also can be defined as $\phi = arctan(\frac{\partial y}{\partial x})$. In that we parameterize the points in the image into a different parameter space r and θ, it is identical to the Hough transform in that the parameter r represents the distance between the line and the origin, while θ is the angle of the tangential vector of this point.

The orientation of the global symmetry axis is the collective representation of the tangential lines' orientations in the image. A single orientational-constraint the axis of global symmetry has is (a more accurate and complete description of the algorithm is given in Chapter 3):

$$\varphi = \frac{\theta_i + \theta_j}{2}, \tag{2.16}$$

where θ_i and θ_j mean the orientations of two corresponding lines and φ is the orientation of symmetry respectively.

Then the problem of finding symmetry angles, or image alignment is simply a matter of discovering φ that minimize the entropy divergence measure between 2 groups of edges,

$$\Theta^{left} = \{\theta_i | \theta_i \leq \varphi\}, \tag{2.17}$$

and

$$\Theta^{right} = \{\theta_j | \theta_j \geq \varphi\}. \tag{2.18}$$

Then moving the value of φ suffices to find the symmetry angles.

$$\varphi_{symmetry} = \arg\min_{\varphi} D(\Theta^{left}, \Theta^{right}). \tag{2.19}$$

Finding bilateral symmetry is not as trivial as sweeping symmetry angles since this time the motion of sweeping is 2-dimensional. By the chain rule for relative entropy [45],

$$D(p(x,y)\|q(x,y)) = D(p(x)\|q(x)) + D(p(x|y)\|q(x|y)). \tag{2.20}$$

Eq. 2.20 means we have to get the marginal probability of $p(x|y)$ and $q(x|y)$, where p represents the angle distribution, and q gives descriptions of the distance distribution from the symmetry axis.

To ease the problem's probability searching space, we can assume these two measures are independent, then Eq. 2.20 becomes a simple addition of two entropy values. We will discuss this problem later and define the concepts more rigorously in Chapter 3.

2.3.5.6 Image Alignment and Bilateral Symmetry Axis Search

Fig.2.24 shows successful results on the data set with assumption of independent measures. Once we get the angle of symmetry axis, the location of the axis

can be easily retrieved by projecting all the edges in the image onto the line perpendicular to the symmetry axis found. Instead of angle, the distance from the origin would be the new histogram data. Yet another approach to computing the location of symmetry axis is to make a 2D histograms with edges and change them into 1D histograms and compute the divergence by Eq. 2.13. We also make 2D histograms of the image out of the edge-map, and compute the distance measures and a likelihood measure in 1D space. The difference of the performance are negligible(91 % versus 89%) and all the entropy measures produce very similar values.

We tested the measures against 42 test images from [161] and 60 symmetric images from internet. Figure 2.25 shows some examples of success and failure during the experiment. The evaluation of the results are done by 2 raters and if the axis of symmetry found is off by 5 degree or 5% of diagonal then marked as a failure of detection. The divergence measures detect the correct axes of symmetry 91% of cases (84/92). Figure 2.25 shows 2 interesting results that should be noted. Figure 2.25(b)(a) gives a correct axis of symmetry even the original image is perspectively distorted. The absolute amount of perspective distortion is mitigated by the probabilistic representation of divergence measures, and we can not expect the benefit like this from other normal distance measures. Figure 2.25(b)(b) and (b)(c) stress the importance of the edge detector. Figure 2.25(b)(b) represents the result from the edge map of Canny edge detector, and Figure 2.25(b)(c) is the result from the more sophisticated edge detector [135] that helps detect the accurate axis of symmetry.

Though there were few attempts [203, 204] to deal with global symmetry,

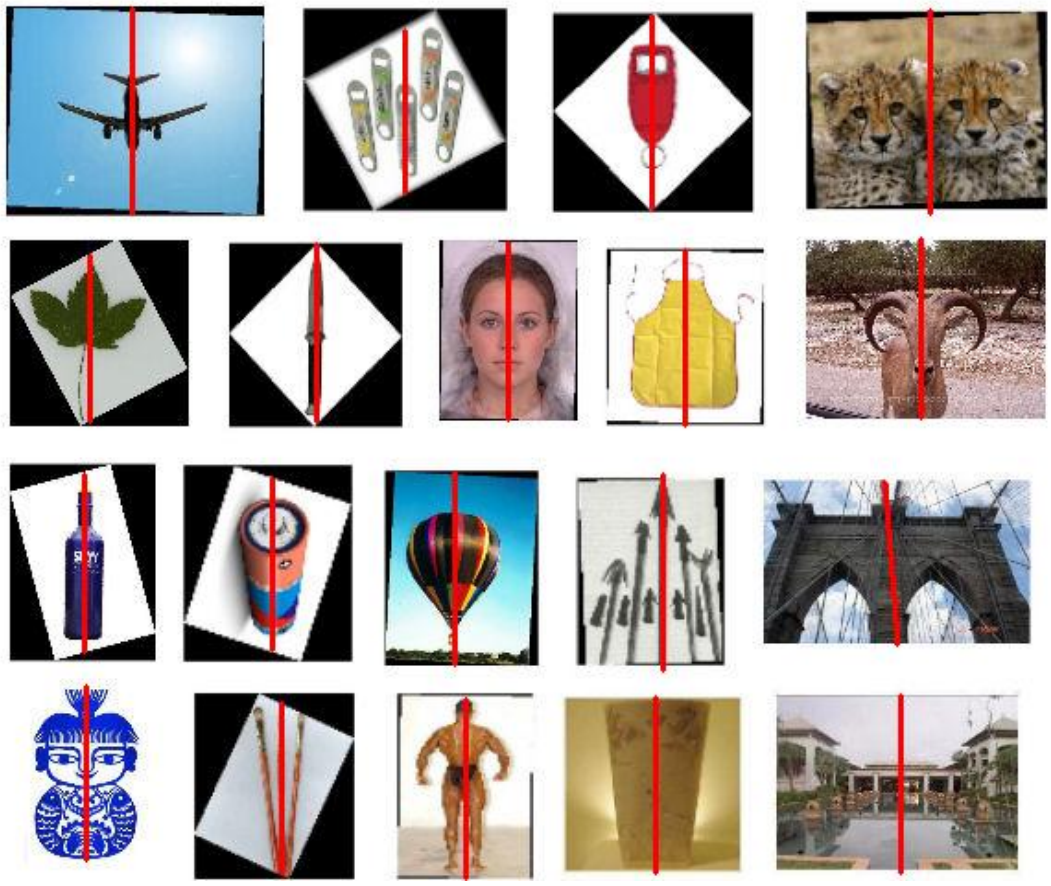

Figure 2.24: Examples of images that the symmetries are successfully found.

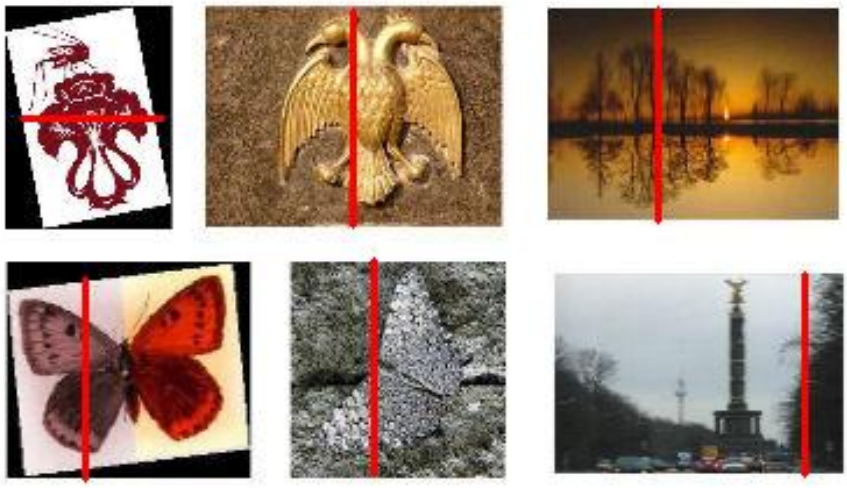

(a) Examples of images that the symmetries are not placed correctly.

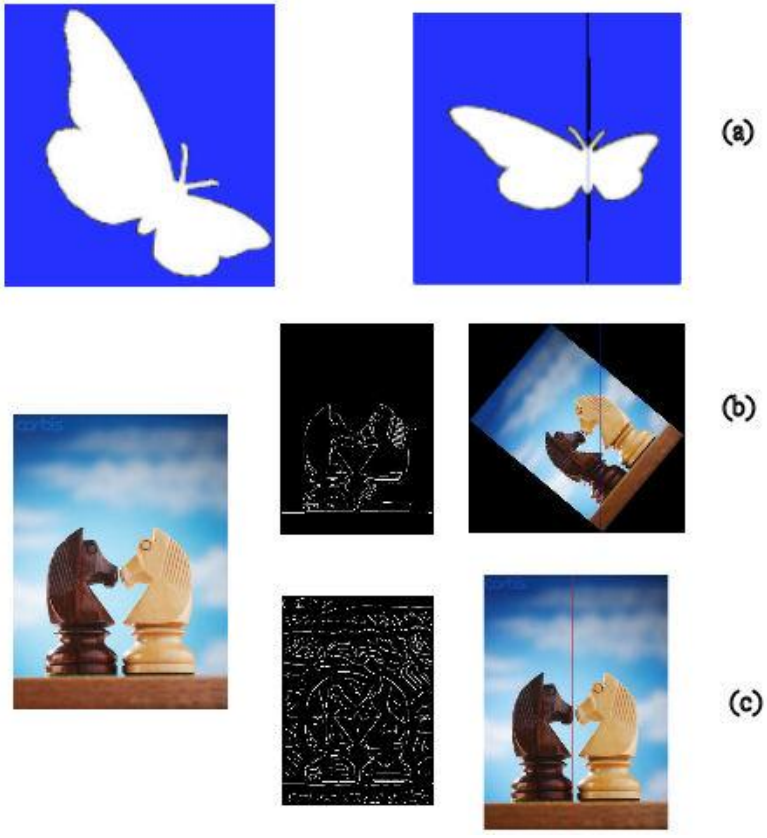

(b) Some interesting examples from the results.

Figure 2.25: Some failed or interesting results.

many previous approaches [231, 126, 175, 127, 181] tried to present ways of grouping feature points for discovering the underlying symmetries embedded in an image by a voting process. In the process, all pairs of feature points in the image plane are made to vote for their axes of symmetry, and these are grouped together to specify the prevailing symmetries presented in the image. This method is able to locate local symmetries and global symmetries on account of accumulated local support but sometimes fails to extract the globally dominant symmetry axis when the image contains strong local symmetries.

The theory is that letting the distance scale wider will invite strong local symmetries to make the cut, and local pairs will be strongly responsive to their local favorites. But this creates a problem. With more candidates, a candidate of symmetry axis will need fewer votes to win. So a local symmetry axis with a strong local following can tip the balance, even if, it isn't anywhere close to being the best axis of global symmetry.

Figure 2.26 provides a lucid example that sometimes the accumulated local contributions fall short of recovering a global symmetry. In Figure 2.26(a), the result of voting is rather uniformly populated into the map so that the local accretion offsets the balance in favor of a candidate with strong local aficionados, whereas Figure 2.26(c) demonstrates its desirable behavior.

We used an attention operator described in [181] and, for the purpose of globally probing the symmetry, employed a distance weight function with a large value of σ. Even more daunting is the fact that the object (butterfly) in the image is a bit off the perfect symmetry. Vigorous local symmetries and unconsummated

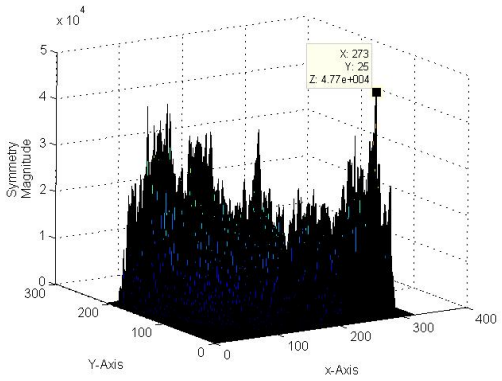

(a) Isotropic Symmetry Map of Generalized Symmetry Transform

(b) Corresponding Symmetry found

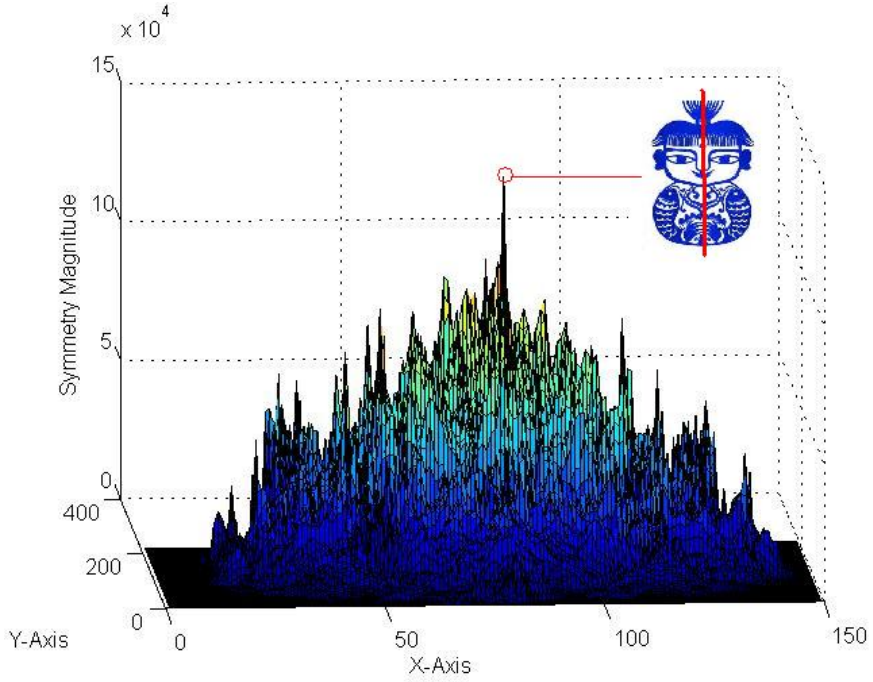

(c) An example that fares well to find the globally dominant symmetry axis

Figure 2.26: An example that fails to find the globally dominant symmetry axis.

global-symmetry structure inherent to natural objects compel many voting schemes to settle for the local winner.

2.3.5.7 Improving Segmentation

Continuous divergence measures could assign a value for each candidate area which stands for the degree of symmetry and interactively get involved with the iteration steps. Figure 2.27 shows the feedback of divergence measures to a segmentation procedure [143] that produces multiple edge maps that corresponds to the candidate areas. One of the main claims of this approach is that the "closeness" can best be explained from the perspective of entropy. The results also support the claim that the divergence measure can be used as a measure that compares different shapes.

2.3.5.8 The Curse of Dimensionality

When we use entropy divergence measures to find symmetry, the actual probability distributions over two partitions of an image are unknown. Then we calculate marginal and joint probabilities on every possible partition of the image from histograms since the measures treat the image as distributions of image features in 1D space. If we shift gears to process higher dimensional data structures, we expose ourselves to the infamous dimensionality curse phenomenon.

In this section, we either assumed that the features, e.g. angle and distance, are approximately uncorrelated in the dimensional space, or computed all joint

Figure 2.27: Symmetry used in evaluating segmentation results. Divergence values for each area: (a) 2.13, (b) 2.25, (c) 4.24, (d) 5.25

distributions. Our assumption of dimensional independence was vindicated by the results obtained. What if, however, the distributions are not normally distributed but correlated to each other? In that case, we need a way to transform the feature space into a new basis where each dimension is uncorrelated. Then the computation of the entropy divergence measures is reduced to projecting the data into the new axes and finding the sum of entropies on these d decoupled distributions by the property of independence in entropy.

Russakoff *et al.* [190] proposed a way to calculate high dimensional histograms on the assumption of normal distribution in $\Re^d$ with covariance matrix Σ_d as:

$$H_g(\Sigma_d) = \log((2\pi e)^{\frac{d}{2}} \det(\Sigma_d)^{\frac{1}{2}}). \tag{2.21}$$

Essentially what we are going to do in the future is to expand our approaches to objects in 3D or even in videos, and this equation will come in handy.

2.3.5.9 Symmetry and Scale

Symmetry has a property that preserves itself invariantly under some transformations, *e.g.*, rotation, translation, inversion and reflection. Amalie Emmy Noether states: Each symmetry of a system leads to a physically conserved quantity.

Unfortunately, the symmetry is not well preserved by the scaling factor. It is a typical problem of "Do you want to see the leaves or the tree". So we follow the change of symmetry on the scale and choose the most invariant one as a real axis of symmetry.

2.4 Conclusion

In this chapter, we have introduced two simple and fast symmetry detection algorithms (in Section 2.3.2 and 2.3.5) based on the line components in an image, and one trace transform based algorithm (explained in Section 2.3.4) that uses the area information of the image. The results show that the proposed algorithms seem to be all effective in finding local and/or global symmetries in images. Yet each approach has its own disadvantages as well as advantages.

For example, the TTS algorithm assumes that a well-segmented image would be given as an input and the image contains a single object. We also observe the following two drawbacks of the LBS: the worst-case time complexity is still quadratic on the number of points, and relatively minor perturbations can lead to the failure of global symmetry detection. The entropy based algorithm may produce many false positives and there is no guarantee that a simple addition of the two entropy values can deliver the global axis of symmetry.

In real-world images, symmetry is approximate: real objects seldom have perfect symmetry, and even perfectly symmetric objects fail to retain their symmetries when they are projected on the image plane. Consequently, we need a continuous value that represents the degree of symmetry.

A continuous symmetry measure can have intermediate values ranging from perfectly symmetrical to completely asymmetrical (we can set aside the psychological validity of the value for a while). It is crucially important when we fancy to use symmetry as a feature that manifests an inherent property of an image. Learning

symmetry and classifying objects by symmetric features are next to impossible if we do not have a measure that represents the degree of symmetry.

From the equation (2.9), it is clear that $H(X)$ is a continuous, positive, and concave function of $[0,1]^n \in R^n$ that maps to $[0,1] \in R$. $H(X)$ also features totality in that it sums over all the microstates the system can be in. That is why $H(X)$ is qualified as a global symmetry measure.

This chapter clearly manifests the divergence measures from the Shannon entropy fit the role of continuous symmetry measures as well as the strong tools for discovering symmetry in the image. In Chapter 3, we delve into a variety of symmetry measures and use them to find approximate symmetries.

Chapter 3

The Detection and Quantification of Approximate Symmetry

In this chapter we present a reliable and computationally efficient method to estimate bilateral symmetry (henceforth referred to as symmetry in this chapter) and compare various measures to compute the degree of it in an image. The principal postulate of the approach taken in this chapter assumes that the image of a bilaterally symmetric object carries two very similar and disjoint feature sets; thus, the problem of finding symmetry from the image is reduced to discovering an optimal bipartition of features embedded in the image so that the distributions of the feature values (*e.g.*, the probability density/mass functions) within each subset are bilaterally similar, and not necessarily identical, to each other. By using the distribution of image gradients, the proposed method estimates the two parameters of the axis of symmetry as two one-dimensional estimation problems, by first solving for the orientation, and then for the translational displacement of the axis. To evaluate the difference between two distributions, we investigate various measures that include but not limited to statistical distance measures, such as Jensen-Shannon divergence (a symmetrized Kullback-Leibler divergence), Bhattacharyya distance, and Matusita distance; and examine the accuracy of detection by each measure. We also provide an empirical comparison of the proposed scheme against another state-of-the-art symmetry detector on a new data set, in which we categorized symmetric

images according to two attributes: the naturalness of the image and the perfectness of the symmetry.

3.1 Introduction

By definition, asymmetries mean any deviations from perfect symmetry, *i.e.*, symmetry and asymmetry should be deemed mutually exclusive and, in consequence, a shape is either perfectly symmetric, or completely asymmetric.

This dichotomous categorization effectively obscures the fact that the assortment of shapes in the world, which has been hitherto considered as symmetric, rarely, if ever, retains perfect symmetry; for example, human faces and bodies are not by any means perfectly symmetrical.

The likelihood of asymmetry is further increased by inevitable real-world constraints: uneven illumination, occlusion, perspective distortion, and quantization distortion. We humans, however, get an impression of symmetry while not noticing the details, and correctly classify "smeared mirror symmetry" as symmetric if the amount of deviation from perfect symmetry falls within an allowable range [11].

The stark chasm between the rigorous definition of symmetry and approximate symmetry perception in humans is also found in computer vision literature. One line of research (hereinafter referred to as an "exact-solution/qualitative approach") is aimed at revealing symmetry through identifying non-empty finite set X on which a mirror (orientation-reversing) isometry $f : X \to X$ and distance function $d\colon X \times X \to \mathbb{R}$ are defined such that $\forall x, y \in X,\ d(f(x), f(y)) = d(x, y)$.

Since the Euclidean metric is the most widely used distance function, a set of pairs $< X_i, f_i >$ (or just a set of f_i) would be given as an exact solution.

If the number of pixels in an image is n, the number of all possible candidate sets X is extremely large at nearly 2^n. Fortunately, some local features, such as local edge gradient [33, 181, 175], edge points [4] or the keypoint descriptor [126] of SIFT (Scale Invariant Feature Transform) [125], provide useful information regarding the possible configuration of symmetry elements, and help reduce the number of comparisons required to retrieve symmetry parameters to $O(n^2)$. In the real world application, the equality constraint of isometry can be relaxed to an ϵ-isometry (or almost isometry) where $|d(f(x), f(y)) - d(x, y)| < \epsilon$ [111]. Some variants of this approach [31, 42, 43] allow even non-isometric symmetries (*e.g.*, symmetries in affine/Möbius/perspective transformations) which preserve cross-ratios.

The main thesis of this line of approaches is that the reflection f_i is a function depends only on the elements in X_i tightly conform to its mirror isometry constraints or, conversely, that the set X_i (usually a set of even number of points) serves as an impeccable evidence that the reflection f_i is the genuine solution. Accordingly, the elements aberrated from being perfectly symmetric with respect to the reflection f_i do not give any influence to the exact solution $< X_i, f_i >$ save the number of evidences ($|X_i|$) of the reflection f_i if they were supposed to belong to X_i.

Because of this equality constraint, the exact solution approach is reputed to be resilient to local disturbances as shown in Figure 3.1, and a voting scheme is commonly used to obtain the symmetry parameters [181, 126, 175] because the voting process is quite effective on sparse and noisy data sets [73].

Figure 3.1: Recovered symmetries from cluttered images. Symmetries are detected by the method described in [126].

For all of its advantages, there are two undesirable features worth considering that are inherent to symmetry detectors with the scheme described above. First, they are resilient against adverse background structures because they exhaustively sift through all possible pairs of elements considered (point-by-point comparison) to confirm $\forall x, y \in X_i,\ d(f_i(x), f_i(y)) = d(x, y)$ with time complexity $O(n^2)$ where n is the number of feature points. This computational complexity is barely adequate as the number n increases. Second, the equality constraint renders the qualitative approach to achieve very high precision but low recall in identifying relevant elements of X_i when a shape in an image exhibits some deviation from perfect symmetry. If the degree of departure from perfect symmetry is high enough to make $|X_i|$ for f_i dwindle away altogether, even an apparent global symmetry would not be distinguished from other trivial symmetries which do not need detection (Figure 3.2).

On the other hand, the second line of research [17, 101, 133, 136, 203, 204, 99, 249] (hereafter referred to as an "optimization/quantitative approach") determines an optimal solution f_o (in general, parameters of symmetry) from a solution space

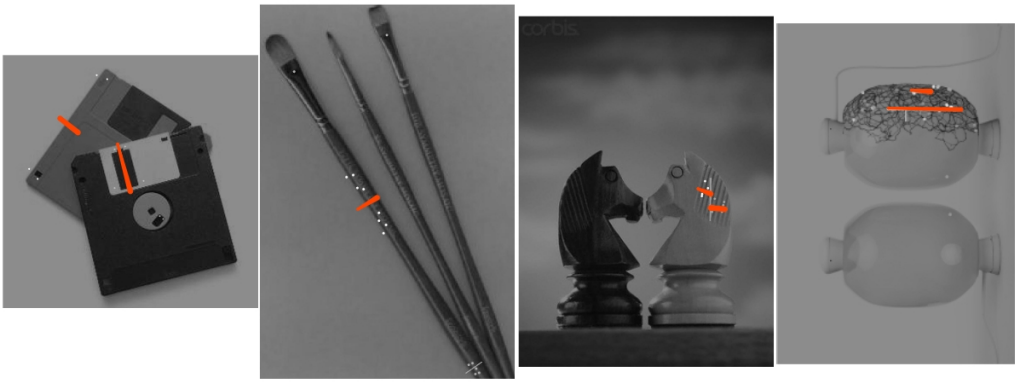

Figure 3.2: Recovered trivial symmetries over global symmetries from approximately symmetric shapes. Symmetries are detected by the method described in [126].

with,

$$f_o = \underset{f \in FS}{\arg\min}\ C(X, f, d). \tag{3.1}$$

Here FS is the set of feasible solutions given a non-empty finite set $X \in \mathcal{P}(I)$ from image feature data I, and $C(X, f, d)$ is the minimal cost function (or maximal utility function for coefficient of symmetry [133], correlation function [136, 203, 204] and a measure of symmetry [101]) of aforementioned X, a candidate solution f and a metric d: $M \times M \to \mathbb{R}$ on a set M (d can be a generalized metric). The term "quantitative" is disparate from the "amount" of symmetry in permutation groups [38] and somewhat similar to "the degree of a non-structural deviation from a perfect symmetry" [177].

The quantitative approach directs its attention to a way to weigh the "degree" of symmetry based on either the relation among the feature values [17, 32, 101, 133,

Figure 3.3: Detected symmetries encased in images – detected by our algorithm.

136, 196, 199, 203, 204, 99], or the minimum work to transform a given shape into a symmetric figure [249]. The optimal solution f_o, which mainly evinces a symmetry in the image (Figure 3.3. Compare this Figure with Figure 3.2), sometimes reflects a balanced distribution of visual weight that creates a harmonious connection between the corresponding elements across the f_o (Figure 3.4). Indeed, the visual cues of the two regions are obviously far from identical in Figure 3.4, but there is a easily recognized sense of equivalence between them. Osborne [155] adduces that the balance, or equivalence of weighting, around an axis is equated by the term "harmony".

For a given subset of image features X and a metric d, an ordered pair $(f_o, C(X, f_o, d))$ of the optimal solution and its corresponding cost denotes the most probable symmetry structure and its departure from an "optimal" symmetry, respectively. Note that the optimization approach does not impose any equality constraint to satisfy on X, and in consequence of that, the elements of features in X that do not agree with an optimal symmetry of an (symmetric) object embedded in the image unfavorably affect the measurement of the optimal symmetry (Figure. 3.5).

Figure 3.4: Detected balances framed in images – detected by the proposed algorithm. Balance is the sense of visual equilibrium and being called approximate symmetry on some occasions in view of carrying equivalent not identical forms side by side.

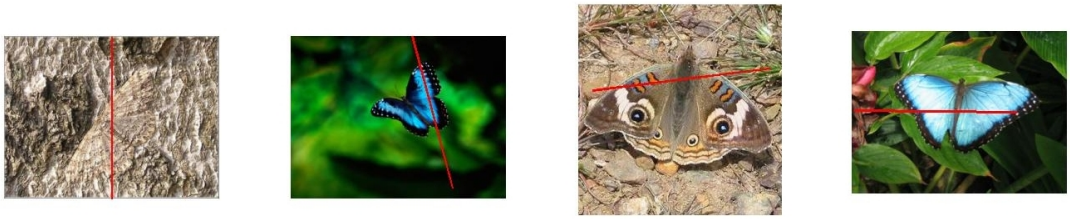

Figure 3.5: Erroneous symmetry detection in cluttered images – detected by the proposed algorithm.

For this reason, the optimization approach normally assumes the input to be an image that contains either a single object or a properly segmented object; otherwise, there are too many (2^n) possible choices for X to be investigated. Considering various segmentation algorithms[187, 143] consistently churn out possible candidate areas as intermediate results, the benefit of quantitative approach is apparent in many disciplines: object recognition [32], image segmentation [205], visual inspection, shape/scene representation and matching. Also pay attention to the word "optimal" instead of "perfect" in describing the exemplar representation of symmetry. The optimization approach in the absence of the isometry constraint carries its own optimal symmetry depends on the objective function $C(X, f, d)$ and the measure d, namely, the optimal symmetry can be different from an isometric symmetry.

By and large, each candidate solution $f_i \in FS$ divides the feature set X into two disjoint sets. Afterwards, a metric on the two sets provides a distance between them to moderate the dichotomous distinction between symmetry and asymmetry. It will give a null distance for reflectively equivalent sets and a positive value inversely proportional to the degree of equivalence for nonequivalent sets. This operation allows the definition of an approximate symmetry as a substantial degree of equivalence between the supposedly symmetrical halves having a close to zero distance with respect to a metric d. The crux of the optimization approach lies here: the metric should be discriminative enough to be used in accurate symmetry detection, and still be tolerant enough to overcome disruptions within the permissible range. The evidently preferred metrics are the Euclidean distance (the coefficient of

symmetry [133], the symmetry distance [169, 249, 253] and the measure of symmetry [101]) and distance correlation [136, 203, 204]. We hypothesize those metrics are not always the best choices, and hazard a guess that there are better metrics or measures that serve to uncover approximate symmetries more reliably and ultimately allow us to make a decision as to whether an object in an image is symmetrical or not. To the best of our knowledge, there has been no comprehensive and rigorous experimental investigation into the role of metrics in symmetry detection yet.

Like everything, different approaches come with their own pros and cons. The exact-solution approach is supposed to excel in dealing images with multiple and independent isometric-symmetries; the optimization approach is assumed to be superior in terms of deciding the most probable symmetries over the given image features. Thereby indiscriminate comparison of the two approaches seldom produces meaningful results. For instance, the comparison of the two symmetry detectors from each approach on a set of images with multiple symmetric objects might give reassurance that the exact-solution approach performs better against the optimization approach, but does not provide more relevant information on their capabilities unless the regions of interest are given to the optimization approach. We are of the opinion that the nature of the relation between these two approaches can better be characterized as complementary rather than competitive. For example, the false positive rate of the exact-solution approach is pretty high in a recent performance evaluation tests [161] and this issue can be resolved by employing the optimization approach that can evaluate the degree of symmetry on the detected region of interest [181].

Interestingly, in a recent seminal study on performance evaluation of symmetry detection algorithms [161], one of the exact-solution approaches [126] outperforms other algorithms [120, 201] in detecting discrete symmetries. Even an algorithm that requires a globally dominant symmetry axis uses this approach for region-based image segmentation [205]. Regrettably, however, the approximation approach [120] the performance evaluation study includes is not sophisticated enough to vie with the well-polished version of generalized symmetry transform (GST) algorithm [181] because fold-and-cut plan is not conceived for bilateral-symmetry detection per se.

In the previous chapter, We briefly introduced previous approaches center on the distance measure of symmetry or similarity. Without any a priori assumption or knowledge of the barycenter (the center of mass) [4], the search of the axes of symmetry is carried out in a two-dimensional parameter space: two orthogonal directions in Cartesian coordinates, or a radial (r) and an angular (θ) coordinates in the polar coordinates [4, 136, 133]. A sweep line algorithm is the bane of most, if not all, approximation models, seeing that we normally need $O(n)$ operations for each feasible solution f in Eq. 3.1 to compute the value of $C(X, f, d)$ where n is the size of image feature data. Section 3.2. specifies symmetry constraints we employ to reduce the number of feasible solution f to a constant number $O(1)$. We also articulate in the section that there are two caveats with this approach when the symmetry constraints are applied (other than the symmetry assumption, to wit, when the shape in the image is not symmetric, the constraints are to no avail). Section 3.3. details the algorithm to find f_o, and Section 3.4. enumerates summarily the measures used in the cost function $C(X, f, d)$. The evaluation results are given

in section 3.5.

3.2 Geometric Constraint of Symmetry

The ultimate goal of symmetry detector has been the estimation of the 1D parameter of the rotation and the 1D translation defining the axis of symmetry. To achieve this goal, many of the previous approaches are either fastidiously try to distinguish the exact values of the parameters by exploring every possible alternative (all matching pairs of features [181, 126] or all possible solutions [120]) or make an assumption on the position of the symmetry axis [203].

Our approach, however, divorces itself from the exacting (and computationally costly) task of precise "point-by-point matching" or "exhaustive searching", and instead imposes much relaxed symmetry-constraints, based on statistical measures without resorting to any parametric assumptions on the symmetry axis, to uncover rather apparent symmetry that is immune to small local perturbations of a symmetry structure.

3.2.1 Constraint of Symmetry Used in Exact-solution Approaches

The GST [181] uses an attention operator predicated on spatial position and gradient information. The algorithm is based on the isometric constraint, and in addition to that, a measure hinged on the similarity between local gradient structure is introduced. The additional measure, a phase weight function, prefers pairs of gradient orientations symmetrically congruent to each other and the intensities of

gradients are not decisive factors in the symmetry magnitude. The GST chalked its success up to its freedom from intricacy but the computational complexity comes with the territory: $O(n^2)$, where n is the total number of pixels in the image. Another improved version [126] of GST also consumes $O(N^2)$ though N is the total number of feature points determined by SIFT and sanguinely expect $N \ll n$.

3.2.2 Constraint of Symmetry Used for Rotational Parameter Recovery

The amount of time the exact-solution approaches expend encouraged us to come up with a more efficient algorithm that transform a line in the image to a point in other parameter space (in polar coordinate system) where we do not have to invent a new procedure to identify symmetry.

It is an educated (as well as mistaken) guess that, by the duality of points and lines in geometry, the barycenter in the Hough space defines the center of lines, hopefully the symmetry line, just like the barycenter in the Euclidean space represents the center of mass (the mean location of all the mass in a system).

Let us assume, just for the sake of argument, there are only two non-collinear line segments in the plane and both segments are of the same length. A genuine relation between two lines (l_1, l_2) and the line that bisects the angle between the two lines (l_c), which can make infinite number of congruent triangles between the lines (Figure 3.6), is defined in the Hough space as follows (see Section 3.8 for the proof):

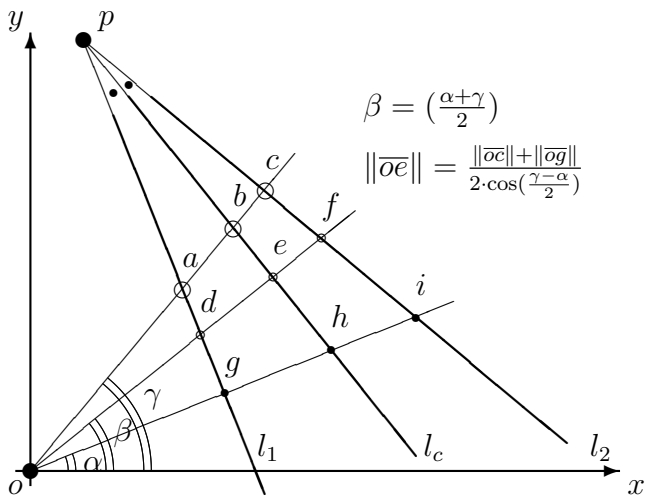

Figure 3.6: Relation between two lines l_1, l_2 and a line bisects the angle $\angle apc$ between them(l_c).

$$\theta(l_c) = \frac{\theta(l_1) + \theta(l_2)}{2}, \tag{3.2}$$

$$r(l_c) = \frac{r(l_1) + r(l_2)}{2 \cdot \cos(\frac{\theta(l_2)-\theta(l_1)}{2})} \tag{3.3}$$

, where $\theta(l_1) = \alpha$, $\theta(l_2) = \gamma$ and $\theta(l_c) = \beta$ in the Figure 3.6.

Although (Eq. 3.3) fails to deliver a linear equation we hoped, (Eq. 3.2) shows that the angular term is completely decoupled from the radial term so that we can recover the angle of symmetry axis independently. This is one of the instrumental geometric constraint that enables previous approaches [136, 203, 204] to retrieve the orientation of the symmetry axis with none of radial coordinate.

For an image $I(x, y)$, the gradient map of $I(x, y)$, $\nabla I(x, y)$, is defined as $\nabla I(x, y) = (\frac{\partial I(x,y)}{\partial x}, \frac{\partial I(x,y)}{\partial y})$. Then its polar angle function on the image Cartesian

coordinates (x, y) is defined by

$$\theta(x, y) = \arctan(\frac{\partial I(x, y)}{\partial x}, \frac{\partial I(x, y)}{\partial y}). \tag{3.4}$$

With a set of given number of data points $\theta(x, y)$, there are various statistical approaches to ascertain an estimate of the probability distribution $p(\theta)$ of a continuous variable θ. The oldest, simplest, and most successful approach is a non-parametric method that bins the data into k regular bins, normalize the bins and smooth the resulting histogram [164]. The parametric methods assume either likelihoods of $p(\theta)$ or its known parametric form and try to locate the best fit from the data $\theta(x, y)$. The mixture model that postulates data $\theta(x, y)$ are consist of multiple parametric distributions mixed in varying proportions can be used when $\theta(x, y)$ come from multiple objects or include significant amount of noises. Considering the nature of the optimization approach and the difficulty of estimating the likelihood of $p(\theta)$, we take a non-parametric approach. Section 3.3 contains the details of the approach we take in our implementation and its rationale.

Suppose now we consider the probability $p(\theta)$ as the relative frequency of very short line segments in an image with the same angular coordinate θ. In case that the θ_o is the angle of symmetry axis, by (Eq. 3.2),

$$p(\theta_o + \theta) = p(\theta_o - \theta),\ \forall \theta : 0 \leq \theta < \pi, \tag{3.5}$$

but the converse is not true. (Eq. 3.5) is the restatement of the the symmetry

constraint in (Eq. 3.2).

On the one hand, the symmetry constraint in (Eq. 3.5) and an estimate of the probability distribution $p(\theta)$ make it possible to get the exact orientation information at speed by properly averaging the $p(\theta)$, but on the other hand, the barycenter approach is very prone to numerical errors and outliers (see Section 2.3.1); accordingly, We use the cost function $C(I, \theta, d)$ identical in all important respects to [203, 204] as

$$C(I, \theta, d) = \int_0^{\pi} d(p(\theta + x), p(\theta - x))dx, \tag{3.6}$$

where d is one of the metrics specified in Section 3.4, and the orientation of the axis of symmetry θ_o is:

$$\theta_o = \underset{0 \le \theta < \pi}{\arg\min}\ C(I, \theta, d). \tag{3.7}$$

By (Eq. 3.6), a set of possible orientations of the axes of symmetry(Θ_o) for the input image I is:

$$\Theta_o = \left\{ \theta_i \middle| \frac{d}{d\theta} C(I, \theta_i, d) = 0,\ \frac{d^2}{d\theta^2} C(I, \theta_i, d) > 0 \right\}. \tag{3.8}$$

Also it is plain that $p(\theta)$ should be a periodic function with period π, that is $p(\theta + 2\pi) = p(\theta)$.

Actually, in real application, the integral operation in (Eq. 3.6) is approxi-

mated by a probability density estimate at discrete number of points covering the range of the data. For example, we can divide the range of θ, $(0, \pi)$, into n discrete intervals with increment $\frac{\pi}{n}$:

$$C(I, \theta, d) = \sum_{i=1}^{n-1} d\left(p(\theta + \frac{i}{n}\pi), p(\theta - \frac{i}{n}\pi)\right) dx. \tag{3.9}$$

Likewise, we can approximate Θ_o in (Eq. 3.8) by

$$\Theta_o(\epsilon) = \{\theta_i | C(I, \theta_i, d) < C(I, \theta, d),\ \forall \theta : |\theta_i - \theta| < \epsilon\}, \tag{3.10}$$

where $\epsilon > 0$ defines a given neighborhood.

We must take heed that some measures of the statistical distance between two probability distributions are defined without summing the pairwise differences between the corresponding points. Thereupon, let P_θ and Q_θ be two non-overlapping and non-empty partitions of a set $p(\theta)$ defined as follows:

$$\begin{aligned} P_\theta &= \left\{p(\theta_i) | \theta_i = \theta + \frac{i}{n}\pi, i = 1, 2, \ldots, n-1\right\}, \\ Q_\theta &= \left\{p(\theta_i) | \theta_i = \theta - \frac{i}{n}\pi, i = 1, 2, \ldots, n-1\right\}, \end{aligned} \tag{3.11}$$

where n has the same definition as in (Eq. 3.9). We define P_θ and Q_θ with the assumption that they share the same support. Now, the $C(I, \theta, d)$ for the metrics that take probability distributions of a discrete random variable θ can be computed:

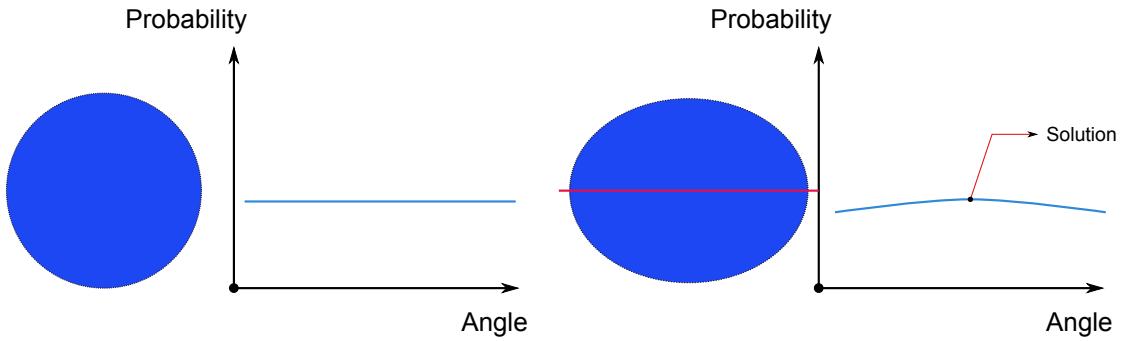

Figure 3.7: A potent problem of angular sweep on $p(\theta)$.

$$C(I, \theta, d) = d(rs(P_\theta), rs(Q_\theta)), \tag{3.12}$$

where the function rs denotes the rescale operation that makes probabilities of P_θ and Q_θ add to 1 respectively with the presumption that they have the same bounded (and reflectively symmetric) support as above, so that we do not have to re-estimate the probability distribution for each P_θ and Q_θ.

A possible drawback of this approach is its sensitivity to noise when the input has the shape of a circle or an ellipse (Figure 3.7). The probability distribution of $p(\theta)$ on these shapes is rather flat in shape and a seemingly small perturbation tip the balance and may turn an obviously implausible direction into a strong candidates. This is the common weakness of the approach. If the optimal solution is not so prominent and conspicuous in the feasible solution space, it can be buried among the surrounding outliers.

The time complexity of the algorithm is $O(n_\theta^2)$ where n_θ is the number of discrete intervals covering the range of the data if the metric d takes constant time

on the given two elements.

3.2.3 Two caveats

The optimization framework to design a 1D structure established on geometric constraints of symmetry is a pretty efficient way of recovering the orientations of symmetry axes accurately, but comes with two caveats: First, the image gradient direction is not always consistent even when its edges are. Second, edges with gradient direction parallel to the symmetry axis should be handled with care.

In general, two edges can have the same direction and their gradient orientations are opposite each other. This property comes in handy when we apply the symmetry constraint to the corresponding image gradients across the axis of symmetry. We cannot, however, anticipate images to be maintaining clear contrast between the background and the foreground objects such that edge gradients between the the symmetrically corresponding edges always hold the constraints in (Eq. 3.5). In addition to that, synthetically generated features, black and white sketch images, signs and logos often consist of black-and-white lines only. The two rectangles on the left in Figure 3.8 have the same shape, yet different set of image gradient orientations. To correct this inconsistency, we change the orientation range from $[0, 2\pi]$ to $[0, \pi]$, namely, $p(\theta) = p(\theta + \pi)$. As a result of this change, the same pairs of gradient orientations are compared to each other at θ and $\theta + \frac{\pi}{2}$. (see Section 3.9 for the proof). This adjustment will double the size of the candidates, but does not affect the order of the time complexity of the algorithm.

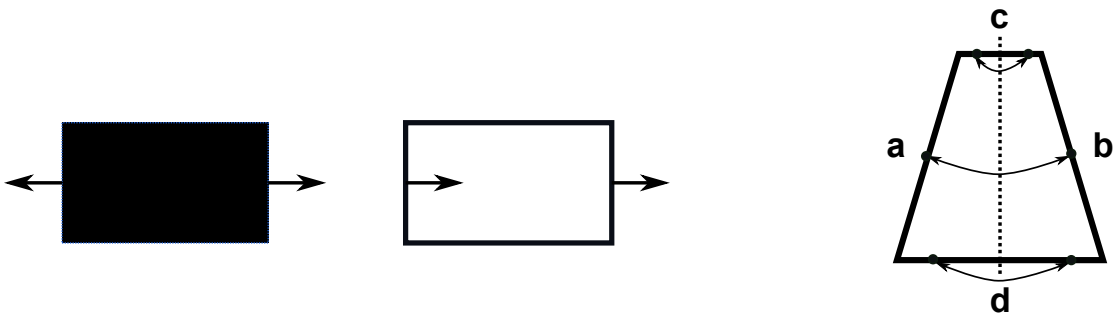

Figure 3.8: The two caveats of the symmetry constraint. Two rectangles on the left are of the same shape but of different pairs of image gradients. A trapezoid on the right has two sides c and d that are not symmetrically related to each other.

The edges with gradient direction parallel to the axis of symmetry (c and d in Figure 3.8) are the symmetrical counterparts not by the gradient orientation, but by the location of the edges. A trapezoid on the right in Figure 3.8 has two sides c and d, and these two line segments are not symmetrically related to each other; the edges in each line segment are symmetrical to each other by the distance from the axis of symmetry (the dotted line). Considering we do not have the distance information yet, we opt for ignoring them. Observe that ignoring them does not impose any penalties on the cost function $C(I, \theta, d)$ and at least some portion of the edge population influences the $C(I, \theta, d)$ by the smoothing bandwidth of kernel density estimation.

3.2.4 Constraint of Symmetry Used for Translational Parameter Recovering

The cosine term in the divisor in (Eq. 3.3) foils the barycenter approach or the optimization approach like in (Eq. 3.7). Now that we have the value of $\theta(l_c)$, the value of $\theta(l_2) - \theta(l_1)$ can be calculated easily:

$$\frac{\theta(l_2) - \theta(l_1)}{2} = \theta(l_c) - \theta(l_1) = \theta(l_2) - \theta(l_c). \tag{3.13}$$

Let the value in (Eq. 3.13) be θ_h and rewrite the (Eq. 3.3):

$$r(l_c) = \frac{\frac{r(l_1)}{cos(\theta_h)} + \frac{r(l_2)}{cos(\theta_h)}}{2}. \tag{3.14}$$

(Eq. 3.14) is another geometric constraint of symmetry, and immediately the problem of finding $r(l_c)$ looks very similar to discovering $\theta(l_c)$. However, the $cos(\theta_h)$ gives rise to the problem of unbounded values in (Eq. 3.14), just like the slope parameter of a line have to brace itself for the infinite value from a vertical line. We may have several different ways available to remedy this problem, such as treating the unbounded values as special cases (they are parallel lines) or just disregarding them. None the less, the problem still persists however expedient the correction may be. First, the $r(l_c)$ is not stable in the "vicinity" of a point $\theta_h = \frac{\pi}{2}$. Second, a trapezoid on the right in Figure 3.8 shows that $r(l_c)$ is swayed by edges in c and d that should be canceled out.

The adopted solution for this situation is the change of parameter space. We

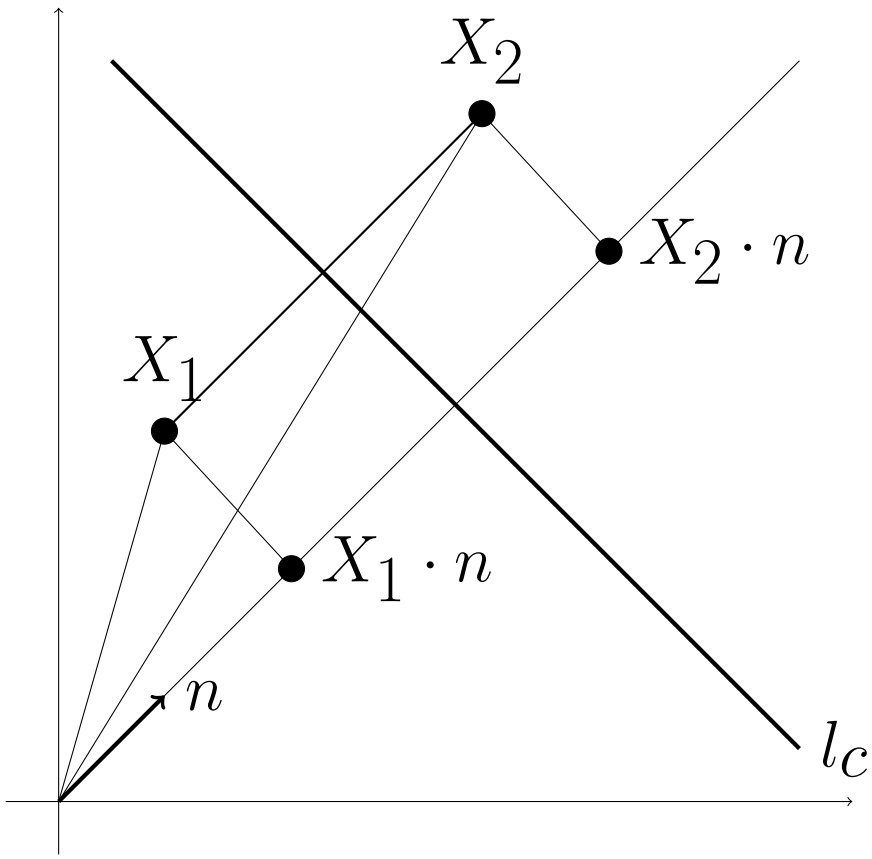

Figure 3.9: Symmetry constraints on the translational displacement $r(l_c)$.

decide it is better to use a different parameter and go back to a Cartesian coordinate system and calculate the translation parameter. Along the candidate normal unit vector $\mathbf{n}$ for θ , the line l_c sweep the Cartesian plane through (Figure 3.9). The geometric constraint of symmetry between two points X_1 and X_2 is:

$$r(l_c, \theta) = \frac{X_1 \cdot \mathbf{n} + X_2 \cdot \mathbf{n}}{2}. \tag{3.15}$$

From a geometric point of view, it means rotating the image so that the symmetry axis is placed orthogonal to x-axis, and obtain the x-coordinates of the

image gradients. Also note that the distance between the symmetry axis and the origin does not change under pure rotation around a point of origin, and similarly the angle of symmetry axis does not change under pure translation.

$p(r, \theta)$ also defines the probability distribution of a continuous variable r given θ and if $r_o(\theta)$ is the distance of symmetry axis from origin:

$$p(r_o + d, \theta) = p(r_o - d, \theta), \forall d : -d_{img} < d < d_{img}, \tag{3.16}$$

where d_{img} is the length of the image diagonal and $p(r, \theta) = 0, \ \forall r : r \leq -d_{img}, \ r \geq d_{img}$.

In the same way,

$$C(I, r(\theta), d) = \int_{-\infty}^{\infty} d(p(r + x, \theta), p(r - x, \theta))dx, \tag{3.17}$$

and the distance of symmetry axis from origin $r_o(\theta)$ is:

$$r_o(\theta) = \underset{-d_{img} < r(\theta) < d_{img}}{\arg\min} \ C(I, r(\theta), d). \tag{3.18}$$

By (Eq. 3.17), a set of possible translational displacements of the axes of symmetry ($D_o(\theta)$) for the input image I is:

$$D_o(\theta) = \left\{ r_i(\theta) \middle| \frac{d}{dr(\theta)} C(I, r_i(\theta), d) = 0, \right. \\ \left. \frac{d^2}{dr(\theta)^2} C(I, r_i(\theta), d) > 0 \right\}. \tag{3.19}$$

Unlike $p(\theta)$, $p(r, \theta)$ is not a periodic function, and we have to define a reasonable range for $r(\theta)$ in (Eq. 3.18), instead of $(-d_{img}, d_{img})$. Let $r(\theta)$ be a random variable represents the scalar projection of image points onto the normal unit vector $\mathbf{n}$ of θ with an expected value μ and a variance σ^2. By the Chebyshev's inequality, less than or equal to 50% of the of the values lie outside of the interval $\mu - \sqrt{2}\sigma \leq r(\theta) \leq \mu + \sqrt{2}\sigma$, and we choose to use this interval for the radial sweep in order to make sure it does not miss a feasible solution that corresponds to an axis of perfect symmetry.

The choice of the sweeping interval, $(\mu - \sqrt{2}\sigma, \mu + \sqrt{2}\sigma)$, inevitably invites us to contemplate a way to make two probability distributions for the metric d. In (Eq. 3.11), we suppose a random variable with the same closed support so that the support of each distribution is contained in the interval $(0, \pi)$, that is to say that regardless of the picking of θ, the support of the distribution is always $(0, \pi)$ thanks to the periodicity of the function $p(\theta)$. Now the selection of a candidate solution $r(\theta)$ in (Eq. 3.18) divides the domain of the probability distribution function $p(r, \theta)$ (range of a random variable r given θ into $(r_{MIN}(\theta), r(\theta))$ and $(r(\theta), r_{MAX}(\theta))$, and

two sets of ranges are usually not equal in size.

There are many different ways to translate distributions using scale and translation parameters in order that their support is enclosed in a fixed interval $(0, k)$. For instance, in (Eq. 3.20), we can choose the smaller of the two sets of ranges and cut out the larger to rebalance ($R_1 = R_2 = \min(r(\theta) - r_{MIN}(\theta), r_{MAX}(\theta) - r(\theta))$), pick the larger of the two and pad the range of the smaller with extra zeros ($R_1 = R_2 = \max(r(\theta) - r_{MIN}(\theta), r_{MAX}(\theta) - r(\theta))$), or leave them as they are ($R_1 = r_{MAX}(\theta) - r(\theta)), R_2 = r(\theta) - r_{MIN}(\theta)$). Ensuingly, we choose the larger of the two and pad the range of the smaller with extra zeros.

$$
\begin{aligned}
P_{r(\theta)} &= \left\{ p(r_i, \theta) | r_i = r(\theta) + \frac{i}{k} R, i = 1, 2, \ldots, k \right\}, \\
Q_{r(\theta)} &= \left\{ p(r_i, \theta) | r_i = r(\theta) - \frac{i}{k} R, i = 1, 2, \ldots, k \right\},
\end{aligned} \tag{3.20}
$$

where $R = \max(r(\theta) - r_{MIN}(\theta), r_{MAX}(\theta) - r(\theta))$. The rationale for choosing R is approximate symmetry we want to recover is closer to perfect symmetry than affinely distorted symmetry. Please note that the time complexity of this step is only $O(k\sigma)$. If selecting multiple candidates for multiple symmetry axes is more appropriate, *e.g.*, identifying all the possible symmetry axes, we can employ all three values of R at the cost of $O(k\sigma)$.

We can observe the computational complexity of this algorithm is $O(k\sigma)$ where k is the number of discrete intervals in $(0, k)$ that serves as a common support of the probability distributions for the metric d, and σ is a standard deviation of the $r(\theta)$.

At this point, we are having Θ_o and for each $\theta_i \in \Theta_o$, $D_o(\theta_i)$. A set of ordered pairs $(\theta_i, r_j(\theta_i))$ represents the set of plausible solutions $PS \subset FS$ in (Eq. 3.1).

3.2.5 2D Constraint of Symmetry for Decision of Parameters

For a given solution $(\theta_i, r_j(\theta_i)) \in PS$, we may impose additional 2D constraints using the value of the gradient as input. We can either match pairs of image gradient points (a tightened constraints in 1D space) or use the summed statistics of the two regions in a bipartite image (a relaxed-constraints in 2D space based on the probability distribution defined on the value of the gradient). In our implementation we select the former one. The corresponding point, X_c, of each image point X can easily be found by:

$$X_c = X + 2(r_j(\theta_i) - X \cdot \mathbf{n})\ \mathbf{n}. \tag{3.21}$$

(Refer Figure 3.9).

(Eq. 3.21) is the 2D constraint of symmetry and the metric d computes $d(X, X_c)$ to decide the f_o in (Eq. 3.1), the optimal solution. Let $f_{i,j}$ be $(\theta_i, r_j(\theta_i))$:

$$C(I, f_{i,j}, d) = \int_{X \in I} d(X, X_c)\, dX, \tag{3.22}$$

and the f_o is

$$f_o = \underset{f_{i,j} \in PS}{\arg\min}\ C(I, f_{i,j}, d). \tag{3.23}$$

This step requires order of $O(n)$ time complexity, where n is the number of elements in the image with gradient magnitude greater than the threshold given. Another good cost function $(I, f_{i,j}, d)$ would be symmetrized Chamfer distance. As the matching parameter f_o is already fixed, the matching cost is also set at $O(n)$.

While we appreciate the fact that we cannot completely guarantee the set of plausible solutions PS contains the globally optimal solution (the corruption of the data sometimes occasions the distortion of symmetry structure) and the globally optimal solution is guaranteed to be found in $O(n\, n_\theta\, d_{img})$, if one exists, the constraints we adopt in this section are the very beneficial and suffice to find most approximate symmetries in an image (our experiments showed that it is almost always the case). The justification of this approach is based on the saliency of the orientation [184] that retinal disorientation has an adverse effect on recognition. Our claim is if human-labeling decides ground truth (the word approximate is somewhat subjective), angular displacement is more critical than distance aberration. Furthermore, a complicated coupling of the angular and the radial components in measuring the loss of symmetry does not guarantee better performance, inasmuch as we do not know perceptual thresholds and weights of factors affecting asymmetry discrimination [206].

Thus, to sum up the complexity of the complete algorithm, the solution is guaranteed to be found in $O(\max(n, n_\theta^2, k\sigma))$ if one exists.

It should also be stressed that usable features are not restricted to the gradient image specified here. Pixel gradients, raw pixel values, filtered pixel information and/or any other information of the image can be used as a feature as long as the

feature can provide a probability distribution.

3.3 Algorithm

Figure 3.10 and Algorithm 2 explains the process of finding rotational parameter, θ, of symmetry axis.

The first step in distinguishing symmetry from a given image is to recover the set of rotation parameters Θ_o in (Eq. 3.10). Algorithm 2 specifies a way to detect a set of candidate rotations from the probability of edge orientations given edge responses computed by an edge detector. We used the Canny edge detector for this purpose, however, note that a better edge detector usually leads to better results.

Algorithm 2 Find rotational parameter θ of symmetry axis.

$[e,\ o] \leftarrow CannyEdgeDetector(Image)$
{e: Edge Strength Image, o: Orientation Image}
for all i such that $e_i \geq$ threshold **do**
  Add o_i to the list O {O: Viable orientation}
end for
$P_{KDE} = KDE(O)$
{$KDE(O)$: Kernel density estimation on O}
for $i = 0$ to $\frac{\pi}{2}$ **do**
  $C_l(i) = C(P_{KDE}, i, d)$
  {$C(P_{KDE}, i, d)$: Cost function, d: Metric}
end for
$OC \leftarrow indices(localMinima(C_l))$
{OC: A set of plausible candidates of θ }

Algorithm 3 $C(\theta, f, d)$: Cost function. θ: A candidate angle, f: An output of Kernel density estimation, d: A metric for cost calculation.

for $i = 0$ to $i < \frac{\pi}{2}$ **do**
  $C \leftarrow C\ +\ d(f(\theta + i), f(\theta - i))$
end for
Return C

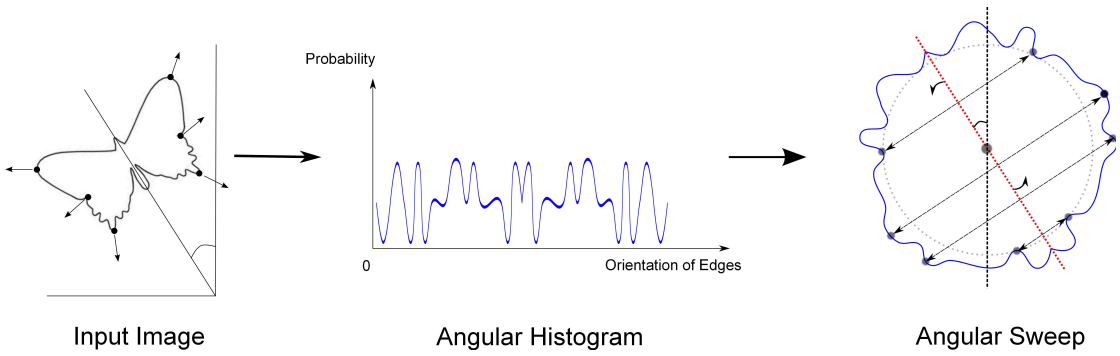

Figure 3.10: Algorithm of recovering symmetry angle(θ)

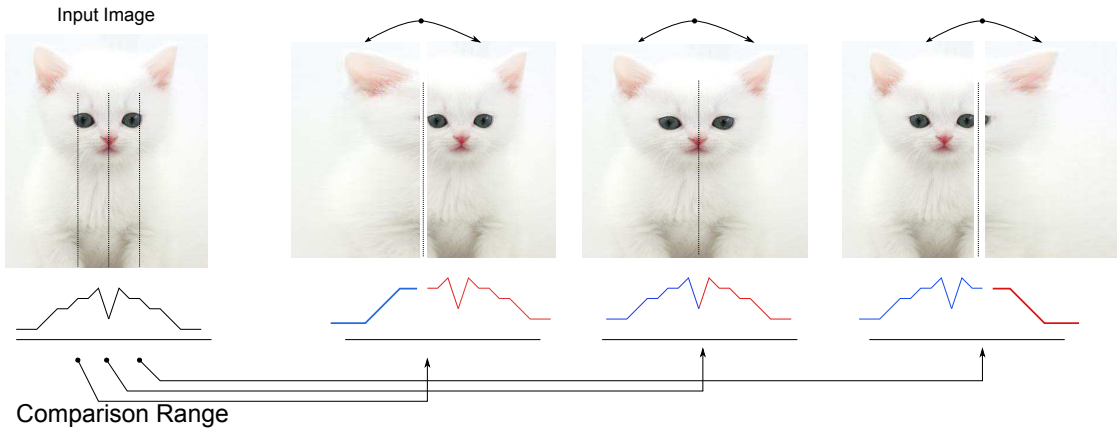

Figure 3.11: Algorithm of recovering the radius of axis of symmetry r_{sym} with scale the ranges up or down to fit.

For each rotational angle θ from OC in Algorithm 2, we compute possible candidates ($r_i(\theta)$) for the position of the symmetry axis. Algorithm 4 explains the process of finding the position (radius r) from the probability distribution of edge distances.

Figure 3.11 shows the case when we decide to compare each region assuming that both sides are equivalent (case of $method = 3$ in Algorithm 5)

Finally, in a last step, we check for every possible candidate solution, a con-

Algorithm 4 Find translational parameter r of symmetry axis along the given angle θ (or unit normal vector $\mathbf{n}$).

Require: *method*: Range Comparison Method
  for all i such that $e_i \geq$ threshold **do**
    Add $X_i \cdot \mathbf{n}$ to EL
    {$\mathbf{n}$: unit normal vector of θ}
    {EL: List of edge distances}
  end for
  $P_{KDE} = KDE(EL)$
  {$KDE(EL)$: Kernel density estimation on EL}
  $d_{min} = \min(f)$; $d_{max} = \max(f)$;
  $\mu = mean(f)$; $\sigma = \sigma(f)$
  for $i = \mu - \sqrt{2}\sigma$ to $\mu + \sqrt{2}\sigma$ **do**
    $CR \leftarrow range(d_{min}, d_{max}, i, method)$ {CR: Comparison Range}
    $C_l(i) = C(P_{KDE}, i, d, CR)$
    {$C(i, f, d)$: Cost function, d: Metric}
  end for
  $OC \leftarrow indices(localMinima(C_l))$
  {OC: A set of plausible candidates of θ }

Algorithm 5 *range*: Range function. d_{min}: minimum index, d_{max}: maximum index, idx: current index, *method*: 1(Choose smaller range), 2(Choose larger range), 3(Keep the ratio).

  $range_{min} = \min(idx - d_{min}, d_{max} - idx)$
  $range_{max} = \max(idx - d_{min}, d_{max} - idx)$
  if $method = 1$ **then**
    Return $(range_{min}, range_{min})$
  else if $method = 2$ **then**
    Return $(range_{max}, range_{max})$
  else
    Return (d_{min}, d_{max})
  end if

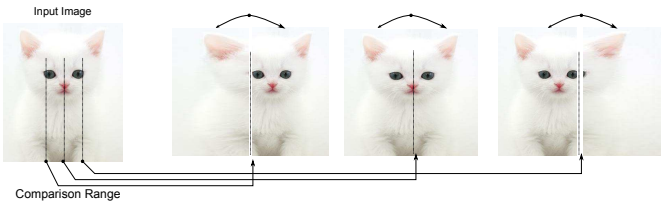

Figure 3.12: Algorithm of recovering the axis of symmetry((r_{sym}, θ_{sym})) with scale the ranges up or down to fit.

straint on the strength of the gradient to find the best symmetry axis. As described in Section 3.2.5, we define the cost function for a candidate solution $f_{i,j}$ as the sum of distances between all corresponding point pairs (Eq. 3.22). We employ 5×5 Gaussian blur (with $\sigma = 1.0$) on the gradient map $\bigtriangledown I(x, y)$ (in order to decrease the influence of noise and increase the chance of recovering the genuine approximate symmetry)

Figure 3.12 shows 3 snapshots pertaining to the calculation of 2D cost function, and illustrates a way of matching by stretching the smaller-sized image patch to fit.

3.4 Measures of Symmetry

In many areas of science and engineering, especially in the computer vision community, deciding "how close or distant two distributions are" is a very important issue. A variety of measures have been proposed for estimating similarity and dissimilarity between images based on statistics of image features, such as image gradient orientations.

Every once in a while a symmetric object in an image is construed as a pair of

identical objects disposed facing each other and juxtaposed in the region of it [64]. Then the problem of finding symmetry is reduced to discovering two similar objects placed side by side in the image, to wit, if we can find two disjoint sets of features that share common reflective attributes with each other, we will be able to identify the location of a symmetric object as well as its characteristics of symmetries. The most important operations here are bipartition of the feature values and measurement of similarity/dissimilarity between these two sets.

Certainly there are subtle differences between measuring image similarity and symmetry. Since two objects are very closely bound together in the same scene in the case of symmetry, we can ignore any transformation between them except the reflection. So if the partition part can give us reliable information on the symmetry axis, we will have much higher degree of similarity between them.

In this paper eight different measures are presented to evaluate the degree of (a)symmetry. Manhattan distance, also known as L_1 distance, is adopted to establish a baseline for the other measures and to give a general idea of how different the two distributions are from each other.

3.4.1 Jensen-Shannon divergence

We employ Jensen-Shannon divergence [116], $D_{JS}(P, Q)$, to measure the difference between two probability distributions P and Q of a discrete random variable, described in Eq. 2.14.

$D_{JS}(P, Q)$ does not occasion a special case when it is computed as in the case

of Kullback-Leibler measure [106] and has several other desirable properties, *e.g.*, non-negativity, boundedness($\leq ln(2)$) and the square root of $D_{JS}(P,Q)$ is a metric [116]. One study found that Jensen-Shannon divergence is superior to Cramér-von Mises test and the Kolmogorov-Smirnov test (K-S test) [176]

3.4.2 Symmetric Chi-squared Divergence

The value of the χ^2 test-statistic is

$$\chi^2 = \sum_{i=1}^{n} \frac{(O_i - E_i)^2}{E_i} \tag{3.24}$$

where O_i is the observed counts of category i, E_i is the expected counts of category i, and n is the number of categories. In symmetry detection, we cannot tell the observed distribution from the expected one, so we modify the original χ^2 test-statistic (3.24) into symmetric χ^2 divergence:

$$\chi_s^2 = \sum_{i=1}^{n} \frac{(O_i - E_i)^2}{O_i + E_i}.$$

3.4.3 Bhattacharyya distance

At first, the Bhattacharyya distance [20] measures the geometric similarity of two discrete or continuous probability distributions and closely related to the Bayes error estimation. For discrete probability distributions P and Q over the domain X,

it is defined as:

$$D_B(P,Q) = -\ln\left(\sum_{x\in X}\sqrt{P(x)Q(x)}\right), \tag{3.25}$$

and the cosine-like term $\sum_{x\in X}\sqrt{p(x)q(x)}$ is called the Bhattacharyya coefficient, BC ($0 \leq BC \leq 1$ and $0 \leq D_B \leq \infty$). D_B does not obey the triangle inequality (so D_B is not a metric), but the Hellinger distance $\sqrt{1-BC}$ does obey the triangle inequality. It is known that if two distributions P and Q are normal, Jensen-Shannon divergence is equal to Bhattacharyya distance up to a constant scale [39].

Previous studies [83, 84] show Bhattacharyya distance performs "noticeably" better than the L_1 and L_2 norms.

3.4.4 The Matusita distance

The Matusita measure [137] between two probability distributions P and Q is given by:

$$\begin{aligned} D_B(P\|Q) &= \int\left(\sqrt{P(x)} - \sqrt{Q(x)}\right)^2 dx \\ &= 2 - 2\int\sqrt{P(x)\cdot Q(x)}\, dx, \end{aligned}$$

where x describe the whole space and $\int\sqrt{P(x)\cdot Q(x)}\ dx$ is the same as Bhattacharyya coefficient,BC, in 3.4.3. Since the Bhattacharyya term is symmetric and invariant to scale, the Matusita distance also symmetric and scale invariant.

3.4.5 Difference of Shannon's Entropy

This measure is introduced to show the extreme type of measure that does not need any alignment of the two given probability distributions P and Q.

$$
\begin{aligned}
D_B(P\|Q) = \|H(P) - H(Q)\| = \\
\|\sum_{i=1}^{n} P(x_i)\log_b \frac{1}{P(x_i)} - \sum_{i=1}^{n} Q(x_i)\log_b \frac{1}{Q(x_i)}\| \\
= \|\sum_{i=1}^{n} Q(x_i)\log_b Q(x_i) - \sum_{i=1}^{n} P(x_i)\log_b P(x_i)\|,
\end{aligned}
$$

3.4.6 Cosine Distance

The cosine distance between two vectors gives the angular distance between them. By the definition of the scalar product ($\mathbf{a}\cdot\mathbf{b} = \|\mathbf{a}\|\,\|\mathbf{b}\|\cos\theta$), the angle ($\theta$) between two vectors $\mathbf{a}$ and $\mathbf{b}$ is:

$$\theta = \arccos\left(\frac{\mathbf{a}\cdot\mathbf{b}}{\|\mathbf{a}\|\,\|\mathbf{b}\|}\right).$$

Sometimes the cosine value of the θ ($\frac{\mathbf{a}\cdot\mathbf{b}}{\|\mathbf{a}\|\|\mathbf{b}\|}$) is used to represent the similarity of the given two vectors $\mathbf{a}$ and $\mathbf{b}$ (cosine similarity).

The cosine distance can have a value from the range $[0, \pi]$ where π means the opposite angle (the longest distance), and 0 means the same angle (the shortest distance). It is known to be less applicable for non-orthogonal vector space.

3.4.7 The Earth Mover's Distance (EMD) [189]

One critical problem of the previous distance measures, except the difference of Shannon's entropy, is the assumption that when a distribution is superimposed on the other, they are well-aligned to each other. This strong presumption of alignment reminds us of the isometry constraint in the exact-solution approach.

The Earth Movers Distance (EMD) [189] is a well-studied cross-bin distance used in the analysis of dissimilarity between two distributions over a region D. This distance is considered more robust than other histogram matching algorithms for the reason that it does not suffer from arbitrary quantization problems attributable to the fixed binning. The EMD provides for partial matching, and can be applied to signatures with different sizes [188].

It reckons the minimal cost required to reconstruct one distribution into another based on a solution to the well-known transportation problem [79].

Given two histograms P, Q the EMD is:

$$EMD(P,Q) = \frac{\min_{f_{ij}} \sum_{i,j} f_{ij} d_{ij}}{\sum_{i,j} f_{ij}}. \tag{3.26}$$

with the following constraints:

$$f_{ij} \geq 0 \qquad sum_j f_{ij} \leq P_i, \qquad \sum_i f_{ij} = Q_i \ , \tag{3.27}$$

where f_{ij} denotes a set of flows that stands for the amount transported from the i-th supply(or the the first signature) to the j-th demand(or the second signature).

The cost d_{ij} is the ground distance between the i-th supply and j-th demand.

To compare two histograms (or signatures that subsume histograms) with the EMD, one must define a distance between features, which is interpreted as the cost of turning a unit mass of one feature into a unit mass of the other. The EMD between two signatures is then the minimum cost of turning one of them into the other.

It does not penalize harshly for the non-exact matchings between the distributions by allowing shifts of mass/density within each distribution. When a mass of earth is scattered over an area of space where a set of empty holes are also dispersed, the EMD measures the minimum amount of work needed to fill the holes with soil. The amount of work is usually computed by multiplying the ground distance by the weight of earth (or the amount of flow) that should be moved along the distance to fill the holes.

This concept is deemed as a natural measure to compare two probability distributions with the same support, especially one distribution is derived from the other by small perturbations, the very definition of approximate symmetry. However, its high computational complexity $O(N^3 \log N)$, where N is the number of feature clusters, prevents itself from being widely used in multidimensional feature clusters. We use EMD only for the rotational parameter recovery due to this computational concern.

3.5 Experiment and Result

A new dataset includes 1051 images, and each of the images holds at least one symmetric structure in it. Out of this dataset we used 693 images that do not contain multiple symmetric objects. The images were obtained from the Microsoft Research Cambridge (MSRC) dataset, the PASCAL Visual Object Classes (VOC) Challenge, the MPEG-7 CE Shape-1 Part-B data set and the web. Each symmetric image was examined carefully by eyes so that there was not a disproportionate share of similar objects (such as butterflies and human faces). The gathered images were then classified and renamed into our own nomenclature. For the evaluation, the images were classified by two attributes. The first attribute has two values and distinguishes "Natural" vs "Synthetic" images, and the second attribute is concerned with the deviation from perfect symmetry and distinguishes into three subordinate groups: "Perfect", "Approximate" and "Clutter".

To evaluate the different methods, we used a computationally defined measure. The evaluation only considers whether the axis of symmetry has been computed correctly or incorrectly. Human labelers who understood the concepts of symmetry were instructed to label ground-truths using a tool developed by us. The angular term θ and the radial term r were stored while they were identifying an axis of symmetry.

When an algorithm presents information on the prevailing axis of symmetry, a program computes its (θ_{sol}, r_{sol}) tuple and evaluates it by the percentage of the distance from the correctly estimated axis of symmetry (PDCeS) that is defined as

follows:

When an algorithm presents information on the prevailing axis of symmetry, a program computes its (θ_{sol}, r_{sol}) tuple and evaluates it by the percentage of the distance from the correctly estimated axis of symmetry (PDCeS) that is defined as follows:

$$PDCeS_{m,n}(sol, GT) =$$

$$\begin{cases} 0 \quad \text{if } \exists\, i:\ 200\frac{\|\theta_{sol}-\theta_{GT(i)}\|}{\pi} \leq m, \\ \qquad\qquad\quad 100\frac{\|r_{sol}-r_{GT(i)}\|}{\|ImgDiag\|} \leq n \\ 1 \quad \text{Otherwise,} \end{cases} \tag{3.28}$$

where $sol = (\theta_{sol}, r_{sol})$, $(\theta_{GT(i)}, r_{GT(i)}) \in GT$ is an $i-th$ elements of a ground-truths set GT and $\|ImgDiag\|$ denotes a diagonal of an image. Whenever the PDCeS generates a value '1', the count of false negative (FN) is increased by 1. Likewise, the count of true positive (TP) gets increased by 1 if the PDCeS results in '0'. By definition, $\|\theta_{sol} - \theta_{GT(i)}\| \leq \frac{\pi}{2}$.

Fig. 3.16 shows the false negative rate that indicates the rate the algorithm failed to detect the actual axis of symmetry under $PDCeS_{4,3}$(within $\pm 3.6°$ and $\pm 3\%$ of a diagonal of the ground truth).

3.6 Discussion

First, there was a parameter not fixed before the evaluation. Figure 3.13 shows different profiles of edge orientations with different bandwidth values of KDE. Before applying KDE, the distribution is too spiky to compare reliably (look at the angle around 90 degree - true orientation parameter of symmetry axis). If we apply too broad bandwidth, the profile's discriminability is significantly damaged. Therefore, we tested 120 symmetric images(Not from the dataset) to find an optimal bandwidth values for KDE (Figure 3.14). The sensitivity value is peaked around 1.5, so we choose this value as a bandwidth of KDE.

Figure 3.15 displays the performance of recovering correct symmetry angle. As expected, EMD shows best performance in correctly selecting symmetry angle, and JSD and MD also demonstrate reliable output. The results point to that, to our chagrin, the overall performance does not show meaningful differences between measures. Either the existence of perfect symmetry and synthetic images(easy case) might contribute this obscure result or what really matters is the algorithm itself not the measures.

As shown in Figure 3.16, our algorithm, which shares some characteristics with the digital paper cutting [120] algorithm, outdoes the best algorithm [126] (using SIFT features) in [161] across the board regardless of the measures used. Some of the results are shown in Figure 3.20. The color images are the results of our algorithm, the gray images the result of [126]. The most conspicuous problem of the algorithm [126] is if the shape is not complex enough, the SIFT features it

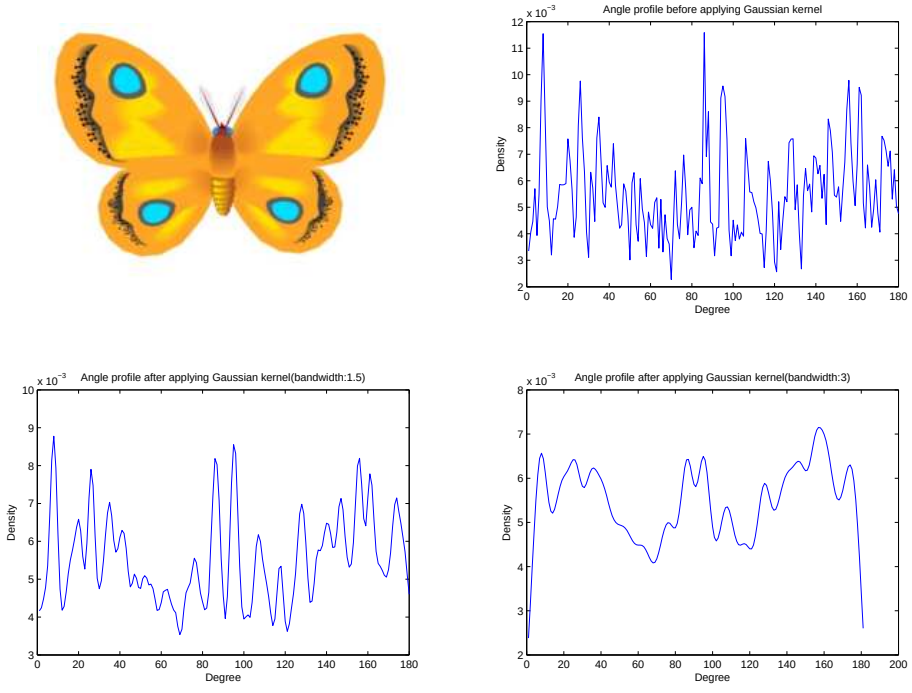

Figure 3.13: Kernel Density Estimation results on the distribution of edge orientation components. When the bandwidth value is 1.5∼2, it gives most reliable results. Figure 3.14 shows the relationship between KDE's bandwidth and performance of the algorithm.

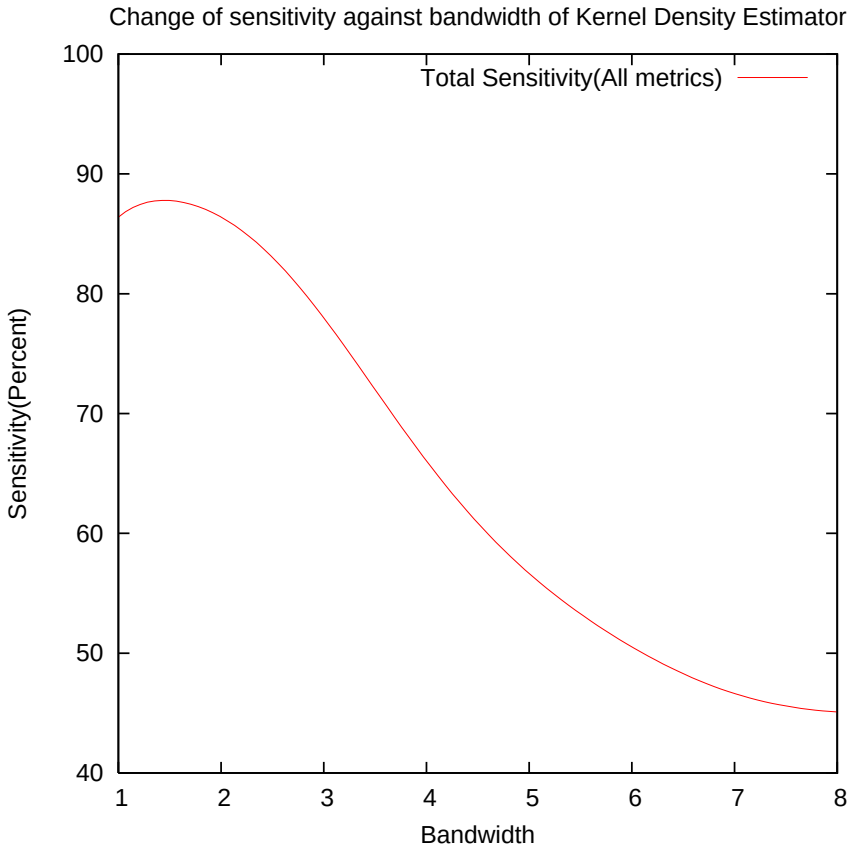

Figure 3.14: Relation between Sensitivity($\frac{TP}{FN+TP}$) and Bandwidth of Kernel Density Estimator.

choose are not informative enough to discern the symmetry. Also if the scene is too complex, it produces a lot of false positives that dwarf the real axis of symmetry, let alone its subquadratic time complexity. Figure 3.21 confirms that algorithm [126] is doing hit or miss depends on the extracted SIFT feature and the SIFT feature does not guarantee it would be the "good" symmetric feature. The performance gap gets bigger when the algorithms are allowed to guess up to 3 best axes of symmetry (Figure 3.17)

Overall, the Jensen-Shannon divergence, Bhattacharyya distance and the Matusita distance manifest the lowest false negative rates and edge out other measures.

The algorithm in [126] fared well on the set of images in cluttered backgrounds, but showed very poor performance (over 40% of the false negative rate) for simple/synthetic images (many of them are perfectly symmetric with relatively simple image structure). This result stands in stark contradiction to the previous study [161] that the same algorithm enjoyed 92% of sensitivity against the single synthetic images.

We want to restate here, that our algorithm is meant to work on images of single symmetric objects. If an image carries perfect or approximate symmetry structure, the algorithm we adduced here does indeed suffice. When a cluttered background is present or multiple symmetric objects are dispersed in the image, we should consider the algorithm in [126].

And what if we do not have any prior information about the given image? Is it possible to find a measurement that can inform us about the symmetric nature of the image? In the next chapter we will investigate whether the distance functions

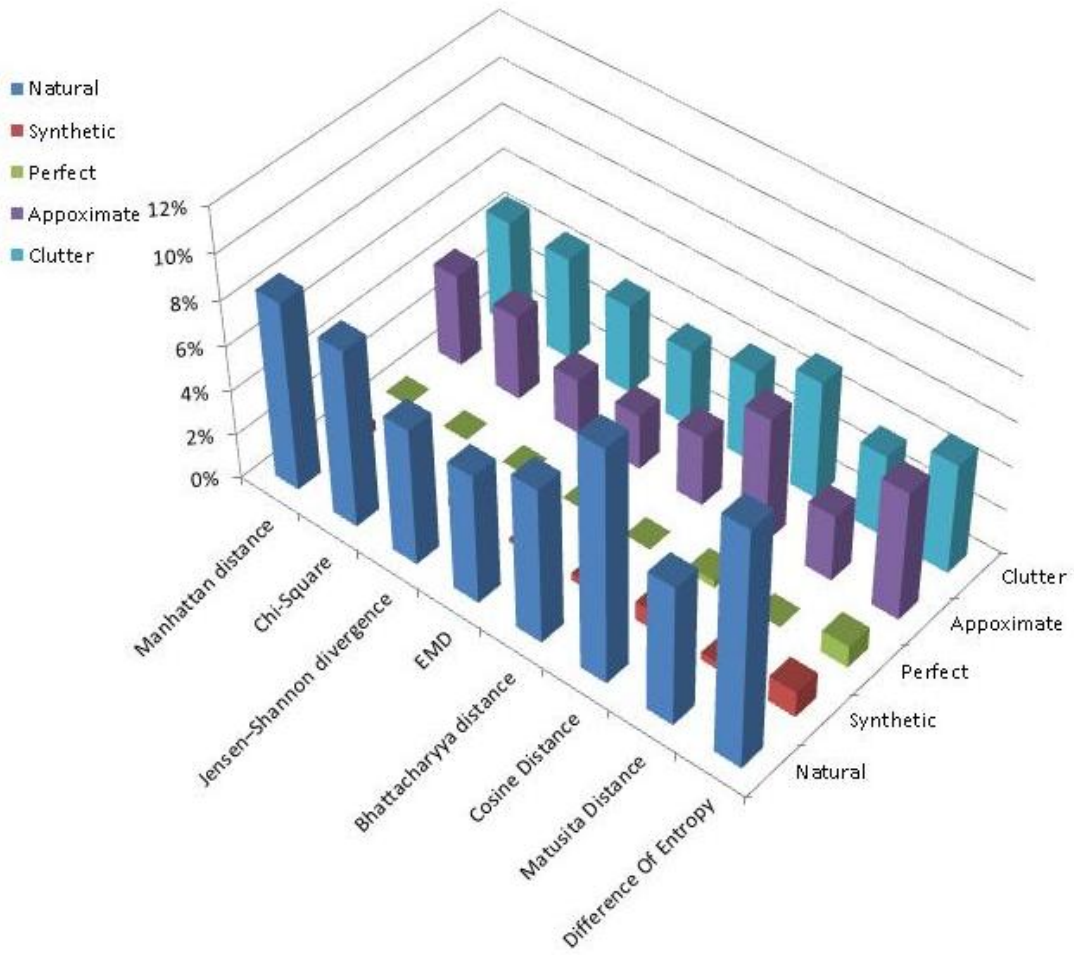

Figure 3.15: False Negative Rate($\frac{FN}{FN+TP}$) symmetry angle detection.

can be used also as measure for evaluating the amount of symmetry.

Figure 3.23 is the result from the algorithm in subsection 3.2.4 that scale the ranges up or down to fit the other. Although that algorithm will generate many false positives, if the structure of angle is preserved (means if the image still satisfies the angular constraint of symmetry), variable scale algorithm can detect symmetry of perspectively distorted images.

Now look to the results in Figure 3.19. These are the images that our algorithm failed to detect the axis of symmetry and the new result after changing the edge

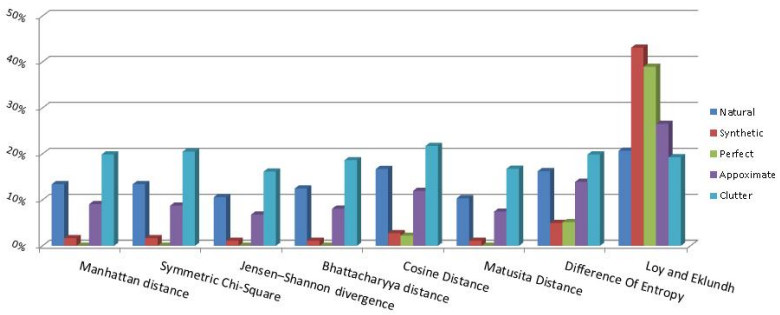

Figure 3.16: False Negative Rate($\frac{FN}{FN+TP}$) of symmetry detection(Best candidate).

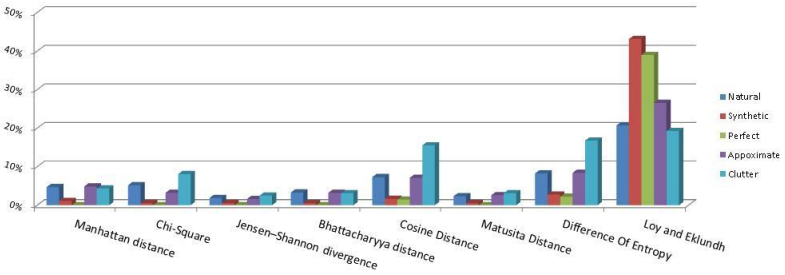

Figure 3.17: False Negative Rate($\frac{FN}{FN+TP}$) symmetry detection(Up to 3 Best candidates).

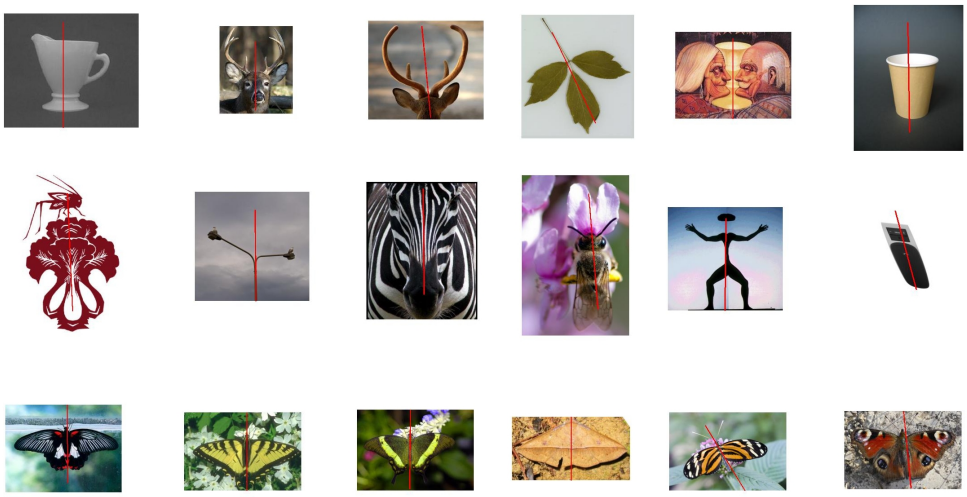

Figure 3.18: Symmetry detection results(Success-Cases).

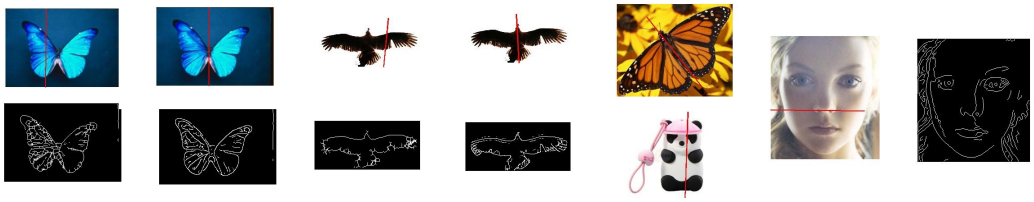

Figure 3.19: Symmetry detection results(Fail-Cases).

Figure 3.20: Comparisons of symmetry detection results. 1.

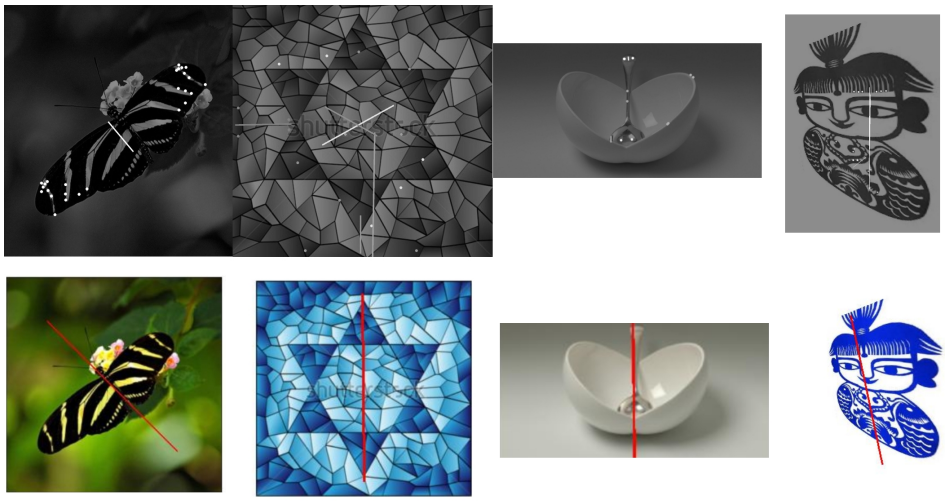

Figure 3.21: Comparisons of symmetry detection results. 2.

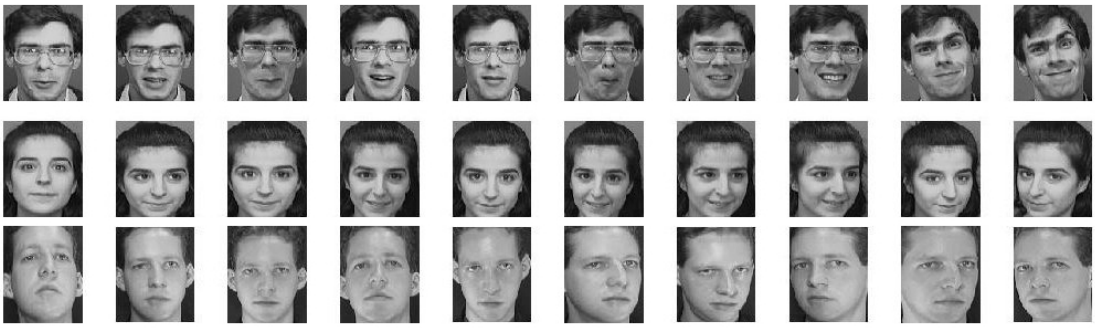

Figure 3.22: Ordering of human faces by their degree of symmetries.

Figure 3.23: Results of symmetry detection from perspectively distorted images.

Figure 3.24: Local symmetry failed.

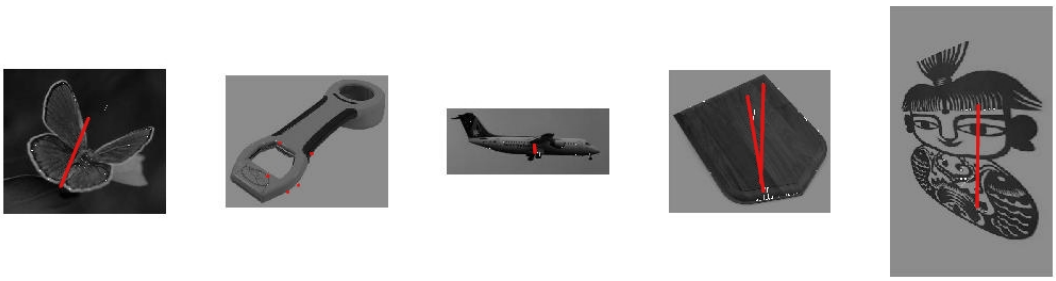

Figure 3.25: Local symmetry failed.

detector from Canny to the boundary detection algorithm [135]. The algorithm presented here is heavily dependent on the edge information. The problem of the boundary detection algorithm [135] is it takes too long to get the result. Adopting the algorithm in [135] might defeat the purpose of the algorithm that provides fast detection, however, if the matching cost is too high for a region then instead of generating unreliable output, applying more reliable boundary detector is not a bad idea.

3.6.1 From Detection to Evaluation

The main topic of this study is the efficient detection of approximate symmetry and we do not dare speculate the optimal cost from a metric is the right measure on the degree of symmetry. The overall degree of symmetry is not the simple sum of similarity between the features of the image but the interactions(including competitions) among the regularities in the image.

Nonetheless, our approach provides the likelihood of the symmetry, $p(C(I, f, d)|w)$, the evidence factor, $p(C(I, f, d))$, and the prior probability, $p(w)$, where w is the state of nature,

$$w = \{w_i|\ w_1 = perfect,\ w_2 = approximate,$$
$$w_3 = clutter,\ w_4 = not\ symmetric\}.$$

Figure 3.26 shows four class-conditional probability density functions for the optimal cost value(distance).

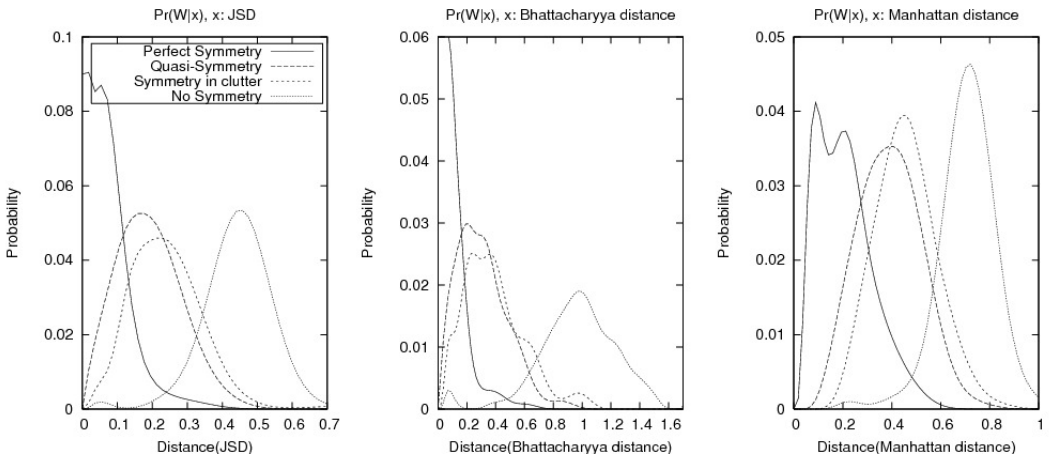

Figure 3.26: Probability distributions of optimal cost on three metrics.

Regrettably, the data gathered are heavily biased towards symmetric images(75% of the images are more or less symmetrical),*i.e.*, the evidence factor, $p(C(I, f, d))$, and most seriously the prior probability, $p(w)$, are probably wrong.

Figure 3.26 shows that the degree of the departure from the optimal symmetry gets larger as the value of optimal cost gets larger, regardless of the metric used. It shed light on the use of the optimal cost value. Though we could not say low cost means more symmetric(it is the inverse of the statement that "if the image is symmetric, then the cost will be low", and is not true), we could say "the high cost means not symmetric"(this is contraposition of our assumption and if the assumption "if the image is symmetric, then the cost will be low" is right, then this statement's truth value is as reliable as the assumption.)

3.6.2 Segmentation by symmetry

The Lipschitz function $\phi(i, j, t)$, where (i, j) is a 2D location of the given image and t is time such that $t \in (0, \infty)$, is called level-set function that defines an edge

contour by the zero level curve($\phi(i,j,t)=0$). The evolution of the zero-level curve defines geometric active contour evolution. The zero-level curve evolves according to differential equation, and hopefully will reach a steady state $\phi(i,j,t+1)=\phi(i,j,t)$ that gives a useful segmentation of the image[34].

The energy functional $F(c_1,c_2,\phi)$ is written as

$$\begin{aligned} F(c_1,c_2,\phi) &= \mu\int_\Omega \delta(\phi(x,y)) \mid \nabla\phi(x,y) \mid dxdy \\ &+ \nu\int_\Omega H(\phi(x,y))dxdy \\ &+ \lambda_1\int_\Omega \mid u_0(x,y)-c_1 \mid^2 H(\phi(x,y))dxdy \\ &+ \lambda_2\int_\Omega \mid u_0(x,y)-c_2 \mid^2 (1-H(\phi(x,y)))dxdy \end{aligned} \tag{3.29}$$

, where H is the Heaviside function, δ is the 1D Dirac measure, and c_1, c_2 are constant that have the average image intensity of inside/outside of the zero level curve respectively.

Function $H(\phi(x,y))$ provides a binary image of the current zero-level curve defined by $\phi(x,y)$, and we can try to detect symmetry from it. Of the two areas the axis of symmetry partitioned, we select a half of the area that is closer to the image edge boundary and create a bounded symmetric area by reflective transformation with respect to the symmetry axis found. To avoid the false positive, we went through the steps above only when the degree of symmetry is high enough.

Let $u_s:\overline{\Omega}\to\mathbb{R}$ be a given symmetric image from $\phi(x,y)$ and rewrite the new energy functional $F(c_1,c_2,1,0,\phi)$

$$
\begin{aligned}
F(c_1, c_2, 1, 0, \phi) = \mu \int_{\Omega} \delta(\phi(x,y)) \mid \nabla\phi(x,y) \mid dxdy \\
+ \nu \int_{\Omega} H(\phi(x,y))dxdy \\
+ \lambda_1 \int_{\Omega} \mid u_0(x,y) - c_1 \mid^2 H(\phi(x,y))dxdy \\
+ \lambda_2 \int_{\Omega} \mid u_0(x,y) - c_2 \mid^2 (1 - H(\phi(x,y)))dxdy \\
+ \lambda_3 \int_{\Omega} \mid u_s(x,y) - 1 \mid^2 H(\phi(x,y))dxdy \\
+ \lambda_4 \int_{\Omega} \mid u_s(x,y) \mid^2 (1 - H(\phi(x,y)))dxdy
\end{aligned}
\tag{3.30}
$$

In short, now we have two fitting terms and by the proportions of the values λ_i, we can control the importance of symmetry in the segmentation. Figure 3.27 shows the two different results on an image that does not delimit the clear boundary of an object.

3.6.3 Heuristic based on Psychological Experiments

One of the well-known psychological findings on human symmetry perception is that there are position effects of symmetry information such that humans are more sensitive to three stripes of regions: a region centered around the axis of symmetry(central region) and outermost stripes(outline region) [11, 234].

To take advantage of this special characteristic, a function of proximity, of symmetry perception as a heuristic approach, we modified the minimal cost function (3.17) to:

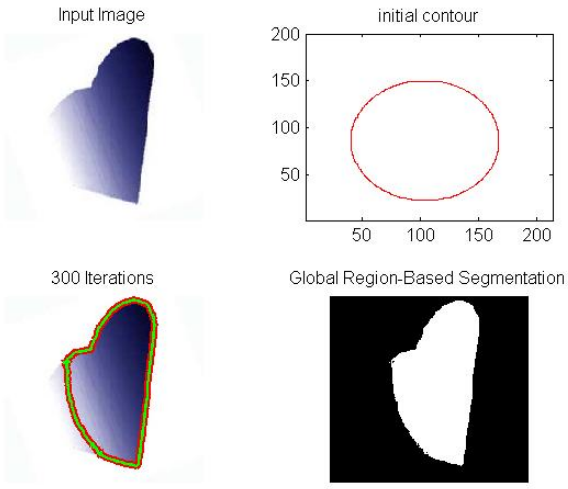

(a) Segmentation without the symmetry constraint

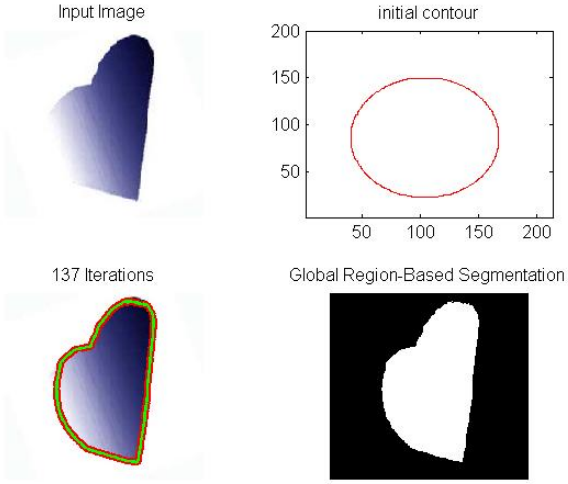

(b) Segmentation with the symmetry constraint

Figure 3.27: Segmentation by level sets and symmetry constraint.

$$C(I, r(\theta), d) = \int_{-\infty}^{\infty} w(x, r(\theta))\ d(p(r+x, \theta), p(r-x, \theta))dx, \tag{3.31}$$

where $w(x, r(\theta))$ is a Gaussian of x with center at $r(\theta)$. Because we do not know the exact location that outlines the shape of an object, and the outermost regions are the areas where clutter is easily seen, we take account of only the central region.

Contrary to our expectations, we observe the performance deterioration as the width of the Gaussian increases. This heuristic fails to return a more feasible solution on the images with perfect or close to perfect symmetry because the detection rate on them are already high at 98$\sim$100%. For a similar reason, we were unsuccessful in finding any single case that gives a better solution for the images with approximate symmetry. Instead, we find out the weight function $w(x, r(\theta))$ in (3.31) amplify the clutter and noise around the symmetry axis.

Admitting the claim that the location of a visual stimulus does not have the same share of influence over symmetry detection is true, the benefit of using it as a heuristic is not apparent at this time and its importance in human perception is not necessarily compatible with computational significance.

3.7 Conclusion

Three measures(JSD, MD and BC) are virtually tied though is marginally better than other measures. This results agrees with the results of previous studies [1, 84, 85, 2] and the choice of measure is not as critical as we thought.

Now we can have "cost" values for various distributions of features(mainly edges) around symmetry axes, and an algorithm that reliably recover the parameters of axis, with an algorithm that provides symmetric area from images, we can complete the automatic symmetry detector.

3.8 Proof of Geometrical Symmetry Constraints

In Figure 3.6,

$$\begin{aligned} \angle(boe) &= \angle(bpc)\ (\triangle boe \sim \triangle bpc) \qquad (3.32) \\ &= \frac{\theta(l_2) - \theta(l_1)}{2}\ (\triangle aod \sim \triangle apb) \\ \theta(L_c) &= \theta(l_2) - \angle(boe) \qquad (3.33) \\ &= \frac{\theta(l_1) + \theta(l_2)}{2} \end{aligned}$$

and,

$$\begin{aligned} |\ \overline{of}\ | &= \frac{r(l_2)}{\cos(\angle(bpc))} \qquad (3.34) \\ |\ \overline{od}\ | &= \frac{r(l_1)}{\cos(\angle(bpc))} \qquad (3.35) \\ |\ \overline{oe}\ | &= \frac{|\ \overline{of}\ | + |\ \overline{od}\ |}{2}\ (\triangle pfe \equiv \triangle pde) \qquad (3.36) \\ &= \frac{r(l_1) + r(l_2)}{2 \cdot \cos(\frac{\theta(l_2) - \theta(l_1)}{2})} \end{aligned}$$

■

3.9 Proof of Periodicity of (3.6) with Period $\frac{\pi}{2}$

Without loss of generality, let us assume $\theta < \frac{\pi}{2}$. During the angular sweep, angles $\theta + a$ and $\theta - a$ are a pair of inputs to the metric d for the angle θ, *i.e.*, $d(\theta - a, \theta + a)$. For the angle $\theta + \frac{\pi}{2}$(still less than π), the angle $\theta + a$ should be coupled with $\theta + \frac{\pi}{2} - a + \frac{\pi}{2}$ by (3.5) and $\theta - a + \pi = \theta - a$.

■

Chapter 4

Fast and Robust Detection of Regions of Symmetry Using Summed Area Tables

How can we differentiate an object from the meaningless chunk of noise? Even flower-naïve bumblebees (*Bombus terrestris*), with no wisdom of symmetric or asymmetric shapes have an intrinsic inclination toward bilateral symmetry [185]. And so flowers in the world have been taking advantage of it for a long time by taking the symmetric form.

Without a prior knowledge of the interesting objects, we have to think a feature model up to distinguish the target objects and draw them apart from the backgrounds so that processing demand and reaction time can be reduced (by limiting computation to smaller subregions). With regard to this step to find significant and discriminative regions of the image that contain objects of interest, the constraint of symmetry could be a sufficient, but not necessary, condition to satisfy.

Symmetry is considered as a crucial visual primitive that can be encoded without overt attention [28, 124, 122], however, it has been mostly overlooked and greatly underutilized. The main reason behind this seemingly unreasonable lack of employment is its disproportionate cost burden. To address this problem, we introduce a simple and fast algorithm to locate regions contain bilateral symmetries.

As it has been already detailed at full length in the Section 1.7.3, symmetry

can be used as stimulus salience[1] that yields a bottom-up bias (sometimes referred to as *exogenous attention*), or a selection goal of the top-down control (also referred to as *endogenous control*).

In the chapter, we concentrate on elucidating how the constraint information about bilateral symmetry is modeled as pop-out stimuli that contrast nicely with surrounding elements, and eventually leads to distinguishing:

- The center of bilateral symmetry serves as a Point of Interest, or PoI, in a scene.
- The Area of Symmetry (AoS) that presents the Area of Interest(AoI) (squares, rectangles).
- Bilateral symmetry parameters (an angle and a distance) that provide topological information about the object resides in the AoS.

During the first stage of the presented algorithm, the locations of features and coded orientations which act as descriptors of regions from a given image are stored in a data cube by the algorithm of a summed area table so that they can be comfortably and efficiently processed by the symmetry detector tailored to find regions of symmetry. Those data cube structure is very similar to the set of feature maps in Figure 1.10 in that the input image given is broken down through a few pre-attentive feature detection systems. Yet our model is different from [102] as neurons in each feature maps that encode for spatial contrast would not spatially

[1]The degree to which a physical feature is likely to attract attention. It is based on low-level physical characteristics and independent of the observer's mental state.

vie for salience, and the model yields multiple layers of feature maps depend on the size of interest regions with the same level of details of visual data instead of multiscale feature maps that might distort or destroy the structure of symmetry.

In the second stage of the algorithm, it generates several conspicuity maps that subsume a degree of symmetry (DoS) map out of the primitive data cube constructed in the first stage. These conspicuity maps indicate which sub-regions of the given image are visually salient and perceptually relevant.

At the final stage, the algorithm distinguishes information of potentially high visual salience (PoIs, AoIs and symmetry parameters) from the conspicuity maps built in the second stage.

We put forward two models that each takes on a different dimension of the problem such as a *perceptually-plausible model of selective attention* or a *computationally efficient symmetry detection model*. The models are tested and verified by computing the conspicuity maps on a wide variety of images, and comparing the fixation locations, areas of symmetry and symmetry parameters of the selected regions obtained from subjects who viewed those images with the computed information at the final stage of the given algorithm.

While admitting that the computational model of the brain that uncovers symmetries around us is not clearly established so far, we present novel and computationally efficient ways to obtain conspicuity maps for the DoS. The models take advantage of the hypothesis of the natural vision systems that choose fairly small areas first and mobilize the most resources toward them to get the information crucial to the survival of life. By doing so, the proposed models can enhance the

performance in efficiency and accuracy, as well as bring themselves into harmony with visual attention models.

The important contributions of the work in this chapter are:

- A complete and automated bilateral symmetry detection system
- A novel and efficient computational method of building up AoS conspicuity maps with the same level of details of visual data in $O(N\,logN)$ where N is the size of a given image.
- A global AoS conspicuity map that is size invariant.
- A set of quantitative evaluation methods for algorithms on AoS detection and labeled image data.

4.1 Introduction

What is intriguing about the picture Las Meninas is that the painter, Diego Velázquez, is pictured to the left and stares nonchalantly at the viewer. His blasé countenance seemingly more pronounced than those of other people in the painting because he is looking back at us, namely, his face looks more symmetric when it comes to our view (Figure 4.1). This picture typifies the problems we tackle in this chapter.

The lovely blond Infanta Margaret Theresa is escorted by the entourage of maids of honor, a chaperon, a bodyguard, two dwarfs and a dog. Diego Velázquez paints himself at a large canvas behind them. There is a mirror in the background

that casts back the images of the king and queen. Out of those entities, how can we weed out all relatively uneventful parts and develop an appreciation for his brilliant ingenuity? Furthermore, we also have to factor in the time complexity that depends on the size of the input image given.

The full resolution of this picture (3,475×4,000) is not overly high. Current consumer digital cameras produce images with excessively high (tens of millions of pixels) resolutions and soon we can easily find cameras with billions of pixels [44]. Since gigapixel images were introduced for viewing [104], the amount of computational time required for analyzing and recognizing them has reached an entirely new order of magnitude. Surely we can and should resize or divide the image so that it falls within a certain manageable range. An efficient symmetry detection algorithm can make all the difference by increasing the manageable size and dividing the image into semantically more meaningful representation (Figure 4.3).

In the study of figural goodness that facilitates fast, precise and stable perception, symmetry, especially bilateral symmetry, is considered asymmetrically superior to other salient visual cues: uniformity, compactness [132] and repetition [19, 47, 220]. Although there are some conflicting claims concerning the preponderance of symmetry over repetition [28, 173], two patterns in Figure 4.4 show a prima facie example where symmetry prevails over repetition in visual grouping. A pair of contours on the right shares the same visual characteristics, such as shape, size and color, however, a pair of contour lines facing each other on the left commands more attention and we tend to associate them into one coherent object.

There are two noteworthy, and not necessarily mutually exclusive [35], cognitive-

Figure 4.1: Las Meninas (The Maids of Honor) painted by Diego Rodrguez de Silva Velázquez, the great realist painter. He is at the center of a looking-glass universe, off to the side, but bigger than anyone else in the painting.

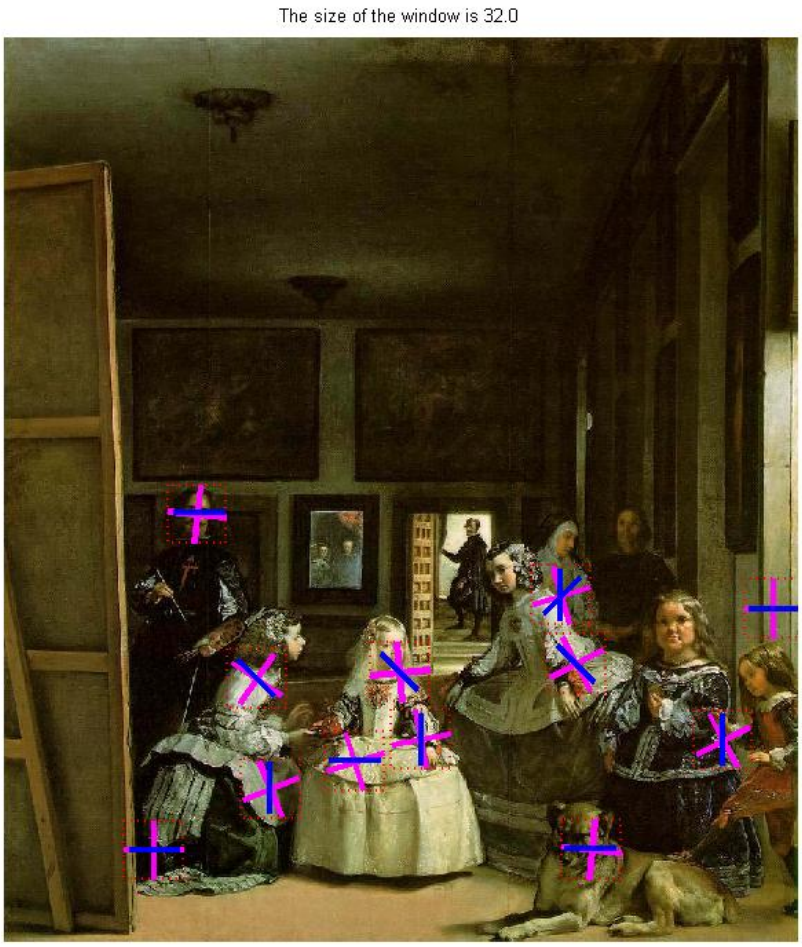

Figure 4.2: The detected regions of symmetry by an algorithm described in this chapter is squared and uncovered bilateral axes of symmetries are marked.

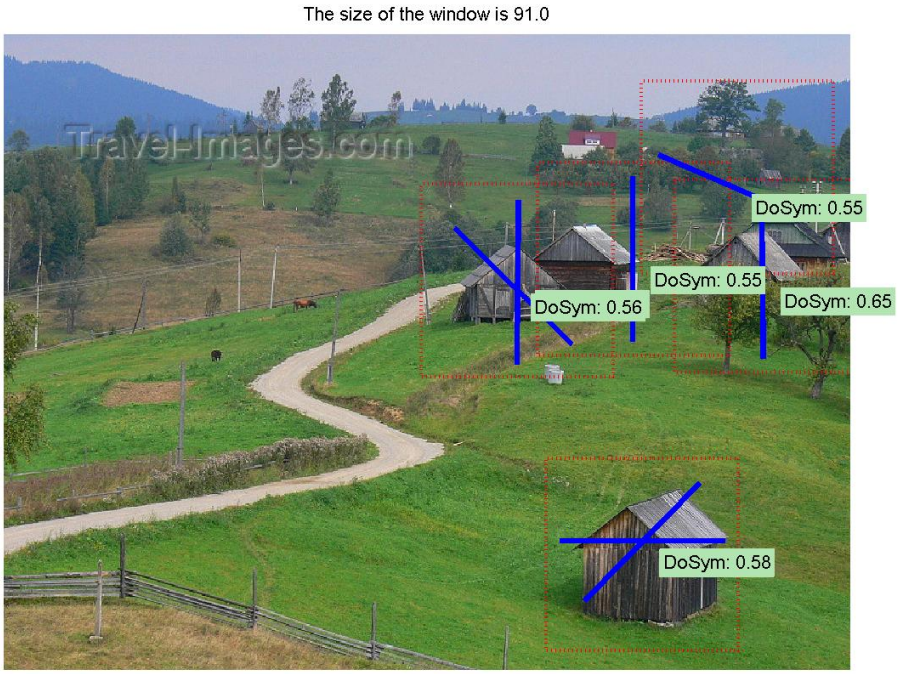

Figure 4.3: Symmetry detection can be used as an intelligent image partitioner.

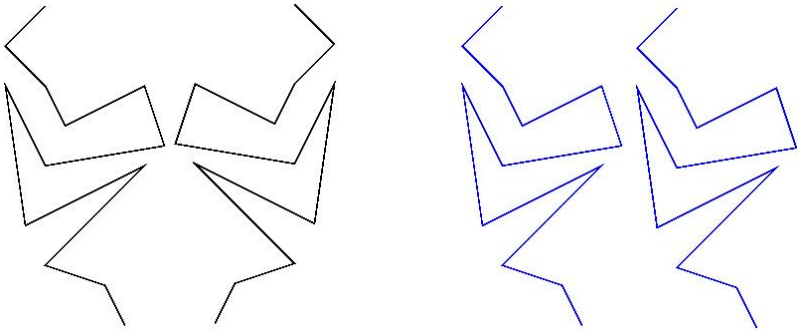

Figure 4.4: The visual regularity formed by the symmetric contours on the left(*black*) tends to be perceived with ease, whereas the regularity engendered by the repeated contours on the right(*blue*) does not seem as apparent. Therefore the relevant contours on the left are more likely perceived to be belonging to a same object. All contours have exactly the same morphological complexity. The shape of contours is adapted from an image found in [173]

(a) (b)

Figure 4.5: The boundary between a camouflaged or disguised butterfly (or moth) and a natural background (or substrate) is hard to perceive. The only remaining visual queue in this case is symmetry. The line represents the detected symmetry by our model, and the circle indicates the size of the detection window.

Figure 4.6: Accidental symmetries found in our dataset images.

architecture principles that try to explain how an objective stimulus feature (*e.g.*, symmetry) affects a subjective evaluation for the given visual stimuli. Each principle also shapes its own answer to what underlying mechanisms enable us to perceive scenes as structured wholes when a visual stimulus can be interpreted in many ways.

The first one is called the *simplicity principle* [80] and it conjectures that the interpretation of a stimulus is selected to be as simple as possible. By this principle, symmetry is a dominant feature of the visual stimuli because it is the simplest of all feature types (perceptual economy).

The second principle, called the *likelihood principle* [78], surmises that perceptual organization is elected to be in agreement to the most likely distal layout. The interpretation of symmetry preference in the frame of the likelihood principle is that the concept of symmetry is a ubiquitous property of objects in nature, and the symmetric shapes are very frequent in the environment. Much as it is possible that the symmetric shapes would be generated by accident, symmetry is considered as one of the five non-accidental[2] properties [21] and the possibility that a given symmetric shape is produced by an accidental alignment should be rejected because it is less likely (Unfortunately, however, Figure 4.6 shows it is not as rare as people like to believe).

The aforementioned principles do not contradict each other; they dovetail perfectly together. Since symmetry is omnipresent, our visual system would get overwhelmed to handle the stimuli unless a system to cope with them is already in place. On the other way around, the facile detection of symmetries enables us to

[2]it is unlikely that a view of an asymmetric object ends up in symmetric image on the retina.

see them in everyday objects.

On account of its ubiquity in every meaningful object and the presence of the visual system that detects it without the application of focal attention, symmetry has been deemed to subserve selective visual attention during a preattentive stage [23, 122]. In the course of preattentive processing, a number of features in a scene (*e.g.*, size, color, location and orientation) that can direct attention to locations of objects are rapidly retrieved, and at a later phase, an attentive stage, attention is converged upon a specific area to give rich and coherent representations of objects (Refer Section 1.7.3).

While there is no denying that symmetrical pattern has great Gestalts and is exceptionally conspicuous so, as a human being, perceiving it is comparably effortless, we rarely, if ever, use symmetry on the computer-vision problem to locate unspecified objects in a scene. One of the reasons for the underutilization of symmetry is that it is consistently expensive to decode image symmetry assuredly, especially for large images. The other reason for the lack of the utilization of symmetry is the dearth of suitable algorithms that are tolerant and sensitive to moderate amounts of disruption in the symmetry structure of the scene.

4.1.1 Overview of the Approach

In this chapter we introduce two new methods to detect regions of symmetry in a scene without consuming too much resources. Conceding that operations like uncovering symmetry for 3D object reconstruction or drawing out non-planar 3D

symmetry under severe perspective distortion would be computationally intensive tasks, context-free symmetry detection, we claim, does not have to be complex or unduly time consuming to be effective. Even if no satisfactory account has been given from cognitive psychophysiology, we decouple the tolerance from the sensitivity.

In lieu of point by point or feature by feature comparisons that take quadratic time relative to the number of image pixels in the worst case, the algorithms proposed here use 2D array operations that would take only linear time. Figure 4.7 presents 4 square quadrants method. In this method, the decomposition step splits the subregion of an image investigated into four equal-sized square quadrants (as a matter of fact, the algorithm divides the subregion into eight isosceles right-triangle regions to detect two oblique orientations). Each of four distributions of image features from the subset quadrants is compared to its counterpart to decide the degree of symmetry of the investigated area (or at the center of the area).

This approach relies on computing an objective function with a sliding window which still has high computational cost as a main limiting factor for performance. A normal sliding window algorithm has time complexity linear to the size of the sliding window and it renders the time complexity of the entire algorithm subquadratic. The algorithms used in this chapter carry an efficient method that has a constant complexity ($O(1)$) to the size of the window. This is achieved by harnessing the spatial coherence of the image and computing the objective function with summed area tables. The significant performance enhancement by this method is demonstrated through testing it on an extensive image dataset. Compared with state-of-the-art

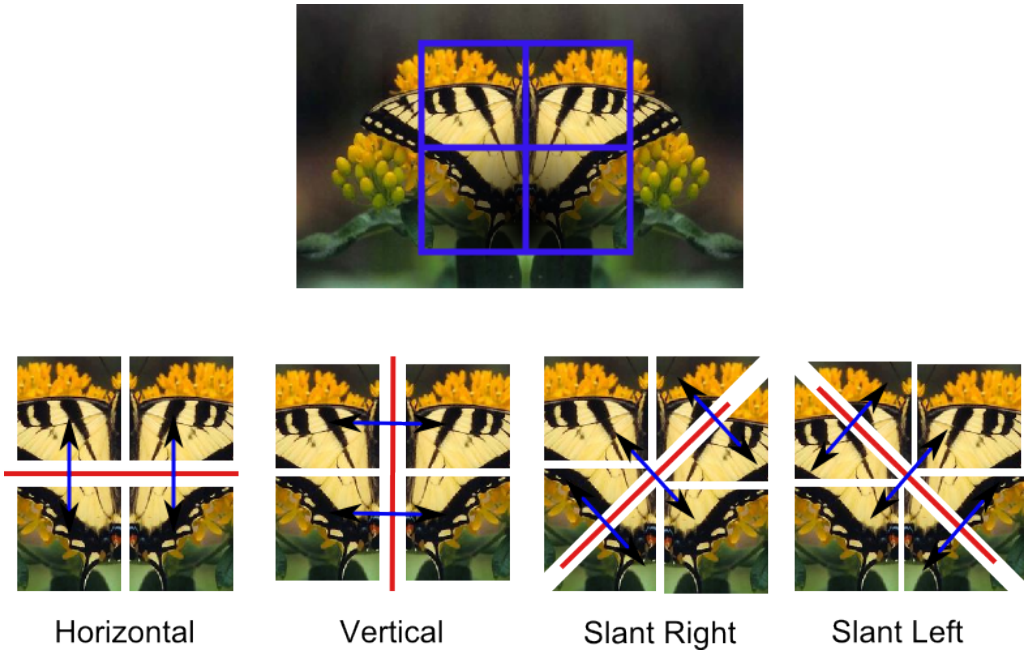

Figure 4.7: A brief and schematic description of the 4 square quadrants algorithm. The blue window in the picture signifies a current sliding window. The window comprises 4 square quadrants and measures the degree-of-symmetry (DoS) on 4 different directions.

techniques, the summed area table based method typically achieves times speed up by several orders of magnitude on large and complex images.

4.2 Previous Work

There are two groups of previous research studies center their attention on symmetry or employ symmetry to find symmetry supporting regions. One is focusing on finding affinely skewed rotation symmetry group [108], and the other is honing in on either a region-based attention model that uses a symmetry map [8] or an attention based active vision system [9]. Since the main subject of this chapter is about region-based visual attention, the later group [8, 9] is reviewed here.

4.2.1 Region-Based Visual Attention Using Symmetry Map [8]

The main idea of this approach is clustering of pixels with common attributes. There are three different approaches for the clustering: Clustering after attention (the authors name it a pixel-based method), Gabor filter based clustering in the frequency domain, and region-segmentation based feature clustering.

Pixel-based approaches usually use the absolute intensity difference between an attended pixel and its surround at six different scales (an image gradient for an edge can be a candidate for the feature). Then the computed difference is compared with those of its neighbors to decide its exclusiveness.

In the frequency domain, high color contrast and the difference in local orientation are mainly used, and the GST generates a symmetry map from the outputs

of Gabor orientation filters [9].

The conspicuity of the region is decided by various factors: the mean gradient of the color along the boundary of the regions, moments of the segmented region, and color and texture contrasts. Since the regions can have size properties, a size contrast map can be applied, but rarely used.

The factors employed by this approach are color contrast saliency, size saliency, three 2D moments, and a symmetry map. The method of generating the symmetry map is rather straightforward. A scanning function, $\Psi(L, P_s)$ totals the number of symmetric points around the point P_s along the line L. It computes equidistant points around 12 predefined orientations on the bounding rectangle and normalizes the value $\Psi(L, P_s)$ by the area of the given region ($\alpha\, R_i$).

4.2.2 Gaze Control for an Active Vision System [9]

According to the mental spotlight model [55], at a given time, attention is concentrated on a certain area of a visual field and within that region the quality of perceptual processing is enhanced while other parts remain unprocessed. When a target comes into view at an unattended location, a mental focus has to be repositioned to that location.

Wolfe's Guided Search model [241] dictates that during the process of a visual search, attention would be given to the most salient item in the display. The items in a scene are ordered in terms of the amount of preattentiveness, and the visual search courses through from the most likely to the least likely until we find the mark

or an "activation threshold" is reached to terminate the search. The preattentive stage guided by the weighted sum of top-down or bottom-up guidance handles basic features, such as color, size, and orientation, in parallel across the visual scene. In attentive stage, serial attention is deployed to find salient locations.

In their model depicted in Figure 4.8, Gabor filters with 12 orientations are used for the GST (though their descriptions on a radius-image and the algorithm used are not clear at all) to generate a symmetry conspicuity map. And to get maps of the dimension eccentricity, segmentation-based gradient fields are used with a principal component analysis to compute moments with cross covariances. Finally, the mean color gradient in the HVC color space along the boundary to the neighbor is calculated for a superimposition with other feature maps obtained above.

4.2.3 Related Works on the Implementation

4.2.3.1 Summed Area Tables

A summed area table (SAT, also known as an integral image [225]) is an entity or an algorithm originally introduced by Crow [46] as an alternative to mip mapping [239]. It is an array that each of its elements holds the value amounts to the sum of all the elements above and to the left of the element to efficiently calculate the sum of the table element values at a fixed amount of time.

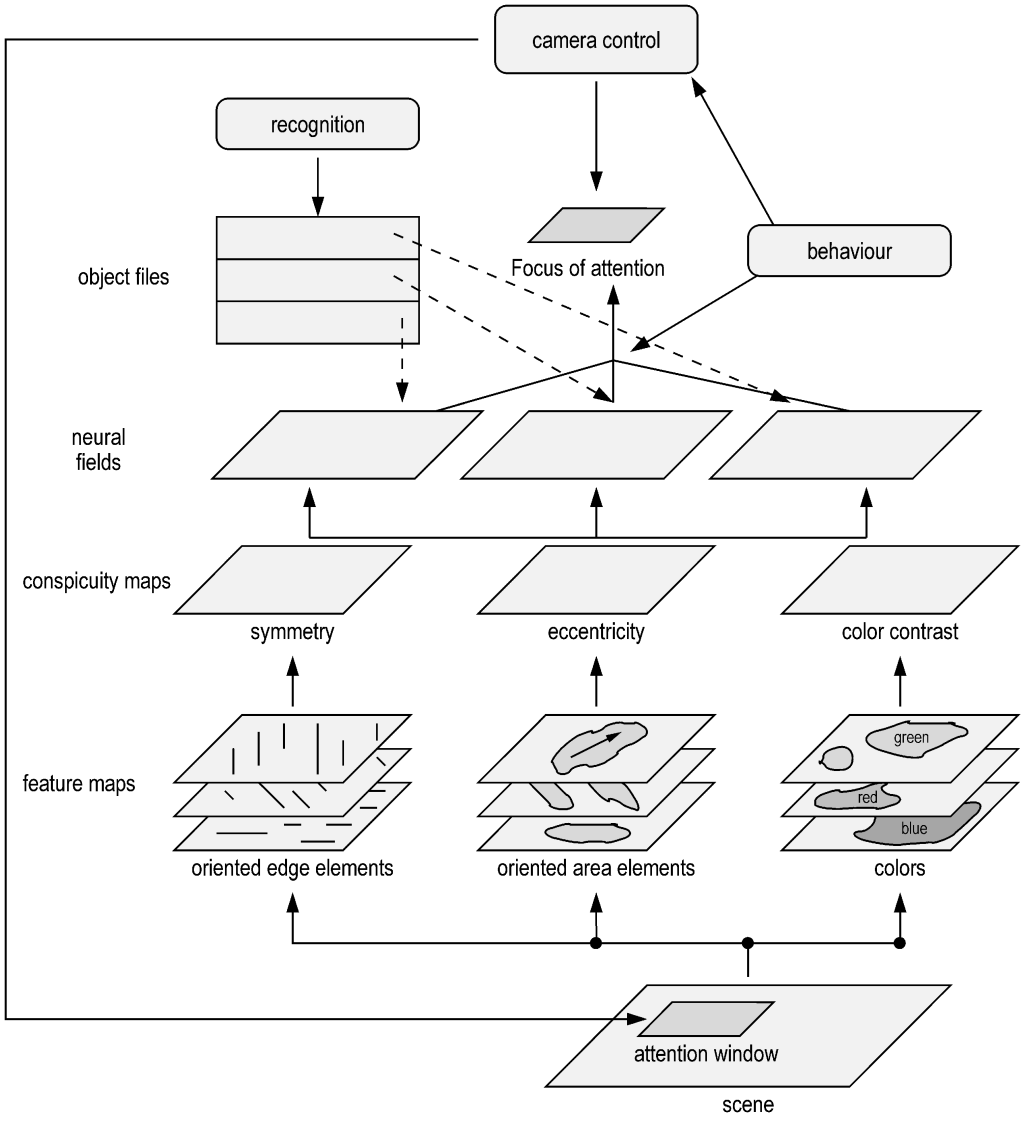

Figure 4.8: An overview of the neural active vision system model architecture. Adapted from [9]

The value at any point (x, y) in the table I is interpreted as follow:

$$I(x, y) = \sum_{\substack{x' \leq x \\ y' \leq y}} i(x', y'), \tag{4.1}$$

where $i(x', y')$ is the original value of the table (or image).

The value $I(x, y)$ can be computed at a cost of two additions and one subtraction per each entry in a single pass.

$$I(x, y) = i(x, y) + I(x - 1, y) + I(x, y - 1) - I(x - 1, y - 1). \tag{4.2}$$

Once the table has been tallied up, the integral of the values in any rectangular region can be carried out in constant time with two subtractions and one addition.

$$\sum_{\substack{A(x) < x' \leq C(x) \\ A(y) < y' \leq C(y)}} i(x', y') = I(A) + I(C) - I(B) - I(D). \tag{4.3}$$

The location of A,B,C, and D are marked in Figure 4.9.

The power of summed area tables is based on the fact that the block operation on the image subset can be done in constant time regardless of its potential block size. It allows for a very fast feature evaluation if our detection system does not work directly with image intensities at the pixel level.

For the purpose of the symmetry detection with a 4 square quadrants algorithm (Figure 4.7) that mandates 2 reflective shapes of isosceles right triangles, we also use a summed area table for an isosceles right triangle (a trapezoid near the boundary)

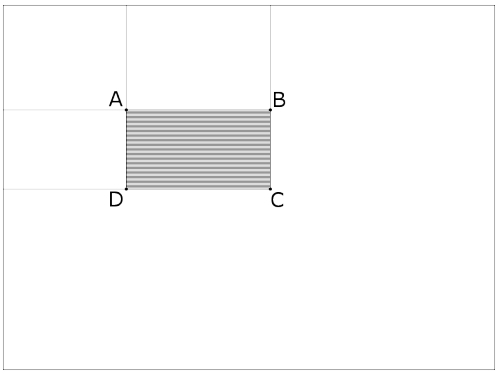

Figure 4.9: A Summed Area Table for fast rectangular region computation.

region so that the value at point (x, y) in the table is

$$I_{triangle}(x, y) = \sum_{\substack{x' \leq x \\ y' \leq x'}} i(x', y'), \tag{4.4}$$

and can be computed at a cost of one addition and one subtraction per each entry in a single pass.

$$I_{triangle}(x, y) = I_{triangle}(x - 1, y - 1) + I(x, y) - I(x - 1, y). \tag{4.5}$$

The integral value in any isosceles right triangle region can be computed by (Figure 4.10)

$$\sum_{\substack{A(x) < x' \leq C(x) \\ A(y) < y' \leq x'}} i(x', y') = I_{triangle}(C) + I(A) - I(B) - I_{triangle}(A). \tag{4.6}$$

A reflection over $y = C(x)$ of this isosceles right triangle region can be defined

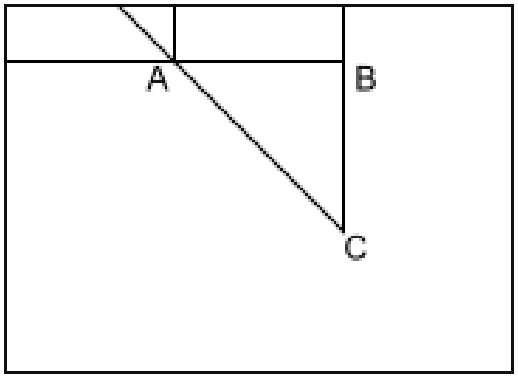

Figure 4.10: Summed Area Table for isosceles right triangle region computation

by the similar way in Eq. 4.4, 4.5, and 4.6.

4.3 The Algorithm - General

The ultimate goal of symmetry detection is the recovery of rotational and translational parameters of symmetry axes. To achieve this goal, most of the previous approaches are fastidiously trying to distinguish and identify the exact values of the parameters. Instead of the pixel-by-pixel probing to find the exact symmetry, we choose algorithms that quickly examine the whole block of area with a bird's-eye view to get the less-than-detail information and make a crude decision mainly based on the orientation spread of the region.

The approaches taken in this chapter abandon the exacting task of a precise parameter-estimation, and impose the most crucial/independent symmetry-constraints in a much relaxed manner to uncover rather apparent symmetry that is immune to small local perturbations to the symmetry structure. In very brief form,

the algorithms described here estimate either differences between quadrants or the most probable orientation parameter directly from a given block.

4.3.1 Application of Log-Gabor Filter Bank and Summed Area Tables

It is well known that the frequency and orientation representations of Gabor filters are analogous to those of the visual system of mammals [166]. Since the associations between activations for a particular spatial location are very unique between objects, the phase symmetry of points in an image can be used as a line and blob detector [105]. Likewise if you want to use a symmetry detector on some locations from the image truly worth your while, walking on the Gabor space is preferable to a random or sequential search.

The receptive-field characteristics of mammalian cortical cells are believed to be well-adapted for the images of the natural environment, and Log-Gabor filters are considered better in capturing the spatial-frequency tuning curves in those cells than ordinary Gabor filters [59].

The filter banks employed here are having a bandwidth of single octave with either 8-orientation selectivities and the angular interval of 22.5° for the 4 Square-Quadrants algorithm, or 16-orientation selectivities (the angular interval of 11.25°) for the single block based algorithm.

Gray intensity values of the pixels in the image are convolved with a bank of filters. Then responses are log filtered. The responses from Log-Gabor filters are

advantageous because the filters give us great flexibility in the angular spread and the range of frequencies to cover. But they are not indispensable. The intensity gradient and orientational information of the image from edge detection operators (e.g. Canny, Roberts, Prewitt, Sobel) also served the purpose in our early experiment.

The filter responses and intensity values of phase-congruency/edges, and positions of high phase-congruency pixels/edges are processed and saved by summed-area tables.

The resulting 2D tables are stacked up to create a 3-dimensional data set, called a data cube. The stored values are made available to the symmetry operator with a specific size parameter upon request. Or, more formally, the transformation ST of image data I to data cube D can be denoted as:

$$ST : I \rightarrow D, I \subset \Re^2, D \subset \Re^3. \tag{4.7}$$

A pixel $I(x, y)$ in the image I is mapped to a vector d ($d \in \Re^k$), where the value of k depends on the number of features needed to represent a block of the image I.

$$d(x, y) = \{(d_1, \ldots, d_k) \mid d_i = D(x, y, i)\}. \tag{4.8}$$

4.4 4 Square Quadrants Algorithm

4.4.1 Overview

This is a perceptually plausible model that reflects the anisotropic symmetry detection (Section 1.7.6). If the upper-left quadrant of the region (in an image) is symmetrically similar (the corresponding orientations should be re-arranged to be compared. See Figure 4.12 for their correspondences) to the upper-right quadrant, and lower-left to lower right, the given region is likely to have vertical symmetry (Figure 4.11 illustrates 4 different orientations of symmetries can be found by the 4 square-quadrants algorithm). But this decidedly simple approach has two caveats come with the territory, *i.e.*, a selection of robust features (particularly features that represent rotational parameters of symmetry) and the computational cost of block operations.

If the 4 square-quadrants contain an object that is a bit off from the 4 preferred orientations, some small aberrations from them could take their toll on the measurement of the degree of symmetry unless the features can compensate this sensitivities. And furthermore, an increase in granularity, *e.g.*, 16 directions instead of 8, often invites an increased computational burden.

4.4.2 Algorithm and Its Implementation

We choose Gabor filtered images along 8 different orientations (Figure 4.13), compile phase congruency or Canny edges, store locations of the feature points (to determine the barycenter of each quadrant) of high phase congruency/edges into a

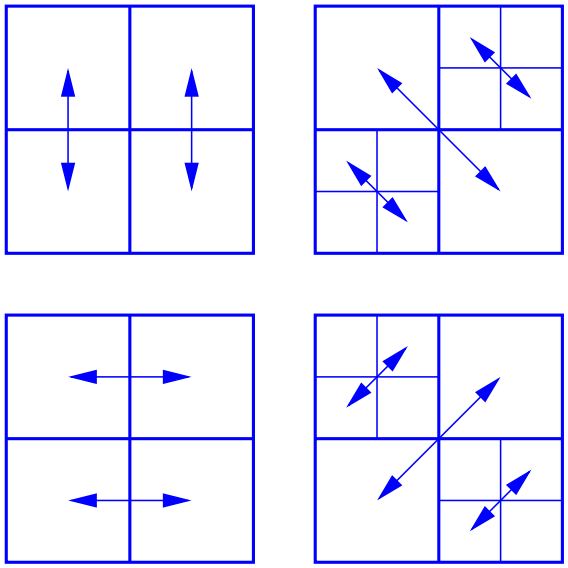

Figure 4.11: 4 filters to detect 4 different orientations of symmetries. Vertical/Horizontal/Slant Right/Slant Left. From the lower left, clockwise.

set of primitive features, and create a data cube out of it (Figure 4.14).

In turn, to get the symmetry information of the block centered at a point (x, y), the algorithm calculates the integral values from all k-layers in the data cube D using Eq. 4.3 and Eq. 4.6 and makes four (or six for oblique orientations) feature-vectors; each represents one quadrant (or one isosceles right triangle region) of the

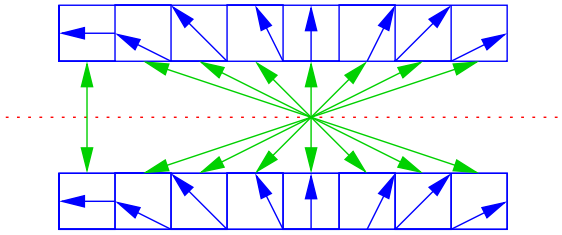

Figure 4.12: Rearrangement of an orientation descriptor symmetrically consistent with the candidate axis of symmetry(red)

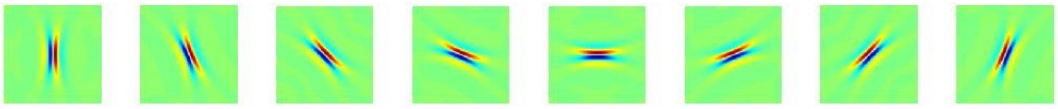

Figure 4.13: Gabor filters used in the 4 square quadrants algorithm.

block queried (See Algorithm 6).

Eventually, then the problem is reduced to matching the four feature-vectors using various measures: a cosine similarity($\frac{A \cdot B}{\|A\|\|B\|}$), EMD (Subsection 3.4.7) or JSD (Subsection 3.4.1) with different combinations of tuples for each preferred direction. We can evaluate the orientational symmetry distance, for instance, with measures including EMD where each $d(i,j)_{orientation}$ is the 8-tuple (8 orientations), and the ground distance is a 1D Gaussian distribution that has a minimum value at the symmetrically consistent combination of orientations (for this reason, it is not a metric).

The three feature maps we want to have are: a symmetry feature map for the degree of symmetry (DoS), an intensity map that decides whether a location $I(x,y)$ has enough stimulus to cause attention, and an eccentricity map that can tell us the location information of the thresholded stimulus. The DoS map is acquired by adequately matching its 4 subregions. The intensity map would be either the output of Gabor filters or high phase congruency/edge response. The eccentricity map is the symmetrically placed image moments ($M_{10}/M_{00}, M_{01}/M_{00}$. Refer Eq. 2.3) from the 4 subregions.

Figure 4.14 shows the entire process that makes use of the SAT and Figure 4.15

demonstrates a course of actions to get one data point in the symmetry feature map at a predefined scale.

In Algorithm 6, the operations $getFeatures$ and $getFeaturesTriangle$ return the sum of values in a square (or an isosceles right triangle) grid defined by two points whose coordinates represent top-left and bottom-right positions. Usually it takes $O(s^2)$ time, where s is the size of the sliding window, to calculate the sum of the values, and renders the computational complexity for the entire process be subquadratic. But thanks to the advantages provided by the SATs, we can complete this operation in $O(1)$ time. The functions $getDoS$ and $getSLDoS$ (for oblique directions) that compute the degree of symmetry between the given fixed-size feature vectors only take $O(1)$ time. The resulting data cube, SFM, contains tuples that stand for the degree of symmetries in four directions (also see Figure 4.15).

Accordingly, the entire computational complexity of the algorithm is linear in the size of the image, $O(n)$, where n is the number of pixels in an image (with one sliding window). The number of locations for local extreme is confined to less than or equal to 5 for each size of interest.

4.4.3 Elements in One Feature Vector

A pixel $I(x, y)$ in the image space corresponds to a vector d ($d \in \Re^k$) in the data cube D. The elements contained in d are:

- Orientational information for the upper left/upper right/down left/down right quadrant: 8×4 elements from 8-direction SATs.

Algorithm 6 Symmetry Feature Map Generation

$D \leftarrow 0s, SFM \leftarrow 0s$
{D: Data Cube, SFM: Symmetry Feature Map}
$ws \leftarrow Size(SlidingWindow)$
$D \leftarrow SummedAreaTable(Image(x, y))$
{$D(x, y, z)$ contains Orientation, Intensity, Location information.}

for all (x, y) in $Image(x, y)$ **do**
  $UL \leftarrow getFeatures(D, (x, y), (x - ws, y - ws))$
  {UL: Upper Left Quadrant}
  $UR \leftarrow getFeatures(D, (x + ws, y), (x, y - ws))$
  {UR: Upper Right Quadrant}
  $DL \leftarrow getFeatures(D, (x, y + ws), (x - ws, y))$
  {UL: Down Left Quadrant}
  $DR \leftarrow getFeatures(D, (x + ws, y + ws), (x, y))$
  {UL: Down Right Quadrant}
  $SL \leftarrow getFeaturesTriangle(D, (x + ws, y + ws), (x - ws, y - ws))$
  {UL: Slant Left Quadrant}
  $SR \leftarrow getFeaturesTriangle(D, (x - ws, y - ws), (x + ws, y + ws))$
  {SR: Slant Right Quadrant}

  $SFM(x, y, Vertical) = getDoS(UL, UR) + getDoS(DL, DR)$
  $SFM(x, y, Horizontal) = getDoS(UL, DL) + getDoS(UR, DR)$
  $SFM(x, y, SlantLeft) = getDoS(UR, DL) + getSLDoS(SL, UL + DR)$
  $SFM(x, y, SlantRight) = getDoS(UL, DR) + getSLDoS(SR, UR + DL)$
end for

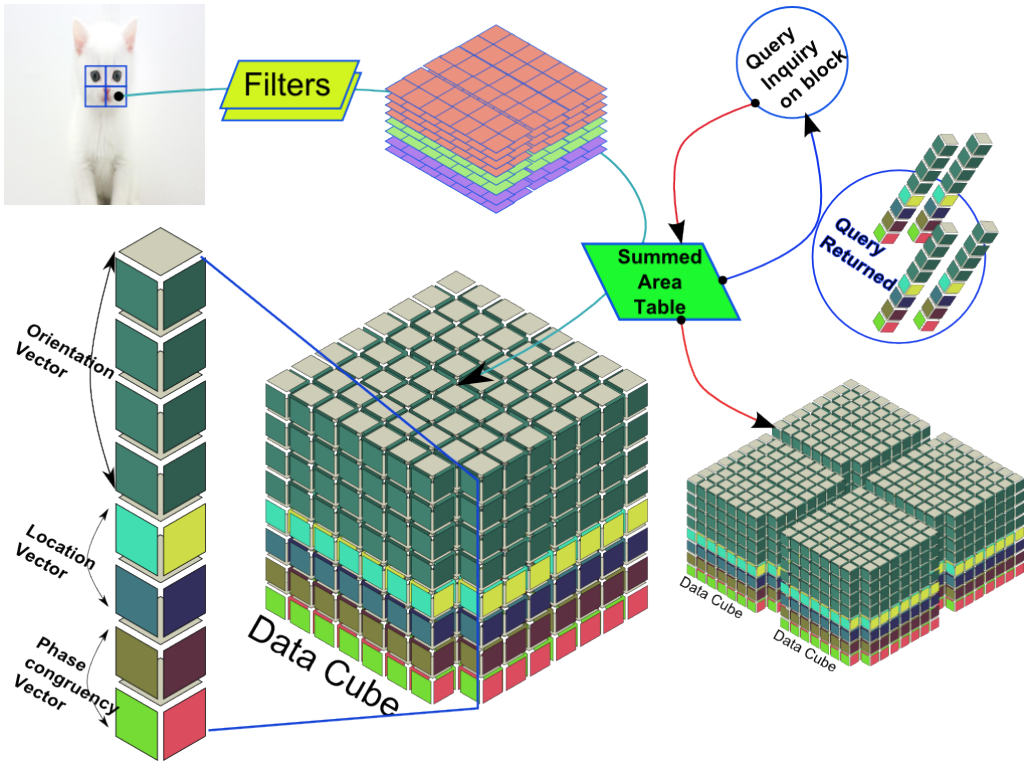

Figure 4.14: Method of utilizing summed are tables for obtaining a symmetry map with an arbitrary window size.

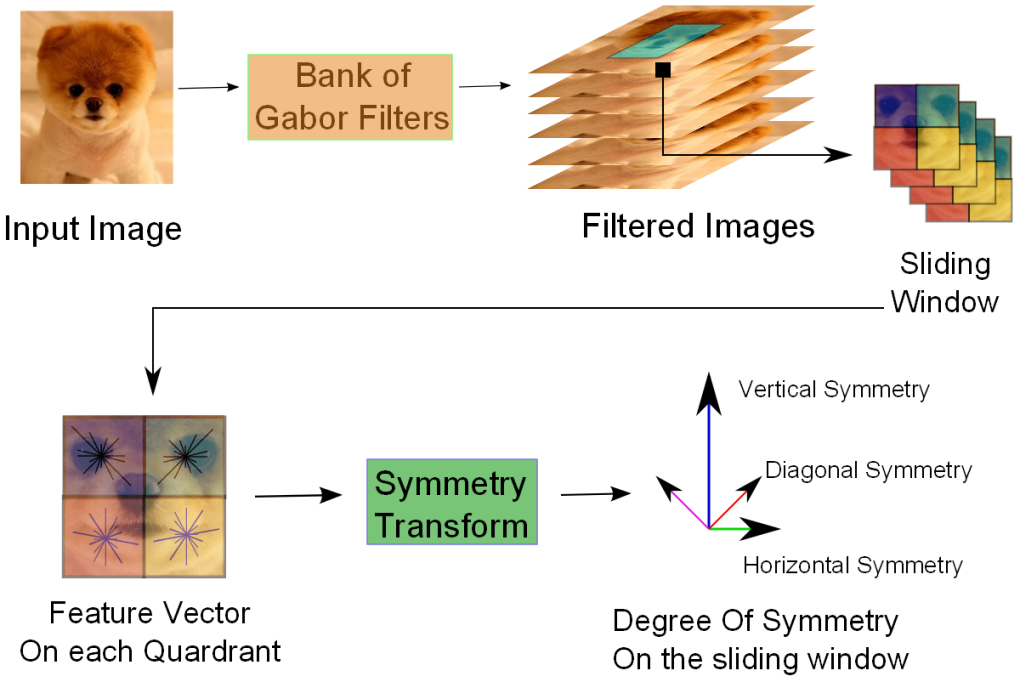

Figure 4.15: Process of acquiring a tuple of the symmetry map.

- Orientational information for the slant left/slant right quadrant: 8×2 elements from 8-direction SATs.
- Phase congruency/edges stimuli for 6 quadrants: 6 elements from 6 SATs.
- (x, y) Coordinate information for 6 quadrants: 6×2 elements from 6 SATs.

The value of k is set at 66, to wit, we have to keep 66 images to find symmetries in one single image. If 4-directional resolution is not satisfactory, then we could rotate the image to increase the resolution to 22.5°. As a result, even the time complexity of the algorithm is still at $O(N)$, N is the size of the image given, the space requirement is pretty high at 132 images for one.

4.4.4 Sliding window sizes

We adopt a variable-sized sliding-window scheme that takes different sizes for the sliding window (from 32×32 to one-quarter the size of the image). It starts with the smallest size 32×32 then increases its size by $\sqrt{2}$ (doubles its area).

4.4.5 Results and Evaluation

To find centers of symmetries, a superimposition of the eccentricity map and the sum of the DoS (only the pixels with an intensity above a certain threshold value are considered) is selected, *i.e.*, add all the responses values from the DoS feature map (responses from all directions, $SFM(x, y, Vertical)+SFM(x, y, Horizontal)+SFM(x, y, SlantLeft) + SFM(x, y, SlantRight)$) and the eccentricity map, then choose the maximum values out of them. This is usually the conspicuity map's job. By doing so, the algorithm prefers closed circular contours with high degree of symmetries. The locations of maximum responses are selected as the PoIs and the size of the window determines the size of the AoIs. The estimated directions of symmetries at selected locations are determined by the max (not the sum) of the DoS map (the most preferred direction). Figure 4.16 shows detected AoIs with red circles.

4.4.5.1 Evaluation Method

Firstly, 153 images were collected and the performance of an algorithm is measured against them. They are obtained from Microsoft Research Cambridge

Figure 4.16: Results of 4 Square Quadrants Algorithm.

Table 4.1: Image file nomenclature

POSITION	MNEMONIC	DESCRIPTION
1	2 — 3	3 for non-planar 3D symmetry (212 images). Otherwise, 2 (839 images)
2	S — M	S: Single object (615 images), M: Multiple objects (436 images)
3	N — S	S: Synthetic image (214 images), N: Natual photograph (837 images)
4	P — Q — C — N	P: Scene of perfect or near perfect symmetry (198 images) Q : Approximate symmetry (352 images). C : Symmetric obj.in cluttered background (102 images) N : Non-symmetric(but locally symmetric) scene (399 images)
5-10		A serial number of the file

(MSRC) dataset, the PASCAL Visual Object Classes (VOC) Challenge [57], MPEG-7 CE Shape-1 Part-B data set and Yahoo and Google images. Just like in Section 3.5, we examined each image carefully by eye to make sure that some types objects in the dataset chosen to display symmetry do not carry a disproportionate share of the image population. The gathered images are then classified and renamed into our own nomenclature (Table 4.1). For instance, "2SNP000388" denotes a 2D natural image that contains a single object with perfect symmetry and 388^{th} image in our dataset .

Secondly, the classified images are labeled by 2 raters who understand the concepts of symmetry. The raters were asked to identify centers of the symmetric objects with circles around each. The annotation tools were written in Java and all the test data reside in web. The annotation values of each data object (total 281 objects) are either averaged into a single value or registered as independent values

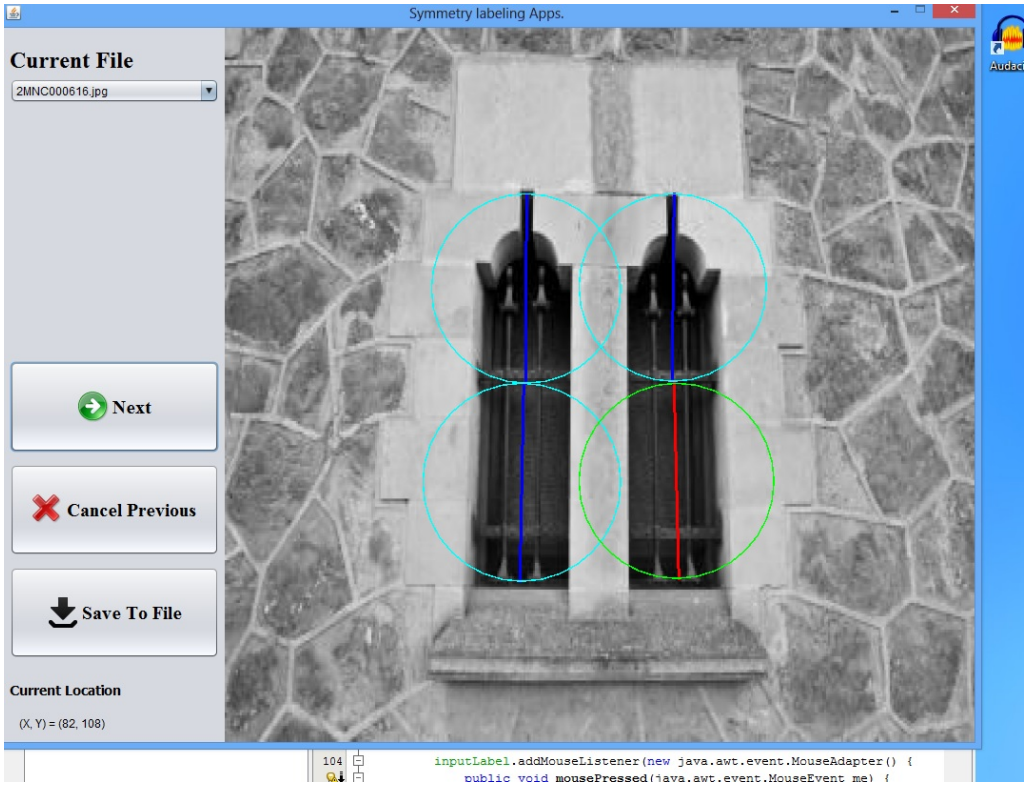

Figure 4.17: Symmetry labeling application to annotate axes and areas of symmetry.

(multiple axes of symmetry) respectively.

Lastly, to appraise the performance of algorithms, only the type II errors (A false negative error. Table 4.2) are measured. Figure 4.6 shows a case that tells us why we still have to resort to type II errors. An accidental symmetry as in Figure 4.6 is not as rare as people like to think and it is not reasonable to treat these cases as false positives. If the detected PoI (the center of symmetry) is inside the symmetric objects, it is considered as a true positive.

Table 4.2: Type II Error

Algorithm	**TP / (TP + FN)**
Algorithm in [126]	0.68 (191/281)
4 Square Quadrants Algorithm	0.79 (221/281)

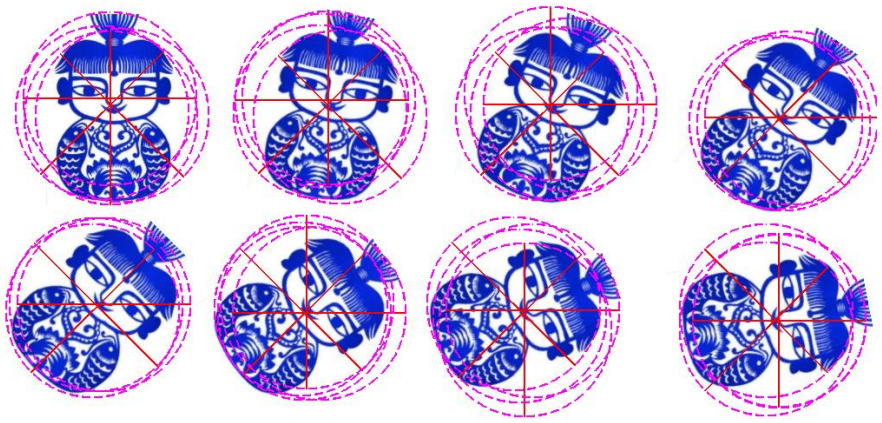

Figure 4.18: Angle spread experiment. A symmetric object is rotated to 8 different orientations.

4.4.5.2 Test for Angle Spread

We always begin our experiment with "Angle Spread Experiment". Though we detect symmetries on 4 different orientations with 8 different orientational measures, we want to make sure our detector covers symmetries between those 4 preferred orientations. Figure 4.18 shows our detector actually covers angles not exactly aligned with 4 predefined orientations. If an orientation of the symmetry falls between two predefined orientations, the symmetry is detected at both orientations.

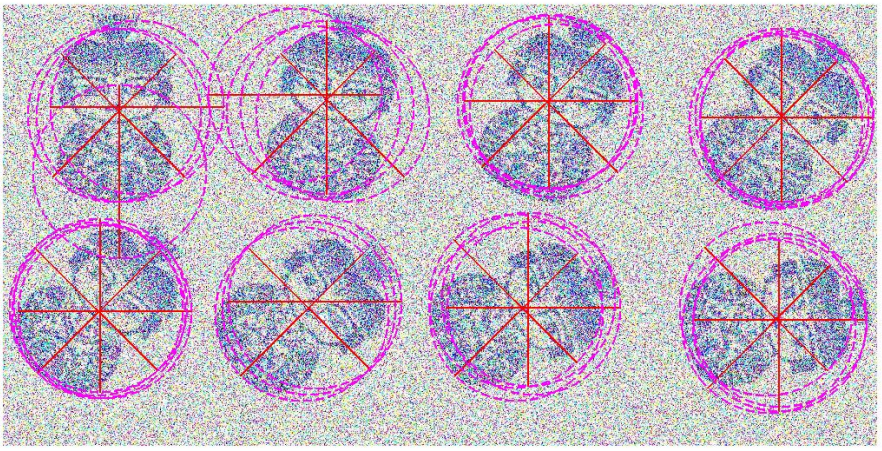

Figure 4.19: A moderate level of image noise.

4.4.5.3 Test for Noises

The proposed PoIs detector also proves its resiliency to noise (Figure 4.19 for the moderate noise, and Figure 4.20 for the severe noise).

Please compare these results with the other algorithm's [126]. (Figure 4.21 for the moderate level of noise, and Figure 4.22 for the severe noise).

4.4.5.4 Max of DoS instead of Sum of DoS

A PoI detector using the sum of the DoS values shows very nice results as a region detector (refer Figure 4.16 and Table 4.2). When the number of candidates is deliberately increased, the locations of the PoIs are mostly preserved (Figure 4.23). However, they are not the most symmetrical PoIs because the sum of the DoS averages the values of the DoS.

If the PoI detector uses a more symmetry-relevant descriptor, the max of the

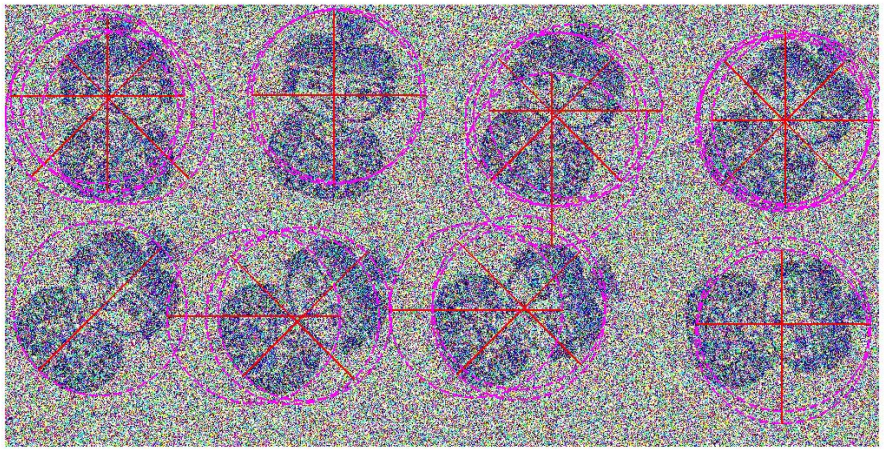

Figure 4.20: A more severe level of noise disruption.

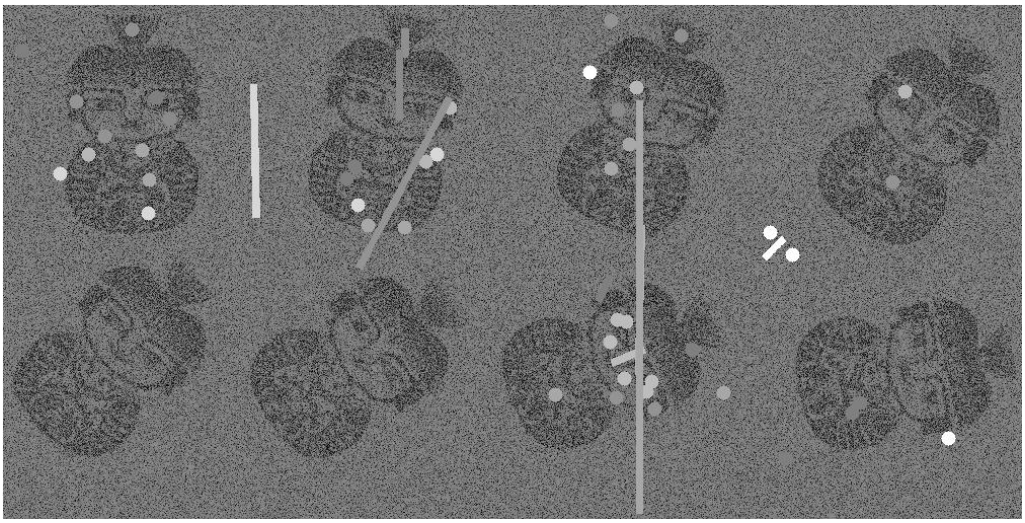

Figure 4.21: A moderate level of image noise. Algorithm in [126]

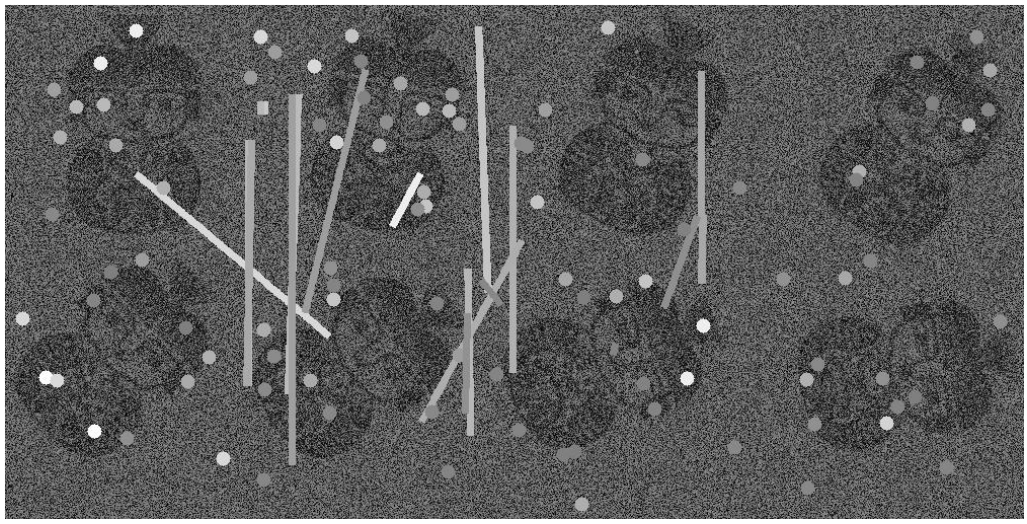

Figure 4.22: A more severe level of image noise disruption. Algorithm in [126]

DoS, the detection of PoIs gets unstable. Figure 4.24 shows two problems in using the maximum value of the DoS for PoIs detection. Just like a human subject, if the axis of symmetry is off from the preferred directions (this case, vertical, horizontal and two slants), the performance gets worse. Secondly, the locations of the local maximum of the DoSs do not agree with the results from human annotators since the maximum of the DoS does not have any information on a "center" of symmetry and the results are pretty local (Figure 4.24).

4.4.5.5 Discussion and Conclusion

Even the sum of the DoS works poorly on a noisy image like Figure 4.25. This test data was made from a perfectly symmetric image and three asymmetric areas have strong symmetry structures in the stimuli. If the PoI detector is not sensitive and tolerant at the same time with asymmetric features, selecting better symmetric

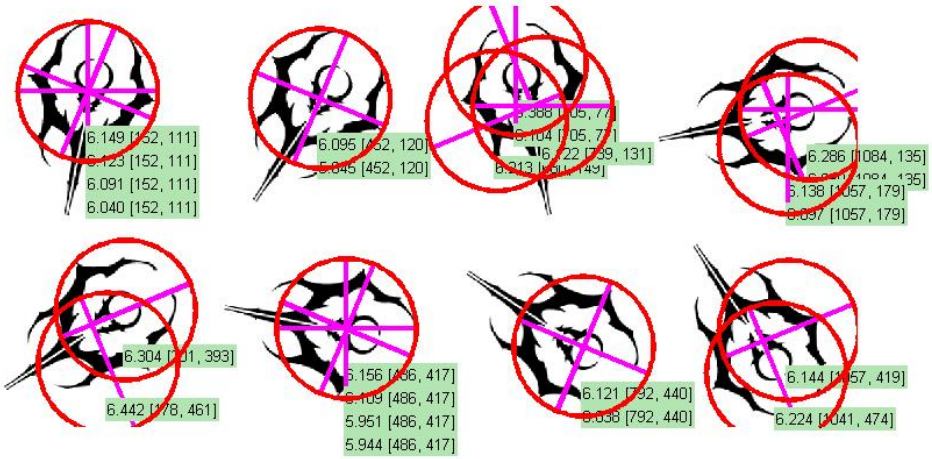

Figure 4.23: The centers of symmetries are focused and correct for the sum of DoS.

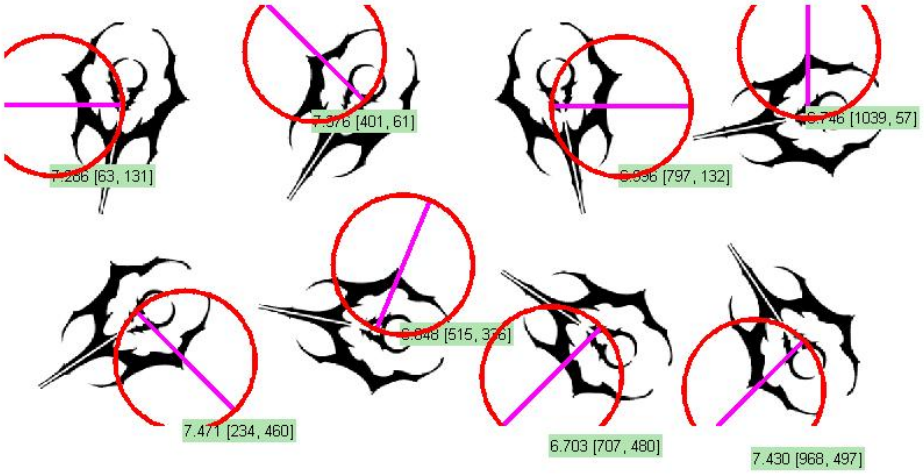

Figure 4.24: The centers of symmetry get shaky when the PoI detector uses the local maximum of the DoSs.

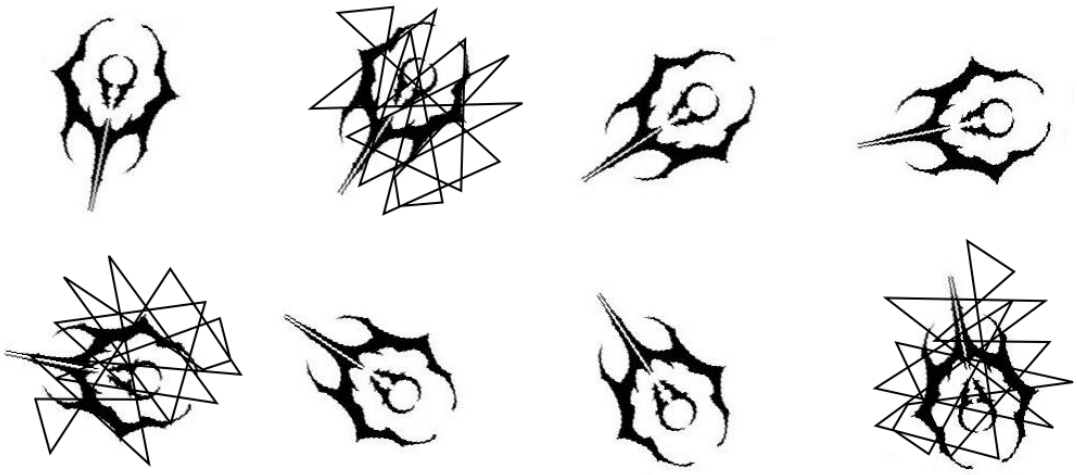

Figure 4.25: Very tricky test data. Some non-symmetric regions have high stimuli and still holds symmetry structure under them.

regions could not be an easy task. To overcome this limitation, there should be a more sensitive but still tolerant symmetric PoI detector.

Though the PoI detector using the sum of the DoS failed to meet the expectation as a symmetric PoI detector, it is, at least, a consistent blob detector (as in [170]).

The other drawback of this algorithm is that if the image features are close to the axis of symmetry, a small displacement of a shape occasions a large difference in the degree of symmetry (Figure 4.26).

4.5 A Single Block Based Algorithm

The 4 square-quadrants approach is too restrictive in that it is quite sensitive to a set of predefined directions and has a strict limitation on the shape of a block (only a square shape is allowed). A novel approach presented in this section involves

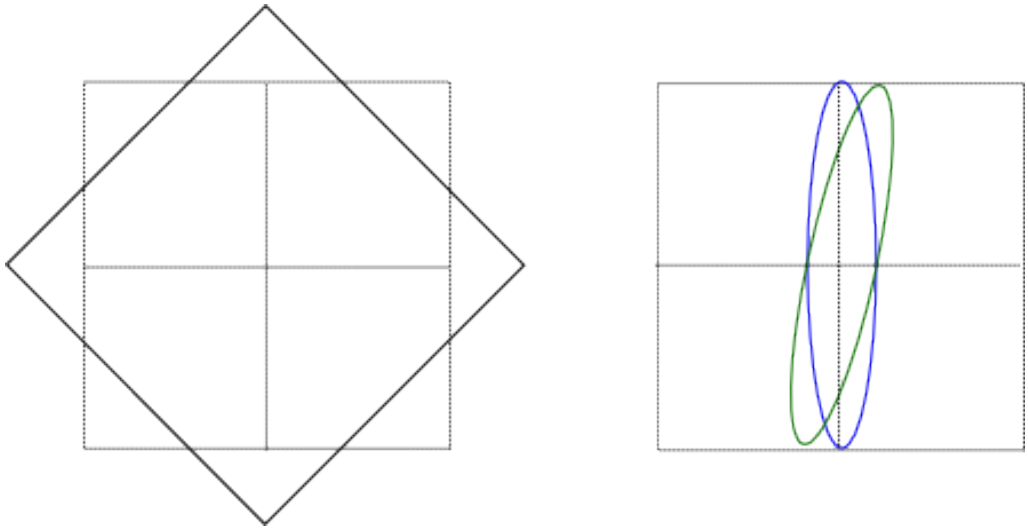

Figure 4.26: The problems of the inconsistent shape of the region for the oblique orientations (left), and of features centered around the axis of symmetry (right).

the symmetry constraint specified at Eq. 3.2. This constraint is very descriptive and nicely fits into the block-constraint operation that the SAT can easily afford. The symmetry constraint adopted for the new algorithm is much less restrictive and certainly much more effective overall than the 4 square-quadrants approach.

4.5.1 Algorithm and Its Implementation

The algorithm is virtually the same as the steps detailed in Section 3.2.2 and Section 4.4.2. The entire algorithm can be construed as iterative applications of the Algorithm 2 to the sliding window. As stated in Section 3.2.2, the time complexity of the Algorithm 2 is $O(max(n, n_\theta^2))$ where n_θ is the number of discrete intervals covering the range of the data, and n is the number of features in the image. Accordingly, the entire time complexity of the algorithm is quadratic, however,

the SATs of the orientation map render the time complexity of the Algorithm 2 $O(n_\theta^2) \approx O(1)$ and the computational complexity of the algorithm is linear in the size of the image, $O(n)$.

During the first stage, the locations of edges (x and y coordinates), the number of edges, and coded orientations which act as descriptors of regions from a given image are stored in a data cube by the algorithm of the SAT.

In the second stage, the algorithm generates several conspicuity maps that subsume a DoS, an intensity, and an image moment.

At the final stage, points (or areas) of high visual salience (PoIs and AoIs) from the conspicuity maps are distinguished (the orientations of symmetry axes also can be identified by the symmetry-orientation feature map).

Algorithm 7 Symmetry Feature Map Generation

$D \leftarrow 0s, SFM \leftarrow 0s$
$\{D$: Data Cube, SFM: Symmetry Feature Map$\}$
$ws \leftarrow Size(SlidingWindow)$
$D \leftarrow SummedAreaTable(Image(x, y))$
$\{D(x, y, z)$ contains Orientation, Intensity, Location information.$\}$

for all (x, y) in $Image(x, y)$ **do**
  $EBLK \leftarrow getFeatures(D, (x + ws, y + ws), (x - ws, y - ws))$
  $\{EBLK$: Entire Block$\}$

  for all θ in $0 \leq \theta < \pi$ **do**
    $SFM(x, y, \theta) = getDoS(EBLK, \theta)$
  end for
end for

In Algorithm 7, the operation $getFeatures$ returns the sum of values in a block defined by two points whose coordinates represent the top-left corner and the bottom-right corner of a rectangle (it does not have to be a square). The function

getDoS that computes the degree of symmetry from the given block $EBLK$ takes only $O(n_\theta^2)$ time. The resulting data cube, SFM, contains tuples that stand for the degree of symmetries in 32 directions.

4.5.2 Elements in One Feature Vector

The elements contained in a vector d from the data cube D are:

- Orientational information for the entire block: 16×1 elements from 16-direction SATs.
- Phase congruency/edges stimuli for the block: 1 elements from 1 SAT.
- (x, y) coordinates information for the block: 2×1 elements from 2 SATs.

The value of k is set at 19.

4.5.3 Evaluation Methods

Since the results of the AoSs detection are a set of lines, line segment Hausdorff distance [67] (Figure 4.27 and 4.28) can be used as measures of the performance. But considering the limited accuracy and insufficient reliability of the human annotation, the Percentage of Correctly estimated body Parts (PCP) [52] that estimates the accuracy of the results by measuring the distance between the segment endpoints and those of the ground-truth segment seems more reliable.

The most conspicuous problem of human annotation comes from the annotation process that is neither bottom-up/preattentive nor context-free. Therefore a

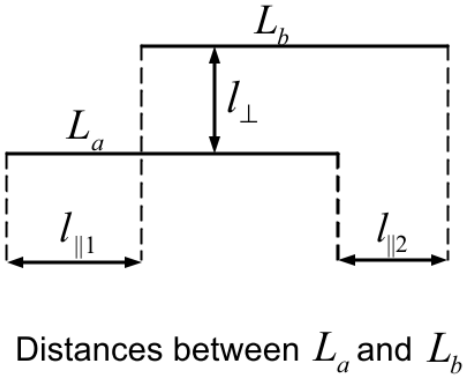

1. Parallel distance:

$$d_{\|}(L_a, L_b) = \min(l_{\|1}, l_{\|2})$$

2. Perpendicular distance:

$$d_{\perp}(L_a, L_b) = l_{\perp}$$

Figure 4.27: Line segment Hausdorff distance(1). Adapted from [67]

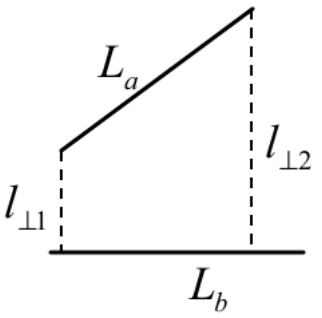

$$d_{\perp}(L_a, L_b) = \frac{1}{2} \cdot (w_1 \cdot l_{\perp 1} + w_2 \cdot l_{\perp 2})$$

Where

$$w_i = \frac{l_{\perp i}}{l_{\perp 1} + l_{\perp 2}}, \qquad (i = 1,2)$$

Figure 4.28: Line segment Hausdorff distance(2). Adapted from [67]

human annotator is prone to label the area only through a serial search to locate the stimulus that the annotator think symmetric. For this reason, we decided to continue with the type II errors.

4.5.4 Results and Evaluation

We work with the Gabor filter bank having a bandwidth of single octave, 16-orientation selectivities and the angular interval is 11.25°. Canny edge detector is selected for an eccentricity map that shows the difference between the current location and the block moment measured at that point. The intensity map also uses the sigmoid function (weight of 5) on the filtered Canny edge detector output. The new assumption is that the intensity map just decides whether the cell should fire or be silent and weeds out the irrelevant symmetry responses from regions with small or no stimulus intensity.

The other settings are much the same as the 4 Square Quadrants algorithm. Since 16-orientation information is handled with edge locations information, at most 16 SATs are used for symmetry detection at a time. Once the size of the interest window is set, the algorithm computes the cost function defined at Eq. 3.2 with the 16 Gabor-filter responses. The resolution of the detected angle parameter is 5.625 °. In order to incorporate the center of symmetry constraint (Figure 4.31) to the conspicuity map, the maximum values of the DoS and the values of the eccentricity map are summed together. The locations of the PoIs are obtained from the local maxima of the symmetry conspicuity map.

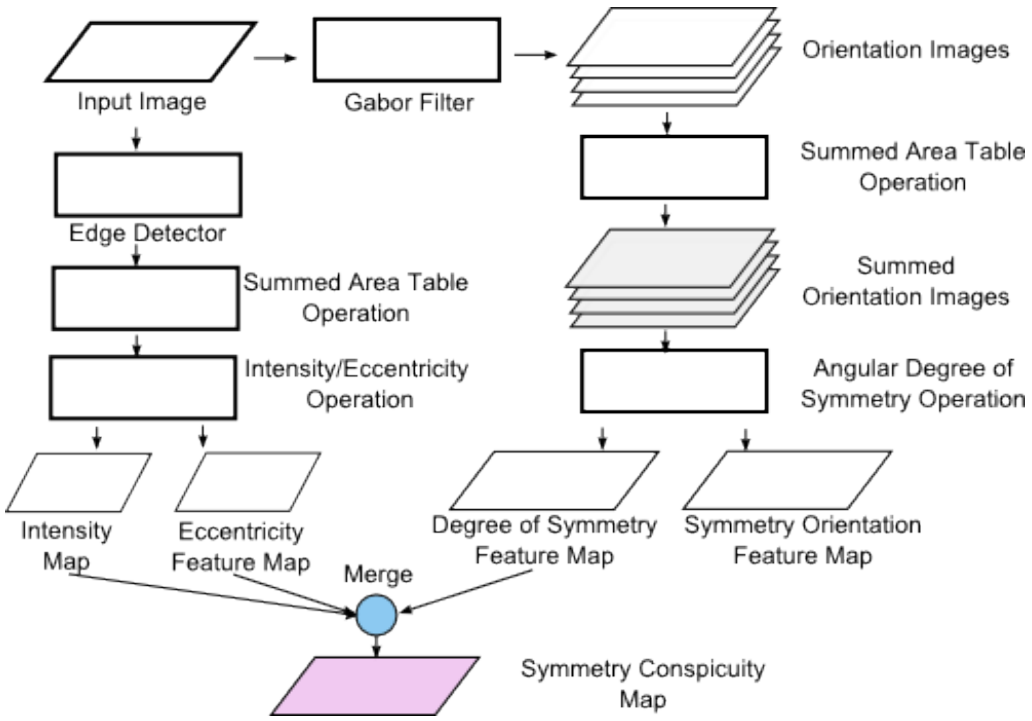

Figure 4.29: A single block based algorithm for the PoI detector.

The algorithm and more illustrative explanations are given in Figure 4.29 and 4.30.

The algorithm passes all the preliminary test cases, such as the angle spread test (Figure 4.32), and the noisy image test. Figure 4.33 and 4.34 confirm that the new measure overcomes the problem of stimuli prevalence.

The Figure 4.35, 4.36, 4.37, 4.38, 4.39, 4.40 contrast the AoIs detection capabilities between the proposed single block based algorithm and the state-of-the-art algorithm proposed in [126]. Those results might be the answer that the scale-invariant features are not necessarily salient features for symmetry detection (refer the question given in Section 2.2.1).

To make the experiment more challenging, we evaluate both algorithms using

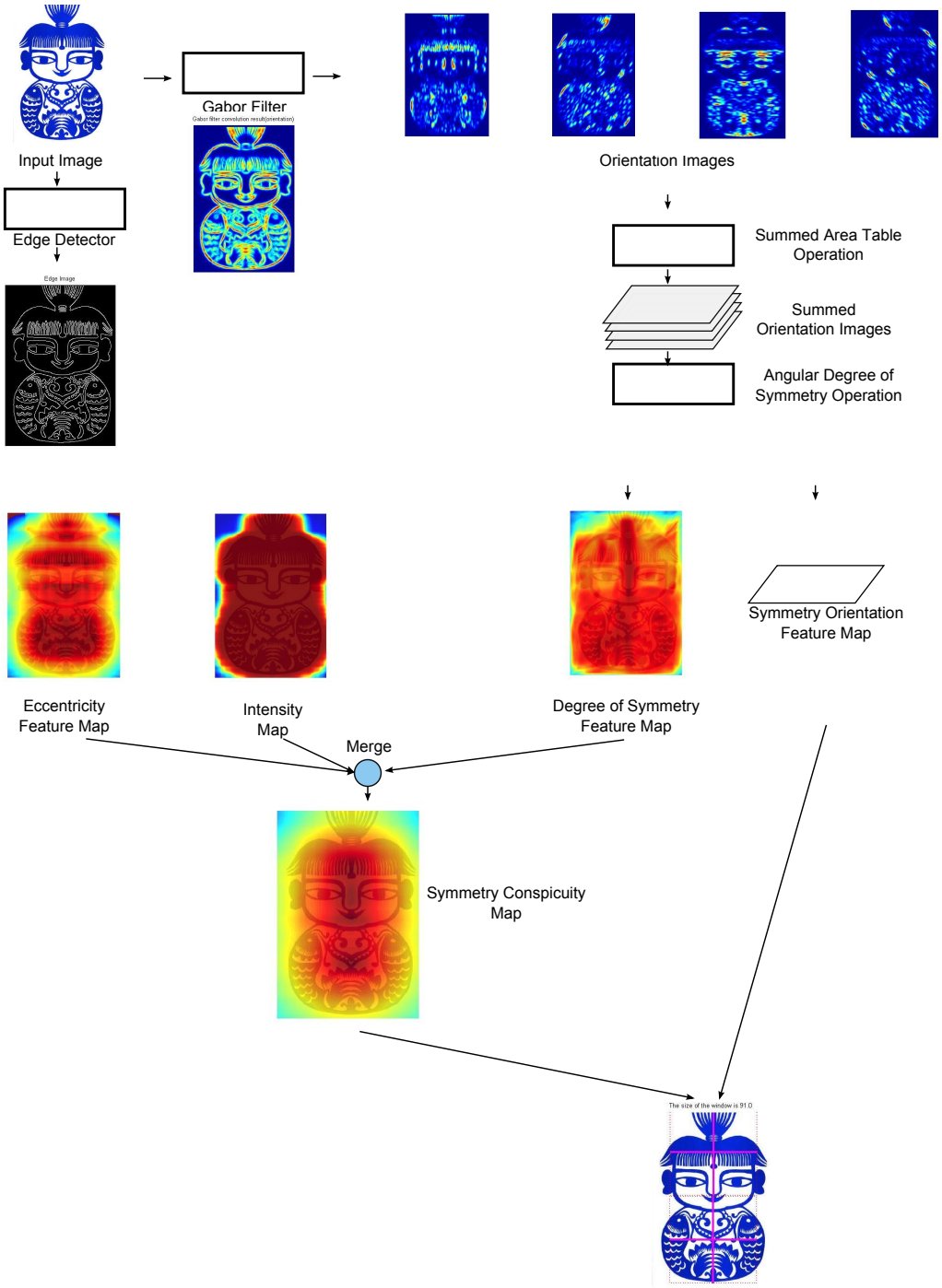

Figure 4.30: Illustrative explanations on the single block based algorithm. The process to find vertical symmetries.

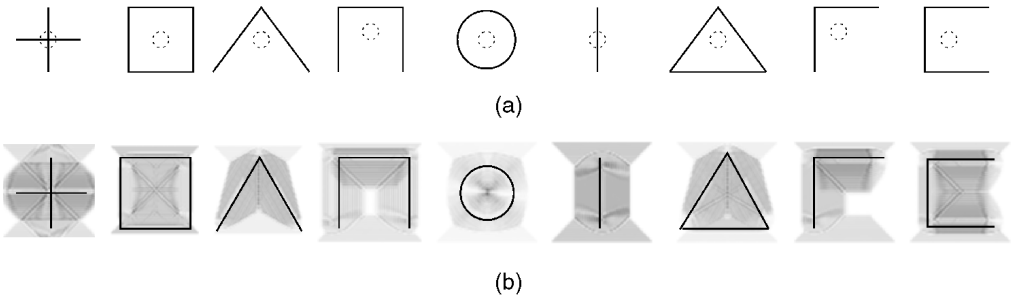

Figure 4.31: (a) Mean spontaneous fixation areas for various geometric figures, each subtends about 2° a visual angle on the retina, adapted from [98]. The small dotted circles indicate the region in which 86% of the fixations occurs.(b) Attractivity map for symmetry (darker values denote higher symmetric saliency). Adapted from [9]

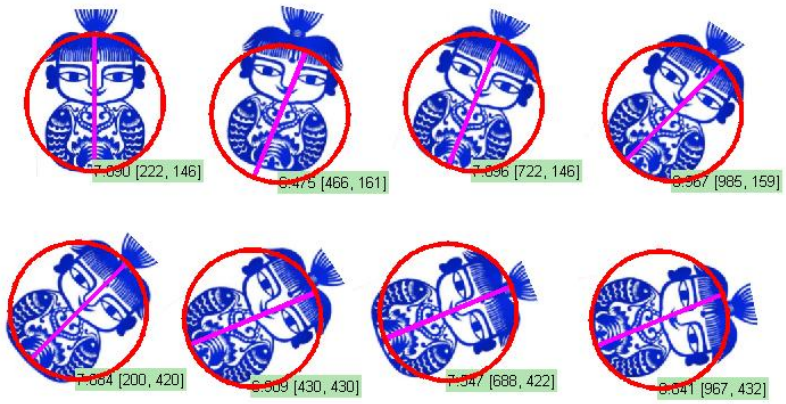

Figure 4.32: The result of the angle-spread test against the single block based algorithm. The circles represent AoIs and the lines mean the orientations correspond to the maximum values of the DoS.

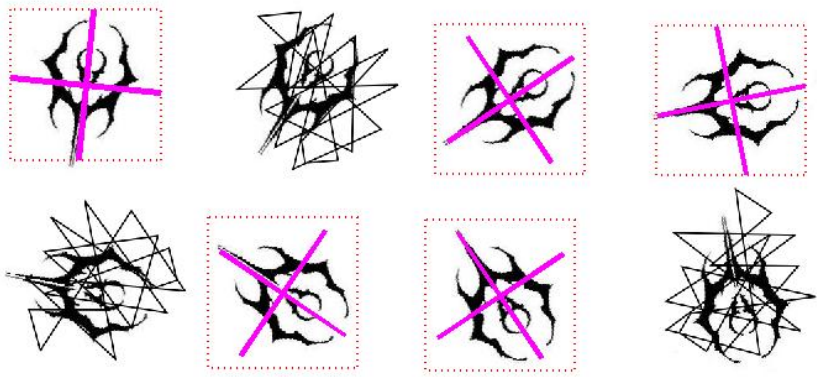

Figure 4.33: AoIs detection result. The dotted boxes represent the AoIs and the magenta lines show the orientations correspond to the maximum values of the DoS

Table 4.3: Type II Error

Algorithm	**TP / (TP + FN)**
Algorithm in [126]	0.492 (159/323)
The single block based algorithm	0.80 (259/323)

the image-dataset contains many images that the 4 square-quadrants algorithm has failed or barely succeeded. Table 4.3 evinces that the single block based algorithm excels the enhanced GST algorithm [126].

4.6 Put It All Together

To make a complete and automated symmetry detection system, we feed the AoIs detected by the single block based algorithm to the approximate symmetry detection system described in Chapter 3.

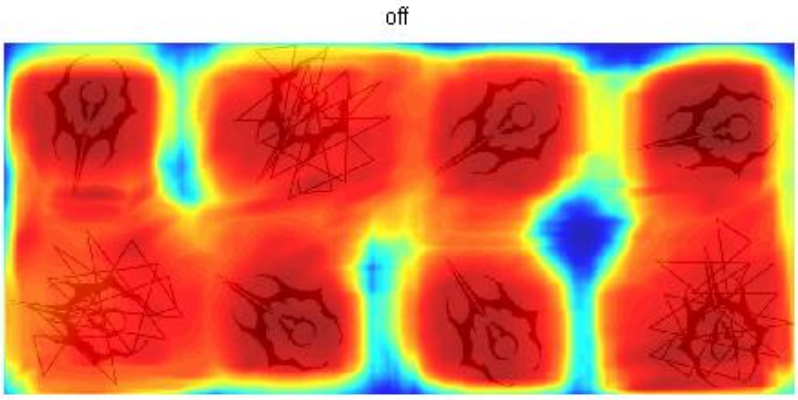

Figure 4.34: The DoS output on the noisy data. Though the intensity of stimuli is much stronger on the noisy parts, the PoI detector correctly identified symmetric areas. The dark red color means a high degree of symmetry.

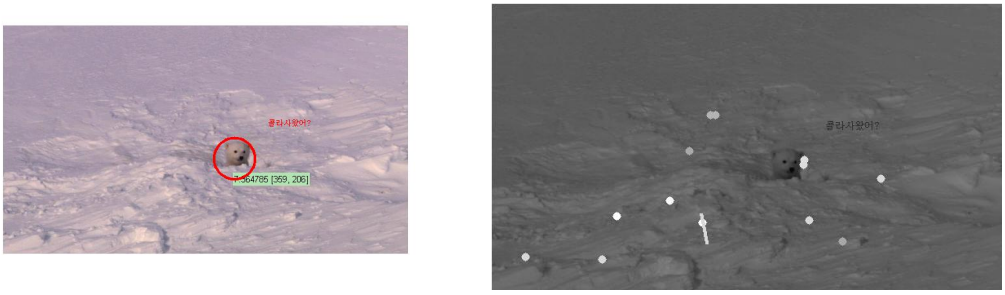

(a) The single block based algorithm (b) The algorithm in [126]

Figure 4.35: Find a baby polar bear. A comparison of the AoIs detection results with an algorithm in [126] (a black and white image).

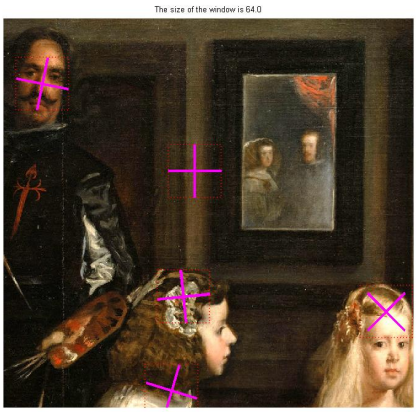

(a) The single block based algorithm

(b) The algorithm in [126]

Figure 4.36: A part of Las Meninas

(a) The single block based algorithm

(b) The algorithm in [126]

Figure 4.37: A girl and a cat.

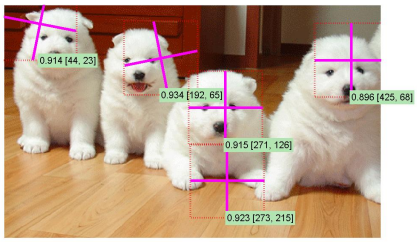

(a) The single block based algorithm

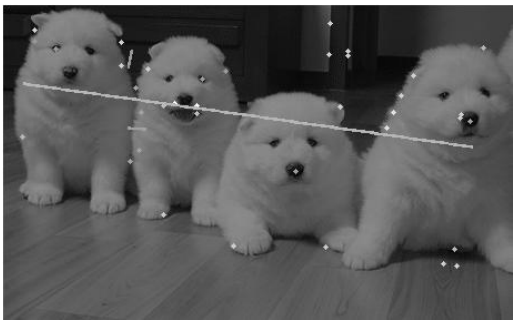

(b) The algorithm in [126]

Figure 4.38: Dogs.

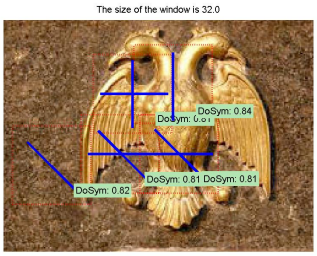

(a) The single block based algorithm

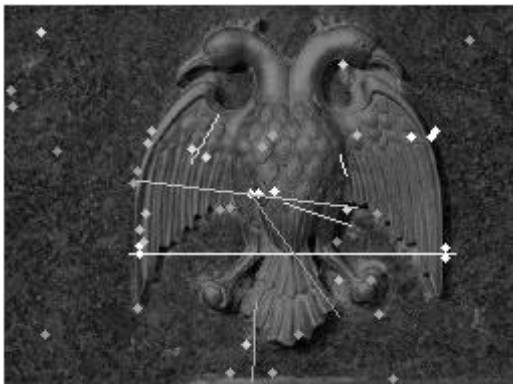

(b) The algorithm in [126]

Figure 4.39: An insignia.

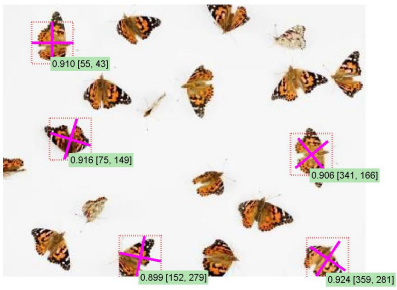

(a) The single block based algorithm

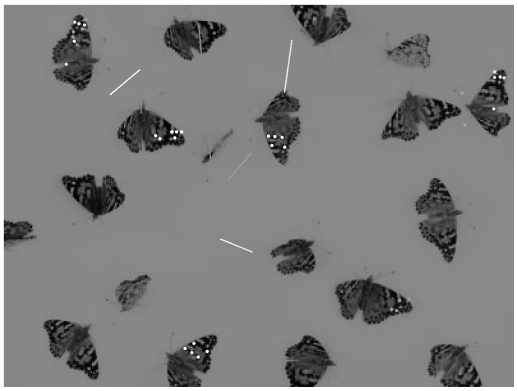

(b) The algorithm in [126]

Figure 4.40: Butterflies.

First, Figure 4.41, 4.42, 4.43, 4.44, 4.45 show that the approximate symmetry detection system can complement the single block based algorithm by correcting the "crude decision".

Second, Figure 4.46, 4.47, 4.48, 4.49 represent results that merge the axes of symmetry retrieved from different sizes of sliding windows, and select the axes with the highest degree of symmetry.

4.7 Discussion and Conclusion

To recapitulate, we address the problem of locating interesting areas in a given image by estimating the symmetry focal. Among the various avenues to explore the image to find points around which the groups of pixels exhibit a good deal of symmetry, we employ a simple estimation algorithm that incorporates Gabor features and summed-area tables.

In general, scale-invariant features are useful features for matching and it seems

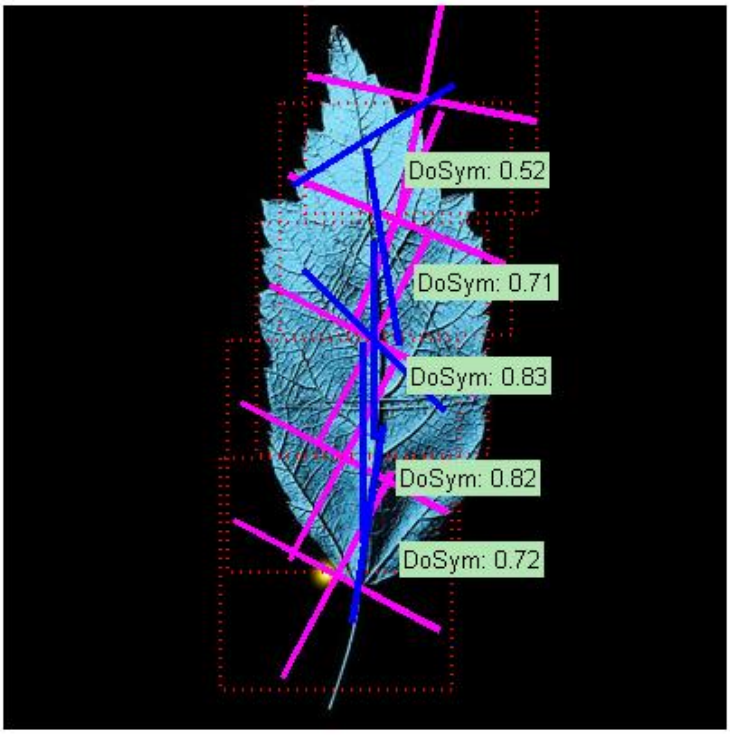

Figure 4.41: A leaf.

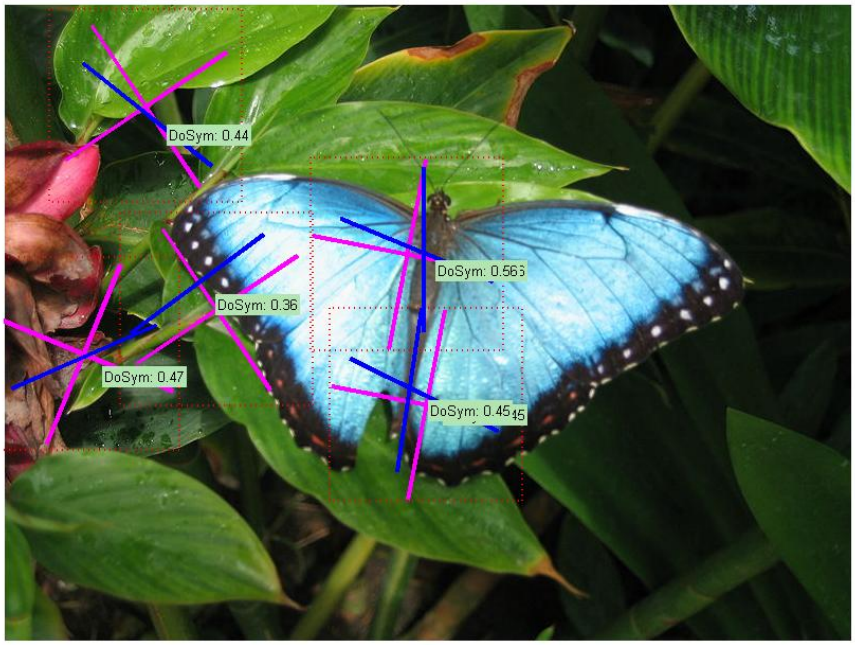

Figure 4.42: A butterfly.

Figure 4.43: A sheep.

Figure 4.44: A butterfly.

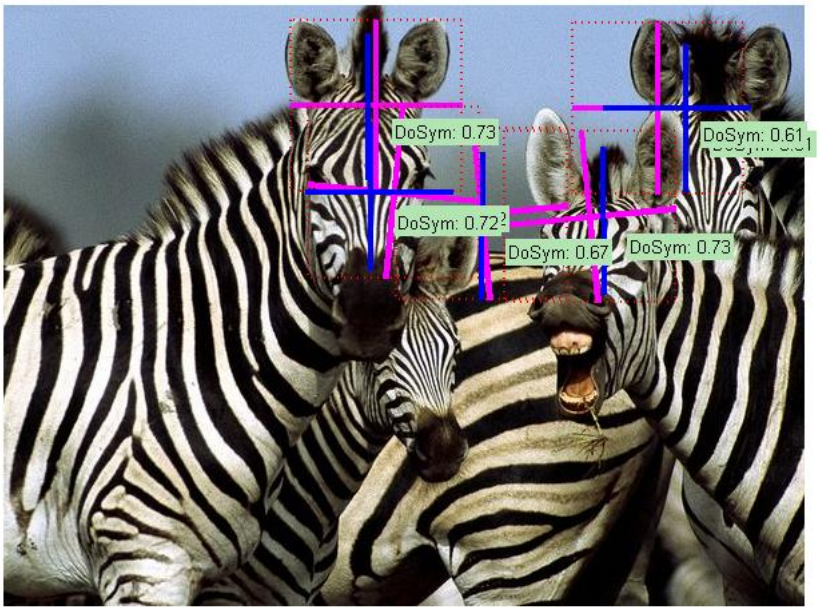

Figure 4.45: Zebras.

Figure 4.46: Cats.

Figure 4.47: A zebra.

Figure 4.48: A butterfly.

natural to employ these features to find symmetry. Unfortunately, most of the false negative results in algorithm [126] stem from the failure of retrieving symmetry relevant features. In other extreme, if the number of scale-invariant features selected are overwhelming, then the performance takes the heat from it. This hit-or-miss property of the scale-invariant features and the sensitivity to the noise make us hesitant to be relying on it.

Figure 4.49: A bear.

Appendix A

Appendix

A.1 Recovering axes of symmetry from perspectively distorted image

A.1.1 Problem statement and notation

Let us assume that there is a symmetric planar object O_{sym} with axis of symmetry L_S. Our goal is to find the axis of symmetry. We denote L_i lines that are perpendicular to L_S. Both L_S and L_i are expressed in homogeneous coordinates (i.e., a column vector with 3 elements). Depending on the context, the same symbols are used for the 3D lines and their 2D projection on the image plane $I : z = 1$. In the rest of the paper, we commonly use the following symbols:

- P_V is the vanishing point, i.e., the point of intersection between any pair of lines L_i. Note that L_i are parallel by virtue of being perpendicular to L_S.
- P_A, P_B denote the intersection of a line L_i with the boundary of the object O_{sym}. P_B is the closest point to P_V, while P_A is the furthest away.
- P_M is the midpoint of P_A and P_B. By definition P_M is also the intersection of L_i with L_S, so it belongs to the symmetry axis.

- the cross ratio of four points is denoted as

$$\begin{aligned}\lambda(P_A, P_B, P_C, P_D) &= \frac{|\overrightarrow{P_C - P_A}|}{|\overrightarrow{P_C - P_B}|} : \frac{|\overrightarrow{P_D - P_A}|}{|\overrightarrow{P_D - P_B}|} \\ &= \frac{|\overrightarrow{AC}|}{|\overrightarrow{BC}|} : \frac{|\overrightarrow{AD}|}{|\overrightarrow{BD}|}, \end{aligned} \tag{A.1}$$

  where $|\overrightarrow{P_C - P_A}| = |\overrightarrow{AC}|$ etc, is the signed distance between points C and A. Note that the order of the points in the cross ratio matters.

A.1.2 Computing the midpoint under perspective projection

If we consider a line L_i perpendicular to the axis of symmetry L_S, then the point P_M of the intersection $L_i \times L_S$ is between the boundary points P_A and P_B and has equal distance from both. The cross ratio of points P_A, P_B, P_M, and the vanishing point P_V is 2.

Since the cross ratio λ is preserved under any projective transformation, we consider the vanishing point to be at infinity $P_V = P_\infty$, i.e., the object is frontoparallel. In this case,

$$\lambda(P_A, P_M, P_B, P_\infty) = \frac{|\overrightarrow{P_B - P_A}||\overrightarrow{P_\infty - P_M}|}{|\overrightarrow{P_B - P_M}||\overrightarrow{P_\infty - P_A}|}. \tag{A.2}$$

If we denote the distance $|\overrightarrow{P_\infty - P_M}| = x$ and consider the limit $x \to \infty$ we have

$$\begin{aligned} \lambda(P_A, P_M, P_B, P_\infty) &= \lim_{x\to\infty} \frac{|\overrightarrow{AB}|x}{|\overrightarrow{MB}|(x + |\overrightarrow{AB}|)} \\ &= \frac{|\overrightarrow{AB}|}{|\overrightarrow{MB}|} = 2 \end{aligned} \tag{A.3}$$

In the general case the point at infinity P_∞ maps to the vanishing point P_V and the parallel lines connecting the boundary points P_A and P_B pass through the vanishing point. If we have the vanishing point we can compute the midpoint along a single line using two equations

$$\begin{aligned} L_i^T P_M &= 0 \\ \lambda(P_A, P_M, P_B, P_V) &= 2, \end{aligned} \tag{A.4}$$

where $L_i = P_A \times P_B$. If we denote with d_M, d_B and d_V the distance of points P_M, P_B and P_V from point P_A respectively, then

$$\lambda(P_A, P_M, P_B, P_V) = \frac{d_B(d_V - d_M)}{(d_B - d_M)d_V} \tag{A.5}$$

From Eqs. A.4, A.5 we find the distance of the midpoint from the boundary point P_A

$$d_M = \frac{d_B d_V}{2d_V - d_B}. \tag{A.6}$$

Algorithm 8 Find the bilateral symmetry of object silhouette

1. Sample the $2D$ plane for candidate vanishing point
2. For each candidate vanishing point P_V
   (a) Randomly select a fixed number of points P_i inside the object
   (b) For each P_i
      i. Find the line $L_i = P_i \times P_V$
      ii. Find the intersection points P_A, P_B of L_i with the object boundary
      iii. Compute the midpoint P_M^i using the cross ratio as described in Sec. A.1.2
3. Fit the least square line L_S through all the midpoints P_M^i and compute the average Euclidean distance of the points from the line
4. Select the vanishing point corresponding to the best fitted line L_S. L_S is the axis of symmetry for the object

A.1.3 The Algorithm

Based on the observation of the previous section detecting the symmetry axis is reduced to finding the vanishing point that gives the best results. In Alg. 8 we present the approach we employ to find the vanishing point (and consequently the symmetry axis). We use a least square based line fitting algorithm and the goodness-of-fit is the average of the squared distance of the midpoints from the line. The line with the smallest value is the best candidate for the symmetry axis L_S.

A.1.4 Conclusions and Future Work

We present a framework for detecting bilateral symmetries in planar $3D$ objects viewed under perspective projection. The method exploits the invariance of the cross ratio under perspective transformations. Using this framework the search

for $3D$ symmetries is reduced to a $2D$ search for the vanishing point of the lines perpendicular to the axis of symmetry. While $2D$ search is computationally expensive, there are ways (e.g., hierarchical search, gradient descent) to reduce the search space, which we will explore in the future.

Bibliography

[1] F. J. Aherne, N. A. Thacker, and P. Rockett. The bhattacharyya metric as an absolute similarity measure for frequency coded data. *Kybernetika*, 34(4):363–368, 1998.

[2] Robert Alterson and Donald B Plewes. Bilateral symmetry analysis of breast mri. *Physics in Medicine and Biology*, 48(20):3431, 2003.

[3] Pablo Arbelaez, Michael Maire, Charless Fowlkes, and Jitendra Malik. Contour detection and hierarchical image segmentation. *IEEE Trans. Pattern Anal. Mach. Intell.*, 33(5):898–916, May 2011.

[4] M.J. Atallah. On symmetry detection. *Computers, IEEE Transactions on*, C-34(7):663 –666, july 1985.

[5] Peter Atkins and Julio De Paula. *Physical Chemistry*. Oxford University Press, 8rev ed edition, March 2006.

[6] F. ATTNEAVE. Some informational aspects of visual perception. *Psychol Rev*, 61(3):183–193, May 1954.

[7] Edward Awh, Artem V. Belopolsky, and Jan Theeuwes. Top-down versus bottom-up attentional control: a failed theoretical dichotomy. *Trends in Cognitive Sciences*, 16(8):437 – 443, 2012.

[8] M. Z. Aziz and B. Mertsching. Fast and robust generation of feature maps for region-based visual attention. *Trans. Img. Proc.*, 17(5):633–644, May 2008.

[9] G. Backer, B. Mertsching, and M. Bollmann. Data- and model-driven gaze control for an active-vision system. *Pattern Analysis and Machine Intelligence, IEEE Transactions on*, 23(12):1415–1429, 2001.

[10] P. Bahnsen. Eine untersuchung nber symmetrie und asymmetrie bei visuellen wahrnehmungen. *Zeitschrift fnr Psychologie*, 108:129–154, 1928.

[11] H. B. Barlow and B. C. Reeves. The versatility and absolute efficiency of detecting mirror symmetry in random dot displays. *Vision research*, 19(7):783–793, 1979.

[12] Timothy C. Bates. Fluctuating asymmetry and intelligence. *Intelligence*, 35(1):41–46, January 2007.

[13] Jean-Yves Baudouin and Guy Tiberghien. Symmetry, averageness, and feature size in the facial attractiveness of women. *Acta Psychologica*, 117(3):313 – 332, 2004.

[14] Driver J Baylis, G. C. Parallel computation of symmetry but not repetition within single visual shapes. *Visual Cognition*, 4:377–400., 1994.

[15] Gordon C. Baylis and Jon Driver. Obligatory edge assignment in vision: The role of figure and part segmentation in symmetry detection. *Journal of Experimental Psychology: Human Perception and Performance*, 21(6):1323–1342, 1995.

[16] S. Belongie, J. Malik, and J. Puzicha. Shape matching and object recognition using shape contexts. *IEEE Trans. Pattern Anal. Mach. Intell.*, 24(4):509–522, April 2002.

[17] Michaela Benz, X. Laboureux, Tobias Maier, Emeka Nkenke, Stephan Seeger, Friedrich Wilhelm Neukam, and Gerd Husler. The symmetry of faces. In Gnther Greiner, editor, *VMV*, pages 43–50. Aka GmbH, 2002.

[18] A.C. Berg, T.L. Berg, and J. Malik. Shape matching and object recognition using low distortion correspondences. In *Computer Vision and Pattern Recognition, 2005. CVPR 2005. IEEE Computer Society Conference on*, volume 1, pages 26–33 vol. 1, 2005.

[19] Marco Bertamini. Sensitivity to reflection and translation is modulated by objectness. *Perception*, 39(1):27–40, 2010.

[20] A. Bhattacharyya. On a measure of divergence between two statistical populations defined by their probability distributions. *Bulletin of the Calcutta Mathematical Society*, 35:99–109, 1943.

[21] Irving Biederman. Recognition-by-components: A theory of human image understanding. *Psychological Review*, 94:115–147, 1987.

[22] Harry Blum and Roger N. Nagel. Shape description using weighted symmetric axis features. *Pattern Recognition*, 10(3):167 – 180, 1978. ¡ce:title¿The Proceedings of the {IEEE} Computer Society Conference¡/ce:title¿.

[23] Luc Boutsen and Christian Marendaz. Detection of shape orientation depends on salient axes of symmetry and elongation: Evidence from visual search. *Perception & Psychophysics*, 63 (3):404–422, 2001.

[24] Y. Boykov and V. Kolmogorov. An experimental comparison of min-cut/max-flow algorithms for energy minimization in vision. *Pattern Analysis and Machine Intelligence, IEEE Transactions on*, 26(9):1124–1137, 2004.

[25] Michael Brady and Haruo Asada. Smoothed local symmetries and their implementation. Technical report, Cambridge, MA, USA, 1984.

[26] M. L. Braunstein. Depth perception in rotating dot patterns: effects of numerosity and perspective. *J Exp Psychol*, 64:415–420, October 1962.

[27] William M. Brown, Lee Cronk, Keith Grochow, Amy Jacobson, Zoran Liu, and Robert Trivers. Dance reveals symmetry especially in young men. *Nature*, 438(7071):1148–1150, December 2005.

[28] V. Bruce and M. J. Morgan. Violations of symmetry and repetition in visual patterns. *Perception*, 4:239–249, 1975.

[29] David M. Buss. Sex differences in human mate preferences: Evolutionary hypotheses tested in 37 cultures. *Behavioral and Brain Sciences*, 12:1–14, 3 1989.

[30] John Canny. Finding edges and lines in images. Technical report, Cambridge, MA, USA, 1983.

[31] Stefan Carlsson. Symmetry in perspective. In *Proceedings of the 5th European Conference on Computer Vision-Volume I - Volume I*, ECCV '98, pages 249–263, London, UK, UK, 1998. Springer-Verlag.

[32] R. Cesar, O. Colliot, Tuzikov, and I. Bloch. Approximate reflectional symmetries of fuzzy objects with an application in model-based object recognition. *Fuzzy Sets and Systems*, 2003.

[33] T. J. Cham and R. Cipolla. Skewed Symmetry Detection Through Local Skewed Symmetries. In *Proc. British Machine Vision Conference*, pages 549–558. British Machine Vision Association, 1994.

[34] T.F. Chan and L.A. Vese. Active contours without edges. *Image Processing, IEEE Transactions on*, 10(2):266–277, 2001.

[35] Nick Chater. Reconciling simplicity and likelihood principles in perceptual organization. *Psychological Review*, 103:566–581, 1996.

[36] M. Chertok and Y. Keller. Spectral symmetry analysis. *Pattern Analysis and Machine Intelligence, IEEE Transactions on*, 32(7):1227–1238, 2010.

[37] Elias H Cohen and Qasim Zaidi. Symmetry in context: Salience of mirror symmetry in natural patterns. *Journal of Vision*, 13(6):1–9, 2013.

[38] Jonathan A. Cohen. Quantifying symmetry, 2005.

[39] Dorin Comaniciu, Peter Meer, and David Tyler. Dissimilarity computation through low rank corrections. *Pattern Recogn. Lett.*, 24(1-3):227–236, January 2003.

[40] L. A. Cooper and R. N. Shepard. Transformational studies of the internal representation of three-dimensional objects. In *Mental Images and Their Transformations*, pages 24–43, 243–262. The MIT Press, Cambridge, 1982.

[41] M. C. Corballis and C. E. Roldan. Detection of symmetry as a function of angular orientation. *Journal of experimental psychology: human perception and performance*, 1(3):221–230, 1975.

[42] H. Cornelius and G. Loy. Detecting bilateral symmetry in perspective. In *Computer Vision and Pattern Recognition Workshop, 2006. CVPRW '06. Conference on*, page 191, 0-0 2006.

[43] Hugo Cornelius, Michal Perd'och, Jiří Matas, and Gareth Loy. Efficient symmetry detection using local affine frames. In *Proceedings of the 15th Scandinavian conference on Image analysis*, SCIA'07, pages 152–161, Berlin, Heidelberg, 2007. Springer-Verlag.

[44] O. Cossairt, D. Miau, and S. K. Nayar. Gigapixel computational imaging. In *IEEE International Conference on Computational Photography (ICCP)*, Mar 2011.

[45] Thomas M. Cover and Joy A. Thomas. *Elements of information theory*. Wiley-Interscience, New York, NY, USA, 1991.

[46] Franklin C. Crow. Summed-area tables for texture mapping. *SIGGRAPH Comput. Graph.*, 18:207–212, January 1984.

[47] Csathó, G. van der Vloed, and P. A. van der Helm. Blobs strengthen repetition but weaken symmetry. *Vision Research*, 43(9):993–1007, 2003.

[48] van der Helm PA. Csatho A, van der Vloed G. The force of symmetry revisited: symmetry-to-noise ratios regulate (a)symmetry effects. *Acta Psychol*, 117:233–50, 2004.

[49] C. Deane-Drummond and P. Scott. *Future Perfect?: God, Medicine and Human Identity*. Bloomsbury, 2006.

[50] R. Desimone and J. Duncan. Neural mechanisms of selective visual attention. *Annual Review of Neuroscience*, 18:193–222–, 1995.

[51] S. S. Agaian E. A. Silva, K. Panetta. Quantifying image similarity using measure of enhancement by entropy. In *International Society for Optical Engineering*, 2007.

[52] M. Eichner and V. Ferrari. Better appearance models for pictorial structures. In *British Machine Vision Conference*, September 2009.

[53] Willis D. Ellis. *A source book of gestalt psychology,*. Routledge & Kegan Paul, January 1969.

[54] Magnus Enquist and Anthony Arak. Symmetry, beauty and evolution. *Nature*, 372:169–172, 1994.

[55] C. W. Eriksen and Y. Y. Yeh. Allocation of attention in the visual field. *Journal of experimental psychology. Human perception and performance*, 11(5):583–597, October 1985.

[56] C. S. Evans, P. Wenderoth, and K. Cheng. Detection of bilateral symmetry in complex biological images. *Perception*, 29:31–42, 2000.

[57] M. Everingham, L. Van Gool, C. K. I. Williams, J. Winn, and A. Zisserman. The pascal visual object classes (voc) challenge. *International Journal of Computer Vision*, 88(2):303–338, June 2010.

[58] Richard Phillips Feynman. *Six Not-so-easy Pieces: Einstein's Relativity, Symmetry, and Space-Time*. Addison-Wesley Pub., Reading, Mass., 1997.

[59] David J. Field. Relations between the statistics of natural images and the response properties of cortical cells. *J. Opt. Soc. Am. A*, 4:2379–2394, 1987.

[60] S. Filipe and L. Alexandre. From the human visual system to the computational models of visual attention: a survey. *Artificial Intelligence Review*, 39(1):1–47, January 2013.

[61] Thomas Schmidt Filipp Schmidt. Rapid processing of closure and viewpoint-invariant symmetry: behavioral criteria for feedforward processing. *Psychological Research*, 2013.

[62] John R Finnerty. The origins of axial patterning in the metazoa: how old is bilateral symmetry? *Int J Dev Biol*, pages 523–9, 2003.

[63] Celia B. Fisher, Kay Ferdinandsen, and Marc H. Bornstein. The role of symmetry in infant form discrimination. *Child Development*, 52(2):pp. 457–462, 1981.

[64] Alexandre R. J. Francois, Gerard G. Medioni, and Roman Waupotitsch. Mirror symmetry=¿2-view stereo geometry. *Image and Vision Computing*, 21(2):137 – 143, 2003.

[65] J. J. Freyd and B. Tversky. Force of symmetry in form perception. *American Journal of Psychology*, 97:109–126, 1984.

[66] S. W. Gangestad and R. Thornhill. The evolutionary psychology of extrapair sex: The role of fluctuating asymmetry. 18:69–88, 1997.

[67] Yongsheng Gao and Maylor K.H. Leung. Line segment hausdorff distance on face matching. *Pattern Recognition*, 35(2):361 – 371, 2002.

[68] M. Gardner. *The ambidextrous universe*. Allen Lane the Penguin Press, 1967.

[69] L. Glass. Moire effect from random dots. *Nature*, 243:578580, 1969.

[70] Karl Grammer and Randy Thornhill. Human (*Homo sapiens*) facial attractiveness and sexual selection: The role of symmetry and averageness. *Journal of Comparative Psychology*, pages 233–242, 1994.

[71] B. Greene. *The Hidden Reality: Parallel Universes and the Deep Laws of the Cosmos*. Penguin, 2012.

[72] R Gurnsey, A M Herbert, and J Kenemy. Bilateral symmetry embedded in noise is detected accurately only at fixation. *Vision Res*, 38(23):3795–803, 1998.

[73] Gideon Guy and Gérard Medioni. Inference of surfaces, 3d curves, and junctions from sparse, noisy, 3d data. *IEEE Trans. Pattern Anal. Mach. Intell.*, 19(11):1265–1277, November 1997.

[74] J. G. Harries. Symmetry in the movements of t'ai chi chuan. *Comput. Math. Appl.*, 17(4-6):827–835, January 1989.

[75] Vi Hart. Symmetry and transformations in the musical plane. In *Proceedings of the 12th Annual BRIDGES Conference: Mathematics, Music, Art, Architecture, Culture (BRIDGES 2009)*, 2009.

[76] Jingrui He, Mingjing Li, Hong-Jiang Zhang, and Changshui Zhang. Symmetry feature in content-based image retrieval. In *Image Processing, 2004. ICIP '04. 2004 International Conference on*, volume 1, pages 417–420 Vol. 1, 2004.

[77] Gunther Heidemann. Combining spatial and colour information for content based image retrieval. *Computer Vision and Image Understanding*, 94(13):234 – 270, 2004. ¡ce:title¿Special Issue: Colour for Image Indexing and Retrieval¡/ce:title¿.

[78] H. Helmholtz and J.P.C. Southall. *Helmholtz's treatise on physiological optics*, volume 3 of *Helmholtz's Treatise on Physiological Optics*. Dover Publications, 1962.

[79] F. L. Hitchcock. The distribution of a product from several sources to numerous localities. *Journal of Math. Phys.*, 20:224–230, 1941.

[80] J. Hochberg and E. McAlister. A quantitative approach to figural "goodness". *Journal of Experimental Psychology*, 46(5):361–364, 1953.

[81] Liqiang Huang and Harold Pashler. Symmetry detection and visual attention: a "binary-map" hypothesis. *Vision research*, 42(11):1421–1430, May 2002.

[82] Kai Huebner. A symmetry operator and its application to the robocup. In Daniel Polani, Brett Browning, Andrea Bonarini, and Kazuo Yoshida, editors, *RoboCup 2003: Robot Soccer World Cup VII*, volume 3020 of *Lecture Notes in Computer Science*, pages 274–283. Springer Berlin Heidelberg, 2004.

[83] Benoit Huet and Edwin R. Hancock. Cartographic indexing into a database of remotely sensed images. In *In Third IEEE Workshop on Applications of Computer Vision (WACV96*, pages 8–14, 1996.

[84] Benoit Huet and Edwin R. Hancock. Structural indexing of infra-red images using statistical histogram comparison benoit huet. In *In Proc. IWISP*, pages 653–656, 1996.

[85] Benoit Huet and Edwin R. Hancock. Relational histograms for shape indexing. *Computer Vision, IEEE International Conference on*, 0:563, 1998.

[86] Kenneth Hugdahl. Symmetry and asymmetry in the human brain. *European Review*, 13:119–133, 10 2005.

[87] M.A.; Gallup G.G. Jr. Hughes, S.M.; Harrison. The sound of symmetry: Voice as a marker of developmental stability. *Evol. Hum. Behav.*, 23:173180, 2002.

[88] Susan M. Hughes, Franco Dispenza, and Gordon G. Gallup Jr. Ratings of voice attractiveness predict sexual behavior and body configuration. *Evolution and Human Behavior*, 25(5):295 – 304, 2004.

[89] Somesh Kashyap Jingchen Liu Ingmar Rauschert, Kyle Brocklehurst and Yanxi Liu. First symmetry detection competition: Summary and results. Technical report, Department of Computer Science and Engineering, The Pennsylvania State University, 2011.

[90] L. Itti. A saliency-based search mechanism for overt and covert shifts of visual attention. *Vision Research*, 40(10-12):1489–1506, June 2000.

[91] L. Itti and C. Koch. Computational modelling of visual attention. *Nature Reviews Neuroscience*, 2(3):194–203, Mar 2001.

[92] Jerzy Jarmasz. Towards the integration of perceptual organization and visual attention: The inferential attentional allocation model. Technical report, 2001.

[93] Harold Jeffreys. An invariant form for the prior probability in estimation problems. *Proceedings of the Royal Society of London. Series A,Mathematical and Physical Sciences*, 186(1007):453461, 1946.

[94] B Julesz and J J Chang. Symmetry perception and spatial-frequency channels. *Perception*, 8(6):711–8, 1979.

[95] Alexander Kadyrov and Maria Petrou. The trace transform and its applications. *IEEE Trans. Pattern Anal. Mach. Intell.*, 23(8):811–828, August 2001.

[96] Alexander Kadyrov and Maria Petrou. Affine parameter estimation from the trace transform. *IEEE Trans. Pattern Anal. Mach. Intell.*, 28(10):1631–1645, October 2006.

[97] G. Kanizsa. *Organization in Vision*. Praeger, New York, 1979.

[98] Lloyd Kaufman and Whitman Richards. Spontaneous fixation tendencies for visual forms. *Perception and Psychophysics*, 5(2):85–88, 1969.

[99] Yosi Keller and Yoel Shkolnisky. An algebraic approach to symmetry detection. *Pattern Recognition, International Conference on*, 3:186–189, 2004.

[100] Davorin Kempf. What is symmetry in music? *International Review of the Aesthetics and Sociology of Music*, 27(2):pp. 155–165, 1996.

[101] Nahum Kiryati and Yossi Gofman. Detecting symmetry in grey level images: The global optimization approach. In *In Proceedings of the 13th International Conference on Pattern Recognition, volume I*, pages 951–956, 1996.

[102] C. Koch and S. Ullman. Shifts in selective visual attention: Towards the underlying neural circuitry. *Human Neurobiology*, 4:219–227, January 1985.

[103] Shigeru Kondo and Rihito Asai. A reaction-diffusion wave on the skin of the marine angelfish Pomacanthus. *Nature*, 376(6543):765–768, August 1995.

[104] Johannes Kopf, Matt Uyttendaele, Oliver Deussen, and Michael F. Cohen. Capturing and viewing gigapixel images. *ACM Transactions on Graphics (Proceedings of SIGGRAPH 2007)*, 26(3):to appear, 2007.

[105] Peter Kovesi. Symmetry and asymmetry from local phase. In *Tenth Australian Joint Converence on Artificial Intelligence*, pages 2–4, 1997.

[106] S. Kullback. A lower bound for discrimination information in terms of variation. *IEEE Trans. on Inform. Theory*, IT-13:126–127, Jan 1967.

[107] Roland Kwitt and Andreas Uhl. Image similarity measurement by kullback-leibler divergences between complex wavelet subband statistics for texture retrieval. In *ICIP*, pages 933–936, 2008.

[108] Seungkyu Lee and Yanxi Liu. Skewed rotation symmetry group detection. *Pattern Analysis and Machine Intelligence, IEEE Transactions on*, 32(9):1659–1672, 2010.

[109] Marius Leordeanu and Martial Hebert. A spectral technique for correspondence problems using pairwise constraints. In *Proceedings of the Tenth IEEE International Conference on Computer Vision - Volume 2*, ICCV '05, pages 1482–1489, Washington, DC, USA, 2005. IEEE Computer Society.

[110] Alex Levinshtein, Cristian Sminchisescu, and Sven Dickinson. Multiscale symmetric part detection and grouping. *International Journal of Computer Vision*, 104(2):117–134, 2013.

[111] Ming Li, Frank C. Langbein, and Ralph R. Martin. Detecting approximate symmetries of discrete point subsets. *Comput. Aided Des.*, 40(1):76–93, January 2008.

[112] Wai Ho Li and L. Kleeman. Real time object tracking using reflectional symmetry and motion. In *Intelligent Robots and Systems, 2006 IEEE/RSJ International Conference on*, pages 2798–2803, 2006.

[113] Wai Ho Li, Alan M. Zhang, and Lindsay Kleeman. Fast global reflectional symmetry detection for robotic grasping and visual tracking. In *in Proceedings of Australasian Conference on Robotics and*, 2005.

[114] W.H. Li, A.M. Zhang, and L. Kleeman. Real time detection and segmentation of reflectionally symmetric objects in digital images. pages xx–yy, 2006.

[115] Leo Liberti. Symmetry in mathematical programming. In *Mixed Integer Nonlinear Programming. Volume IMA*. Springer, 2010.

[116] J. Lin. Divergence measures based on the shannon entropy. *Information Theory,IEEE Transactions on*, 37(1):145151, August 2002.

[117] A.C. Little, C.L. Apicella, and F.W. Marlowe. Preferences for symmetry in human faces in two cultures: data from the uk and the hadza, an isolated group of hunter-gatherers. *Proc Biol Sci*, 2007.

[118] Jingchen Liu and Yanxi Liu. Curved reflection symmetry detection with self-validation. In *Proceedings of the 10th Asian conference on Computer vision - Volume Part IV*, ACCV'10, pages 102–114, Berlin, Heidelberg, 2011. Springer-Verlag.

[119] Yanxi Liu. Computational symmetry, 2000.

[120] Yanxi Liu, James H. Hays, Ying-Qing Xu, and Heung-Yeung Shum. Digital papercutting. In *Technical Sketch, SIGGRAPH*. 2005.

[121] Yanxi Liu, Hagit Hel-Or, Craig S. Kaplan, and Luc J. Van Gool. Computational symmetry in computer vision and computer graphics. *Foundations and Trends in Computer Graphics and Vision*, 5(1-2):1–195, 2010.

[122] P. Locher and C. Nodine. The perceptual value of symmetry. *Comput. Math. Appl.*, 17:475–484, January 1989.

[123] PaulJ. Locher and CalvinF. Nodine. Influence of stimulus symmetry on visual scanning patterns. *Perception & Psychophysics*, 13(3):408–412, 1973.

[124] P.J. Locher and C.F. Nodine. Symmetry catches the eye. *Eye Movements: From Physiology to Cognition*, pages 353–361, 1987.

[125] David G. Lowe. Object recognition from local scale-invariant features. In *Proceedings of the International Conference on Computer Vision-Volume 2 - Volume 2*, ICCV '99, pages 1150–, Washington, DC, USA, 1999. IEEE Computer Society.

[126] Gareth Loy and Jan-Olof Eklundh. Detecting symmetry and symmetric constellations of features. In *9th European Conference on Computer Vision (ECCV 2006)*, page 508521, May 2006.

[127] Gareth Loy and Alexander Zelinsky. Fast radial symmetry for detecting points of interest. *IEEE Transactions on Pattern Analysis and Machine Intelligence*, 25(8):959–973, 2003.

[128] Hongxia Luan, Feihu Qi, Zhong Xue, Liya Chen, and Dinggang Shen. Multimodality image registration by maximization of quantitative-qualitative measure of mutual information. *Pattern Recogn.*, 41(1):285–298, 2008.

[129] Peterson M.A., de Gelder B., Rapcsak S.Z., Gerhardstein P.C., and Bachoud-Levi A.-C. Object memory effects on figure assignment: conscious object recognition is not necessary or sufficient. *Vision Research*, 40(10):1549–1567, 2000.

[130] E. Mach and C.M. Williams. *Contributions to the analysis of the sensations.* The Open court publishing company, 1897.

[131] J. T. Manning and L. J. Pickup. Symmetry and performance in middle distance runners. *Int J Sports Med*, 19(3):205–209, April 1998.

[132] Slobodan Markovic. Objective constraints of figural goodness. *Psihologija*, 35(3-4):245–260, 2002.

[133] G. Marola. On the detection of the axes of symmetry of symmetric and almost symmetric planar images. *IEEE Transactions on Pattern Analysis and Machine Intelligence*, 11:104–108, 1989.

[134] D. Marr and H. K. Nishihara. Representation and recognition of the spatial organization of three-dimensional shapes. *Royal Society of London Proceedings Series B*, 200:269–294, February 1978.

[135] D. Martin, C. Fowlkes, D. Tal, and J. Malik. A database of human segmented natural images and its application to evaluating segmentation algorithms and measuring ecological statistics. In *Proceedings IEEE International Conference on Computer Vision, 2001*, volume 2, pages 416–423, 2001.

[136] Takeshi Masuda, Kazuhiko Yamamoto, and Hiromitsu Yamada. Detection of partial symmetry using correlation with rotated-reflected images. *Pattern Recognition*, pages 1245–1253, 1993.

[137] K. Matusita. Decision Rules, Based on the Distance, for Problems of Fit, Two Samples, and Estimation. *Annals of Mathematical Statistics*, 26:631–640, 1955.

[138] M. K. McBeath, D. J. Schiano, and B. Tversky. Three-dimensional bilateral symmetry bias in judgments of figural identity and orientation. *Psychological Science*, 8:217–223, 1997.

[139] . C. McMANUS. Symmetry and asymmetry in aesthetics and the arts. *European Review*, 13(S2):157–180, 2005.

[140] I. C. McManus, D. Edmondson, and J. Rodger. Balance in pictures. *British Journal of Psychology*, 76(3):311–324, 1985.

[141] Guangnan Meng, Natalie Arkus, Michael P. Brenner, and Vinothan N. Manoharan. The Free-Energy Landscape of Clusters of Attractive Hard Spheres. *Science*, 327(5965):560–563, January 2010.

[142] P. Minovic, S. Ishikawa, and K. Kato. Three-dimensional symmetry measurement of medical entities. In *Pattern Recognition, 1992. Vol.I. Conference A: Computer Vision and Applications, Proceedings., 11th IAPR International Conference on*, pages 457–460, 1992.

[143] Ajay Mishra and Yiannis Aloimonos. Active segmentation with fixation. In *ICCV*, 2009.

[144] N. J. Mitra, L. Guibas, and M. Pauly. Partial and approximate symmetry detection for 3d geometry. *ACM Transactions on Graphics (SIGGRAPH)*, 25(3):560–568, 2006.

[145] Moller. Parasites and sexual selection: Current status of the hamilton and zuk hypothesis. *Journal of Evolutionary Biology*, 3:319–328, 1990. Journal.

[146] Anders Pape Moller and Mats Eriksson. Patterns of fluctuating asymmetry in flowers: Implications for sexual selection in plants. *Journal of Evolutionary Biology*, 7(1):97–113, 1994.

[147] Anders Pape Moller, Manuel Soler, and Randy Thornhill. Breast asymmetry, sexual selection, and human reproductive success. *Ethology and Sociobiology*, 16(3):207 – 219, 1995.

[148] D. Morales and H. Pashler. No role for colour in symmetry perception. *Nature*, 399(6732):115–6, 1999.

[149] Ken Nakayama and Gerald H. Silverman. Serial and parallel processing of visual feature conjunctions. *Nature*, 320(6059):264–265, March 1986.

[150] Mark B. Neider and Gregory J. Zelinsky. Scene context guides eye movements during visual search. *Vision Research*, 46(5):614 – 621, 2006.

[151] E Noether and M A Tavel. Invariant variation problems. Technical Report physics/0503066, Mar 2005.

[152] M. Nucci and J. Wagemans. Goodness of regularity in dot patterns: global symmetry, local symmetry, and their interactions. *Perception*, 36(9):1305–19, 2007.

[153] American Society of Zoologists and American Society of Zoologists. Meeting. *Parasites and Sexual Selection: The American Society of Zoologists, 1889-1989, a Century of Integrating the Biological Sciences*. American zoologist. American Society of Zoologists, 1990.

[154] ChristianN.L. Olivers and PeterA. Helm. Symmetry and selective attention: A dissociation between effortless perception and serial search. *Perception & Psychophysics*, 60(7):1101–1116, 1998.

[155] Harold Osborne. Symmetry as an aesthetic factor. *Computers & Mathematics with Applications*, 12(12, Part B):77 – 82, 1986.

[156] Harold Osborne. Symmetry as an aesthetic factor. *Computers & Mathematics with Applications*, 12(12, Part B):77 – 82, 1986.

[157] D. Osorio. Symmetry detection by categorization of spatial phase, a model. *Proceedings: Biological Sciences*, 263(1366):pp. 105–110, 1996.

[158] S. E. Palmer. The psychology of perceptual organization: A transformational approach. *Human and machine vision*, pages 269–339, 1983.

[159] S. E. Palmer and K. Hemenway. Orientation and symmetry: effects of multiple, rotational, and near symmetries. *Journal of experimental psychology. Human perception and performance*, 4(4):691–702, November 1978.

[160] Heechan Park, Abhir Bhalerao, Graham Martin, and Andy C. Yu. An affine symmetric approach to natural image compression. In *Proceedings of the 2nd international conference on Mobile multimedia communications*, MobiMedia '06, pages 33:1–33:6, New York, NY, USA, 2006. ACM.

[161] Minwoo Park, Seungkyu Lee, Po-Chun Chen, Somesh Kashyap, Asad A. Butt, and Yanxi Liu. Performance evaluation of state-of-the-art discrete symmetry detection algorithms. In *Computer Vision and Pattern Recognition Conference (CVPR '08)*, June 2008.

[162] G. Parovel and S. Vezzani. Mirror symmetry opposes splitting of chromatically homogeneous surfaces. *Perception*, 31(6):693–709, 2002.

[163] P A Parsons. Fluctuating asymmetry: an epigenetic measure of stress. *Biol Rev Camb Philos Soc*, 65(2):131–45, 1990.

[164] Karl Pearson. Contributions to the mathematical theory of evolution. ii. skew variation in homogeneous material. *Philosophical Transactions of the Royal Society of London. A*, 186:pp. 343–414, 1895.

[165] I.S. Penton-Voak, B.C. Jones, A.C. Little, S. Baker, B. Tiddeman, D.M. Burt, and D.I. Perrett. Symmetry, sexual dimorphism in facial proportions and male facial attractiveness. *Proc Biol Sci*, 268(1476):1617–23, 2001.

[166] Nikolay Petkov. Biologically motivated computationally intensive approaches to image pattern recognition. *Future Gener. Comput. Syst.*, 11:451–465, August 1995.

[167] S. M. Pizer, W. R. Oliver, and S. H. Bloomberg. Hierarchical shape description via the multiresolution symmetric axis transform. *IEEE Trans. Pattern Anal. Mach. Intell.*, 9(4):505–511, April 1987.

[168] P.M. Plantec. *Virtual Humans: A Build-it-yourself Kit, Complete with Software and Step-by-step Instructions*. Number v. 1 in Virtual Humans: A Build-it-yourself Kit, Complete with Software and Step-by-step Instructions. AMACOM, American Management Association, 2004.

[169] Joshua Podolak, Philip Shilane, Aleksey Golovinskiy, Szymon Rusinkiewicz, and Thomas Funkhouser. A planar-reflective symmetry transform for 3d shapes. *ACM Trans. Graph.*, 25(3):549–559, July 2006.

[170] Frdric J A M Poirier and Hugh R Wilson. A biologically plausible model of human shape symmetry perception. *Journal of Vision*, 10(1):9.1–16, 2010.

[171] J. R. Pomerantz and E. A. Pristach. Emergent features, attention, and perceptual glue in visual form perception. *Journal of Experimental Psychology: Human Perception and Performance*, 15:635–649, 1989.

[172] M.H. Pornstein and S.J. Krinsky. Perception of symmetry in infancy: the salience of vertical symmetry and the perception of pattern wholes. *J Exp Child Psychol*, 39(1):1–19, 1985.

[173] E. M. Pothos and R. Ward. Symmetry, repetition, and figural goodness: An investigation of the weight of evidence theory. *Cognition*, 75:B65–B78, 2000.

[174] Nicholas Pound, Ian S. Penton-Voak, and William M. Brown. Facial symmetry is positively associated with self-reported extraversion. *Personality and Individual Differences*, 43(6):1572 – 1582, 2007.

[175] V. Shiv Naga Prasad and B. Yegnanarayana. Finding axes of symmetry from potential fields. *IEEE Transactions on Image Processing*, 13(12):1559–1566, 2004.

[176] J. Puzicha, T. Hofmann, and J.M. Buhmann. Non-parametric similarity measures for unsupervised texture segmentation and image retrieval. In *Computer Vision and Pattern Recognition, 1997. Proceedings., 1997 IEEE Computer Society Conference on*, pages 267 –272, jun 1997.

[177] D. Gentner R. W. Ferguson, A.. Aminoff. Modeling qualitative differences in symmetry judgments. In *Proceedings of 18th Cognitive Science Conference*, 1996.

[178] S.J.M. Rainville and F.A.A. Kingdom. Scale invariance is driven by stimulus density. *Vision Res*, 42(3):351–67, 2002.

[179] Stphane J.M. Rainville and Frederick A.A. Kingdom. The functional role of oriented spatial filters in the perception of mirror symmetry psychophysics and modeling. *Vision Research*, 40(19):2621 – 2644, 2000.

[180] J L Reilly, P T Murphy, M Byrne, C Larkin, and Gill. Dermatoglyphic fluctuating asymmetry and atypical handedness in schizophrenia. *Schizophr Res*, 50(3):159–68, 2001.

[181] Daniel Reisfeld, Haim Wolfson, and Yehezkel Yeshurun. Context free attentional operators: the generalized symmetry transform. *International Journal of Computer Vision*, 14:119–130, 1995.

[182] Xiaofeng Ren and J. Malik. Learning a classification model for segmentation. In *Computer Vision, 2003. Proceedings. Ninth IEEE International Conference on*, pages 10–17 vol.1, 2003.

[183] G. Rhodes, S. Yoshikawa, A. Clark, K. Lee, R. McKay, and S. Akamatsu. Attractiveness of facial averageness and symmetry in non-western cultures: in search of biologically based standards of beauty. *Perception*, 30(5):611–25, 2001.

[184] I. Rock. *Indirect Perception*. A Bradford book. Mit Press, 1997.

[185] I. Rodríguez, A. Gumbert, N. Hempel de Ibarra, J. Kunze, and M. Giurfa. Symmetry is in the eye of the beeholder: innate preference for bilateral symmetry in flower-naïve bumblebees. *Naturwissenschaften*, 91(8):374–377, August 2004.

[186] Joe Rosen. Symmetry at the foundation of science and nature. *Symmetry*, 1(1):3–9, 2009.

[187] Carsten Rother, Vladimir Kolmogorov, and Andrew Blake. "grabcut": interactive foreground extraction using iterated graph cuts. *ACM Trans. Graph.*, 23(3):309–314, August 2004.

[188] Yossi Rubner, Carlo Tomasi, and Leonidas J. Guibas. A metric for distributions with applications to image databases. In *Proceedings of the Sixth International Conference on Computer Vision*, ICCV '98, pages 59–, Washington, DC, USA, 1998. IEEE Computer Society.

[189] Yossi Rubner, Carlo Tomasi, and Leonidas J. Guibas. The earth mover's distance as a metric for image retrieval. *Int. J. Comput. Vision*, 40(2):99–121, November 2000.

[190] D. Rueckert, M. Clarkson, D. Hill, and D. Hawkes. Non-rigid registration using higher order mutual information. In *Proc. SPIE*, volume 3979, pages 438–447, 2000.

[191] Jukka Saarinen. Detection of mirror symmetry in random dot patterns at different eccentricities. *Vision Research*, 28(6):755 – 759, 1988.

[192] Victor Sanchez, Rafeef Abugharbieh, and Panos Nasiopoulos. 3d scalable lossless compression of medical images based on global and local symmetries. In *Proceedings of the 16th IEEE international conference on Image processing*, ICIP'09, pages 2497–2500, Piscataway, NJ, USA, 2009. IEEE Press.

[193] Kevin W.; Heath Michael D.; Sarkar Sudeep Sanocki, Thomas; Bowyer. Are edges sufficient for object recognition? *Journal of Experimental Psychology: Human Perception and Performance*, 24(1):340–349, 1998.

[194] Knutsen T Tyler C Tootell R Sasaki Y, Vanduffel W. Symmetry activates extrastriate visual cortex in human and nonhuman primates. *Proceedings of the National Academy of Sciences of the United States of America*, 102(8):3159–3163, February 2005.

[195] G. L. Scott and Christopher. An algorithm for associating the features of two images. *Proceedings: Biological Sciences*, 244(1309):21–26, 1991.

[196] Konstantinos Sfikas, Theoharis Theoharis, and Ioannis Pratikakis. Rosy+: 3d object pose normalization based on pca and reflective object symmetry with application in 3d object retrieval. *International Journal of Computer Vision*, pages 262–279, 2011.

[197] C.E. Shannon. A mathematical theory of communication. *Bell System Technical Journal*, 27:379–423, 623–656, 1948.

[198] A. Shawn. *Wish I Could Be There: Notes from a Phobic Life*. Penguin Group USA, 2008.

[199] Dinggang Shen, Horace Ho-Shing Ip, and Eam Khwang Teoh. An energy of asymmetry for accurate detection of global reflection axes. *Image Vision Comput.*, 19(5):283–297, 2001.

[200] Jianbo Shi and Jitendra Malik. Normalized cuts and image segmentation. *IEEE Trans. Pattern Anal. Mach. Intell.*, 22(8):888–905, August 2000.

[201] V. Shiv Naga Prasad and L.S. Davis. Detecting rotational symmetries. In *Computer Vision, 2005. ICCV 2005. Tenth IEEE International Conference on*, volume 2, pages 954 – 961 Vol. 2, oct. 2005.

[202] A. Souto, B.M. Bezerra, and L.G. Halsey. Alcohol intoxication reduces detection of asymmetry: an explanation for increased perceptions of facial attractiveness after alcohol consumption? *Perception*, 37(6):955–8, 2008.

[203] C. Sun and D. Si. Fast reflectional symmetry detection using orientation histograms. *Real-Time Imaging*, 5(1):6374, 1999.

[204] Changming Sun. Symmetry detection using gradient information. *Pattern Recogn. Lett.*, 16(9):987996, 1995.

[205] Yu Sun and Bir Bhanu. Reflection symmetry integrated image segmentation. *IEEE Transactions on Pattern Analysis and Machine Intelligence*, 99(PrePrints), 2011.

[206] John P. Swaddle. Visual signalling by asymmetry: A review of perceptual processes. *Philosophical Transactions: Biological Sciences*, 354(1388):pp. 1383–1393, 1999.

[207] J P Szlyk, I Rock, and C B Fisher. Level of processing in the perception of symmetrical forms viewed from different angles. *Spat Vis*, 9(1):139–50, 1995.

[208] Randy Thornhill and Steven W. Gangestad. Human fluctuating asymmetry and sexual behavior. *Psychological Science*, 5:297–302, 1994.

[209] M. Toews and T. Arbel. Entropy-of-likelihood feature selection for image correspondence. In *ICCV '03: Proceedings of the Ninth IEEE International Conference on Computer Vision*, page 1041, Washington, DC, USA, 2003. IEEE Computer Society.

[210] G. Tolias, Y. Kalantidis, and Y. Avrithis. Symcity: Feature selection by symmetry for large scale image retrieval. In *in Proceedings of ACM Multimedia (Full paper) (MM 2012)*, Nara, Japan, October 2012. ACM.

[211] Matthias S Treder and Ruud G J Meulenbroek. Integration of structure-from-motion and symmetry during surface perception. *J Vis*, 10(4):5.1–17, 2010.

[212] Matthias Sebastian Treder. Behind the looking-glass: A review on human symmetry perception. *Symmetry*, 2(3):1510–1543, 2010.

[213] Anne Treisman and Hilary Schmidt. Illusory conjunctions in the perception of objects. *Cognitive Psychology*, 14(1):107 – 141, 1982.

[214] Anne M. Treisman and Garry Gelade. A feature-integration theory of attention. *Cognitive Psychology*, 12(1):97–136, January 1980.

[215] Stavros Tsogkas and Iasonas Kokkinos. Learning-based symmetry detection in natural images. In Andrew Fitzgibbon, Svetlana Lazebnik, Pietro Perona, Yoichi Sato, and Cordelia Schmid, editors, *Computer Vision ECCV 2012*, volume 7578 of *Lecture Notes in Computer Science*, pages 41–54. Springer Berlin Heidelberg, 2012.

[216] A. M. Turing. The chemical basis of morphogenesis. *Philosophical Transactions of the Royal Society (B)*, 237:37–72, 1952.

[217] C. W. Tyler. Empirical aspects of symmetry perception. *Spatial Vision*, 9:1–7, 1995.

[218] C.W. Tyler. *Human Symmetry Perception and Its Computational Analysis*. Lawrence Erlbaum Associates, 2002.

[219] P. A. van der Helm and E. L. J. Leeuwenberg. Goodness of visual regularities: A nontransformational approach. *Psychological Review*, 103(3):429–456, 1996.

[220] P A Van Der Helm and E L J Leeuwenberg. A better approach to goodness: Reply to wagemans (1999). *Psychological Review*, 106(3):622–630, 1999.

[221] Peter A. van der Helm. Natural selection of visual symmetries, 2002.

[222] Peter A. Van der Helm. The influence of perception on the distribution of multiple symmetries in nature and art. *Symmetry*, 3(1):54–71, 2011.

[223] G. van der Vloed, A. Csath, and P.A. van der Helm. Symmetry and repetition in perspective. *Acta Psychol (Amst)*, 120(1):74–92, 2005.

[224] R. van der Zwan, E. Leo, W. Joung, C. Latimer, and P. Wenderoth. Evidence that both area v1 and extrastriate visual cortex contribute to symmetry perception. *Curr Biol*, 8(15):889–92, 1998.

[225] Paul Viola and Michael Jones. Robust real-time face detection. *International Journal of Computer Vision*, 57:137–154, 2004.

[226] J. von Neumann. *Mathematical foundations of quantum mechanics*. Princeton University Press,Princeton, 1955.

[227] T. Joel Wade. The relationships between symmetry and attractiveness and mating relevant decisions and behavior: A review. *Symmetry*, 2(2):1081–1098, 2010.

[228] T.J. Wade. Evolutionary theory and self-perception: Sex differences in body-esteem predictors of self-perceived physical and sexual attractiveness and self-esteem. *Int. J. Psychol.*, 35:3645, 2000.

[229] J. Wagemans. Detection of visual symmetries. *Spatial Vision*, 9:9–32, 1995.

[230] J. Wagemans, L. Van Gool, and G. d'Ydewalle. Detection of symmetry in tachistoscopically presented dot patterns: effects of multiple axes and skewing. *Percept Psychophys*, 50(5):413–27, 1991.

[231] Alan M. Wai Ho Li, and Zhang and Lindsay Kleeman. Bilateral symmetry detection for real-time robotics applications. *Int. J. Rob. Res.*, 27(7):785814, 2008.

[232] Zhou Wang, Alan C. Bovik, Hamid R. Sheikh, and Eero P. Simoncelli. Image quality assessment: from error visibility to structural similarity. *IEEE Transactions on Image Processing*, 13(4):600–612, 2004.

[233] P Wenderoth. The salience of vertical symmetry. *Perception*, 23(2):221–36, 1994.

[234] P. Wenderoth. The role of pattern outline in bilateral symmetry detection with briefly flashed dot patterns. *Spatial Vision*, 9:57–77, 1995.

[235] P. Wenderoth. The effects on bilateral-symmetry detection of multiple symmetry, near symmetry, and axis orientation. *Perception*, 26(7):891–904, 1997.

[236] Peter Wenderoth. Monocular symmetry is neither necessary nor sufficient for the dichoptic perception of bilateral symmetry. *Vision Research*, 40(16):2097 – 2100, 2000.

[237] Eric Werner. The origin, evolution and development of bilateral symmetry in multicellular organisms. *CoRR*, pages –1–1, 2012.

[238] Hermann Weyl. *Symmetry*. Princeton Univ. Press, 1952.

[239] Lance Williams. Pyramidal parametrics. In *Computer Graphics (SIGGRAPH 83 Proceedings*, 1983.

[240] Natalie Wolchover. As supersymmetry fails tests, physicists seek new ideas. *Scientific American*, 2012.

[241] J. M. Wolfe. Guided Search 4.0: Current Progress with a model of visual search. In W. Gray, editor, *Integrated Models of Cognitive Systems*, pages 99–119. Oxford, New York, 2007.

[242] J. M. Wolfe, K. R. Cave, and S. L. Franzel. Guided search: an alternative to the feature integration model for visual search. *Journal of experimental psychology. Human perception and performance*, 15(3):419–433, August 1989.

[243] Jeremy M. Wolfe and Stacia R. Friedman-Hill. On the role of symmetry in visual search. *Psychological Science*, 3(3):pp. 194–198, 1992.

[244] K. Yamasaki and K.Z. Nanjo. A new mathematical tool for analyzing the fracturing process in rock: Partial symmetropy of microfracturing. *Physics of the Earth and Planetary Interiors*, 173(34):297 – 305, 2009.

[245] R. K K Yip, P.K.-S. Tam, and D. N K Leung. A hough transform technique for the detection of rotational symmetry under parallel projection. In *Industrial Electronics, Control and Instrumentation, 1991. Proceedings. IECON '91., 1991 International Conference on*, pages 1259–1263 vol.2, 1991.

[246] E. Yodogawa. Symmetropy,an entropy-like measure of visual symmetry. *Perception and Psychophysics*, 32:230–240, 1982.

[247] Hagit Zabrodsky. Symmetry - a review. Technical report, Leibniz Center for Research in Computer Science, Department of Computer Science, Hebrew University of Jerusalem, 1990.

[248] Hagit Zabrodsky, Daniel Algom, and Dr. Hagit Zabrodsky. Continuous symmetry: A model for human figural perception, 1994.

[249] Hagit Zabrodsky, Shmuel Peleg, and David Avnir. Symmetry as a continuous feature. *IEEE Trans. Pattern Anal. Mach. Intell.*, 17(12):11541166, 1995.

[250] Dahlia W. Zaidel and Jennifer A. Cohen. The face, beauty, and symmetry: Perceiving asymmetry in beautiful faces. *International Journal of Neuroscience*, 115(8):1165–1173, August 2005.

[251] Dahlia W. Zaidel and Marjan Hessamian. Asymmetry and symmetry in the beauty of human faces. *Symmetry*, 2(1):136–149, 2010.

[252] Djemel Ziou and Salvatore Tabbone. Edge detection techniques - an overview. *International Journal of Pattern Recognition and Image Analysis*, 8:537–559, 1998.

[253] H. L. Zou and Y. T. Lee. Skewed mirror symmetry detection from a 2d sketch of a 3d model. In *Proceedings of the 3rd international conference on Computer graphics and interactive techniques in Australasia and South East Asia*, GRAPHITE '05, pages 69–76, New York, NY, USA, 2005. ACM.